

# In situ PMD Monitoring Using Coherent Detection and Polarization Tracking

*Sathyanarayanan Sundhararajan*

Submitted to the Department of Electrical Engineering &  
Computer Science and the Faculty of the Graduate School  
of the University of Kansas in partial fulfillment of  
the requirements for the degree of Master's of Science

## Thesis Committee:

---

Dr. Rongqing Hui: Chairperson

---

Dr. Christopher Allen

---

Dr. Shannon Blunt

---

Date Defended

The Thesis Committee for Sathyanarayanan Sundhararajan certifies  
That this is the approved version of the following thesis:

**In situ PMD Monitoring Using Coherent Detection and Polarization  
Tracking**

Committee:

---

Chairperson

---

---

---

Date Approved

*To my mother, father and Lav*

# Acknowledgements

I would like to acknowledge and thank people who have supported me in the research work. I would like to thank Dr. Hui for his benevolent support and encouragement throughout the research work at the Lightwave laboratory. I would like to thank Dr. Allen, for numerous discussions on the hardware implementation used for this research. I would like thank Dr Blunt for serving on my thesis committee and taking time to review my work. I am deeply grateful Dr. Jiang for his help in theoretical analysis of the research and for the many collaborations we shared for this research work.

I would like to thank Sprint and Nortel networks for providing financial support for this research work. Finally I would like to thank all my friends at KU for their support and numerous rides to the research lab at night.



# Abstract

Polarization mode dispersion (PMD) is a major impairment in high bit rate optical communication systems, causing system degradation. Although the random nature of PMD makes it difficult to be characterized, many measurement techniques have been developed to measure PMD and its effects on network reliability. However, the lack of in situ measurement techniques that can measure PMD on traffic carrying fibers has made it difficult for engineers to characterize the effects of PMD on wide bandwidth wavelength division multiplex (WDM) optical systems. The objective of this research is to develop an in situ PMD monitoring technique for long haul fiber optic links and use this technique to characterize the magnitude and distribution of PMD on these links.

Towards this end, a systematic approach was followed to develop a monitoring equipment that can measure PMD on traffic carrying links. First, an earlier implementation of the PMD monitoring equipment based on coherent detection and polarization scrambling [16] was improved in terms of size, speed and accuracy to make it more suitable for field measurements of PMD in traffic carrying fiber optic links. The coherent PMD monitor can measure differential group delay (DGD) values in the range of 0 to 50 ps. Secondly, using theoretical analysis, it was ascertained that the magnitude of PMD, the DGD measured by the PMD monitor, is the apparent DGD of the fiber and not its true DGD. Mathematical analysis was used to derive a relationship between the true DGD and the apparent DGD of the fiber. Also, it was found that the distribution of the apparent DGD is Rayleigh, unlike the true DGD which is Maxwellian.

Thirdly, the hardware and software for implementing a polarization tracking algorithm to measure PMD was developed and tests were conducted to validate the algorithm in terms of speed, accuracy and the characteristics of the measured DGD. The polarization tracking algorithm has a higher measurement speed and

lesser memory requirements than polarization scrambling. A number of laboratory experiments and field trials on traffic carrying fibers were conducted for a comparative analysis of polarization scrambling and polarization tracking. Using the polarization tracking algorithm to measure DGD, the measurement speed was found to be 20 times higher and the memory requirements about 80 times less than the memory required for DGD measurements using polarization scrambling. Results of the laboratory experiments and field trials agree with our theoretical analysis and the two algorithms have similar statistics for the measured DGD. Finally, the possibility of a more efficient implementation of polarization tracking was explored to measure PMD in real time. A run time implementation with the existing hardware and software was developed where the advantages of polarization tracking over polarization scrambling was made evident. The use of the in-situ PMD monitoring technique will enable network engineers to monitor the impact of PMD in live traffic carrying links and to select the wavelength bands that are relatively less affected by PMD.

# Contents

Acceptance Page	i
Acknowledgements	iii
Abstract	iv
<b>1 Introduction</b>	<b>1</b>
<b>2 Polarization mode dispersion (PMD) - Basic concepts</b>	<b>4</b>
2.1 Description of Polarization Optics . . . . .	4
2.2 The Jones Polarization Calculus . . . . .	5
2.3 Degree of Polarization (DOP) . . . . .	6
2.4 Stokes Parameter Representation of Polarization . . . . .	7
2.5 The Poincare Sphere . . . . .	8
2.6 Polarization Effects in Light Wave Systems . . . . .	9
2.7 Birefringence and PMD . . . . .	10
2.8 Polarisation Mode Coupling . . . . .	12
2.9 Principal States Model . . . . .	14
2.10 Vector form of PMD . . . . .	16
2.11 PMD in short and long fibers . . . . .	17
2.11.1 Frequency domain behavior of PMD . . . . .	17
2.11.2 Time domain behavior of PMD . . . . .	17
2.12 Random behavior of PMD . . . . .	18
2.13 Effects of PMD . . . . .	19
<b>3 PMD Measurement Techniques</b>	<b>21</b>
3.1 Time-domain measurement techniques . . . . .	22

3.1.1	Pulse delay technique . . . . .	22
3.1.2	The interferometric method . . . . .	23
3.1.3	The modulation phase-shift method . . . . .	25
3.2	Frequency domain techniques . . . . .	26
3.2.1	The Fixed Analyzer method . . . . .	26
3.2.2	The Poincare Arc method . . . . .	28
3.2.3	The Jones-Matrix Eigenanalysis (JME) method . . . . .	28
3.3	Summary of PMD measurement techniques . . . . .	30
<b>4</b>	<b>In situ PMD monitoring</b>	<b>33</b>
4.1	Need for in-situ PMD measurement techniques . . . . .	33
4.2	The coherent PMD monitor . . . . .	34
4.2.1	Block diagram of the coherent heterodyne detector . . . . .	34
4.2.2	The theory of PMD measurement . . . . .	35
4.3	Polarization Scrambling . . . . .	41
4.3.1	The hardware for implementing polarization scrambling . . . . .	43
4.3.2	Data acquisition algorithm for polarization scrambling . . . . .	50
4.4	Polarization tracking . . . . .	50
4.4.1	Hardware implementation for polarization tracking . . . . .	53
4.4.2	Algorithm used for polarization tracking . . . . .	54
4.5	Time-interleaved implementation of polarization scrambling and tracking . . . . .	56
4.5.1	The Microcontroller algorithm . . . . .	57
4.5.2	The Data Acquisition algorithm . . . . .	59
4.6	Algorithm for extracting DGD information from the acquired data . . . . .	60
4.6.1	Extracting DGD information from polarization tracking . . . . .	60
4.6.2	Extracting DGD information from polarization scrambling . . . . .	63
4.7	Performance analysis of polarization scrambling and polarization tracking . . . . .	64
4.7.1	Range of DGD measured by the PMD monitor . . . . .	65
4.7.2	Measurement speed . . . . .	65
4.7.3	Accuracy of the measurement . . . . .	66
4.7.4	Dead zone of the polarization controller . . . . .	67

4.7.5	Measurement period and Statistics of data collected for extracting DGD . . . . .	69
4.7.6	Noise characteristics . . . . .	70
4.8	Advantage of polarization tracking over polarization scrambling .	76
<b>5</b>	<b>Experiments and Results</b>	<b>77</b>
5.1	Measuring the DGD of a PM fiber . . . . .	77
5.2	Measuring the DGD of a PMD emulator . . . . .	80
5.3	PMD monitor in field measurement trial . . . . .	86
5.3.1	Trials in optical switch station for polarization scrambling	86
5.3.2	Field trial results of polarization tracking . . . . .	88
5.4	DGD measurement of a scrambled input signal . . . . .	89
5.5	Run time implementation of polarization tracking . . . . .	92
5.5.1	Hardware and Software used for real time DGD calculation	92
5.5.2	Test for real time implementation using polarization tracking	93
<b>6</b>	<b>Summary</b>	<b>95</b>
6.1	Conclusion . . . . .	95
6.2	Future work . . . . .	96
	<b>References</b>	<b>97</b>
<b>A</b>	<b>Microcontroller code for polarization tracking and scrambling</b>	<b>100</b>
<b>B</b>	<b>MATLAB code for acquiring data from the PMD monitor</b>	<b>111</b>
<b>C</b>	<b>MATLAB code for extracting DGD from polarization tracking data</b>	<b>113</b>
<b>D</b>	<b>MATLAB code for extracting DGD from polarization scrambling data</b>	<b>117</b>
<b>E</b>	<b>Visual Studio 2005 C sharp code for acquiring data from the PMD monitor</b>	<b>123</b>

# List of Figures

2.1	A polarization ellipse [8] . . . . .	5
2.2	Cartesian Coordinate representation of the stokes parameters [8]	8
2.3	The Poincare Sphere . . . . .	9
2.4	Optical modes and stresses in a single mode fiber [18]. . . . .	11
2.5	Evolution of SOP along the length of a single mode fiber due to Polarization mode coupling [18]. . . . .	12
2.6	Time domain behavior of PMD in short fibers [22] . . . . .	18
3.1	The pulse delay technique for measuring DGD [19] . . . . .	22
3.2	The interferometric technique for measuring DGD [8] . . . . .	23
3.3	The modulation phase-shift method [8] . . . . .	25
3.4	The Fixed Analyzer technique using (a) a broadband source and (b) a narrowband laser [8] . . . . .	27
3.5	The Jones-Matrix Eigenanalysis technique [8] . . . . .	29
3.6	Summary of PMD measurement techniques [8, 19]. . . . .	32
4.1	A coherent heterodyne detection setup for PMD monitoring . . .	35
4.2	An illustration of polarization walk off between the two frequency selected components $f_1$ , point A and $f_2$ , pointB . . . . .	37
4.3	An illustartion of polarization states of frequency components and their relative orientations with the PMD vector of a long fiber . .	38
4.4	Hardware implementation for PMD monitoring using polarization scrambling technique . . . . .	43
4.5	A picture of the hardware used for our reserach . . . . .	44
4.6	The BATI polarization controller . . . . .	45

4.7	Polarization control of the SOP of the local oscillator using two retardation plates . . . . .	46
4.8	Amplifier and filter circuits used for reducing the effects of noise .	49
4.9	Data Acquisition algorithm for polarization scrambling . . . . .	51
4.10	The DAC waveform generated for polarization controller driver . .	52
4.11	Hardware implementation for polarization tracking . . . . .	53
4.12	Algorithm for polarization tracking . . . . .	57
4.13	Microcontroller algorithm to implement time interleaved implementation of scrambling and tracking . . . . .	58
4.14	Data acquisition algorithm for time interleaved implementation of scrambling and tracking . . . . .	59
4.15	Data acquisition algorithm for time interleaved implementation of scrambling and tracking . . . . .	61
4.16	Output waveform for polarization tracking . . . . .	62
4.17	Voltage values obtained data processing and DGD extraction . . .	63
4.18	Output waveform for polarization scrambling . . . . .	64
4.19	Simulation results for error in the DGD measurement due to threshold used for validating polarization tracking . . . . .	68
4.20	The dead zone of the polarization controller . . . . .	69
4.21	The RF spectrum at the output of the RF amplifier without attenuating the LO output . . . . .	73
4.22	The RF spectrum at the output of the RF amplifier with attenuation of the LO output . . . . .	74
5.1	Experimental setup for the PM fiber experiment . . . . .	78
5.2	Plot for DGD calculated by the PMD monitor using polarization scrambling for the PM fiber experiment . . . . .	78
5.3	Histogram for DGD calculated by the PMD monitor using polarization scrambling for the PM fiber experiment . . . . .	79
5.4	Plot for DGD calculated by the PMD monitor using polarization tracking for the PM fiber experiment . . . . .	80
5.5	Histogram for DGD calculated by the PMD monitor using polarization tracking for the PM fiber experiment . . . . .	81
5.6	Experimental setup for the PMD emulator experiment . . . . .	82

5.7	Plot for DGD calculated by the PMD monitor using polarization scrambling for the PMD emulator experiment . . . . .	82
5.8	Histogram for DGD calculated by the PMD monitor using polarization scrambling for the PMD emulator experiment . . . . .	83
5.9	Plot for DGD calculated by the PMD monitor using polarization tracking for the PMD emulator experiment . . . . .	84
5.10	Histogram for DGD calculated by the PMD monitor using polarization tracking for the PMD emulator experiment . . . . .	85
5.11	Histogram for DGD calculated by the PMD monitor using polarization scrambling for the KC-Chicago fiber optic link . . . . .	87
5.12	Plot for DGD calculated by the PMD monitor using polarization scrambling for the KC-Chicago fiber optic link . . . . .	88
5.13	Histogram for DGD calculated by the PMD monitor using polarization tracking . . . . .	89
5.14	Plot for DGD calculated by the PMD monitor using polarization tracking . . . . .	90
5.15	Plot for DGD calculated by the PMD monitor using polarization scrambling for an unstable probing signal . . . . .	91
5.16	Plot for DGD calculated by the PMD monitor using polarization tracking for an unstable probing signal . . . . .	92
5.17	Algorithm for run time extraction of DGD (a) The MCU algorithm for tracking and (b)The software algorithm for DGD calculation in run time . . . . .	93
5.18	Histogram for DGD calculated real time by the PMD monitor using polarization tracking . . . . .	94



# List of Tables

4.1	Characteristics of polarization controller . . . . .	45
4.2	Characteristics of polarization controller driver. . . . .	47
4.3	Characteristics of DT9832 DAQ . . . . .	48
4.4	Characteristics of ADuC7026 microcontroller . . . . .	54
5.1	DGD statistics for the PM fiber experiment. . . . .	81
5.2	DGD statistics for the PMD emulator experiment. . . . .	85
5.3	DGD statistics for the measurement trial with polarization scrambling	87
5.4	DGD statistics for the measurement trial with polarization tracking	90
5.5	DGD statistics for the run time implementation of the PMD monitoring with polarization tracking . . . . .	94

# Chapter 1

## Introduction

The phenomenon of polarization mode dispersion (PMD), its characteristics and effects on light wave systems has been a well- researched topic since 1970. With the advent of fourth and fifth generation fiber optic systems where erbium doped fiber amplifiers (EDFAs) are used to increase the repeater spacing in optical links and wavelength division multiplexing (WDM) is used to increase data rate up to  $100Gb/s$ , the transmission capacity of fiber optic links have increased beyond other communication technologies. This calls for very low dispersion on fibers carrying the traffic at such high rates. As a result, there is a need for characterizing fibers and the wavelengths at which fiber dispersion can be manageable by use of dispersion compensation mechanisms. The fifth generation fiber optic systems use optical pulses that preserve their shape while propogating through the fiber by minimising the dispersion by use of fiber non-linearity. But, for bit rates higher than  $10Gb/s$ , the PMD effects on the system can be adverse if not compensated for.

PMD in fiber optic systems is a property of single mode fibers, and is caused by optical birefringence. PMD is due to a light wave propogating in two orthogonal

polarization modes of a fiber with different propagation velocities. PMD results in pulse broadening and distortion resulting in degradation of system performance [18]. PMD is a stochastic process and varies with temperature, pressure and manufacturing defects or stresses in the circular symmetry of the fiber core. These dependencies make PMD a very difficult phenomenon to measure, to counter or to compensate for. PMD is a vector quantity whose magnitude is called the differential group delay (DGD) with a direction along the fast axis of the PSPs. This thesis focuses on measuring the DGD of the fiber that can be easily measured.

The efforts of many researchers have helped engineers better understand the characteristics of PMD. A number of techniques were proposed for PMD measurement [13,17] such as the Jones Matrix Eigenanalysis method, Poincare sphere analysis, fixed analyzer method and the interferometric method. All these measurement techniques require control of polarization state and optical frequency of the signal that is being measured and, as such, they are unsuitable for monitoring the PMD of optical systems carrying live traffic. They also require access to both ends of the fiber. At the lightwave laboratory at the University of Kansas, we recently proposed a simple technique to measure DGD in live traffic carrying fiber optic links using coherent heterodyne detection and RF signal processing [16]. In earlier research at KU, it has been demonstrated that the system Q margin is inversely proportional to the instantaneous DGD measured by the technique [10]. This result serves as a validation of our technique. Using this technique as a conceptual base, different algorithms have been implemented for in-situ measurement for PMD in live traffic carrying links. This thesis is a presentation of the algorithms for measuring PMD.

The basic concepts of light wave polarization, their representation and origin,

nature and effects of PMD in fiber optic links is discussed in chapter 2. Chapter 3 discusses the traditional PMD measurement techniques, their limitations and capabilities. The coherent PMD monitor developed in the light wave laboratory in KU, theoretical analysis of our method, the algorithms used to measure the DGD along with their hardware implementations, a time interleaved implementation of these algorithms for comparative analysis and the performance analysis of the hardware and software used in the equipment are discussed in detail in chapter 4. In chapter 5, the experiments conducted to characterize the algorithms and field trials to measure DGD and the results of the experiments are given. Conclusions of our research and recommendations for future work are made in chapter 6.

# Chapter 2

## Polarization mode dispersion (PMD) - Basic concepts

### 2.1 Description of Polarization Optics

Any electromagnetic wave can be represented by the electric and magnetic field vectors at right angles to one another on a transverse plane that is perpendicular to the direction of propagation. The pattern of electric field vectors traced out by the wave as a function of time is defined as the polarization of the wave. The concept of polarization applies to the light wave as well. Polarization is a time snapshot of electric field vectors as a function of distance from the source [8]. Any polarization state can be represented by a polarization ellipse shown in figure 2.1, that shows the locus and direction of the electric field vector in a given direction. If the propagation of the light wave is along the  $z$ -axis, then the electric field vectors oriented in the  $xy$  plane can be represented by

$$E_x(z, t) = E_{0x} \cos(\tau + \delta_x) \tag{2.1}$$

and

$$E_y(z, t) = E_{0y} \cos(\tau + \delta_y), \quad (2.2)$$

where  $\tau = \omega t - kz$ .  $E_{0x}$  and  $E_{0y}$  are the peak amplitudes of the field vector in the  $x$  and  $y$  axis respectively, and  $\delta_x$  and  $\delta_y$  are their phase components. Also, the field pattern of the electric field vector in an  $xy$  plane is given by,

$$\frac{E_x^2}{E_{0x}^2} + \frac{E_y^2}{E_{0y}^2} - 2 \frac{E_x}{E_{0x}} \frac{E_y}{E_{0y}} \cos \delta = \sin^2 \delta. \quad (2.3)$$

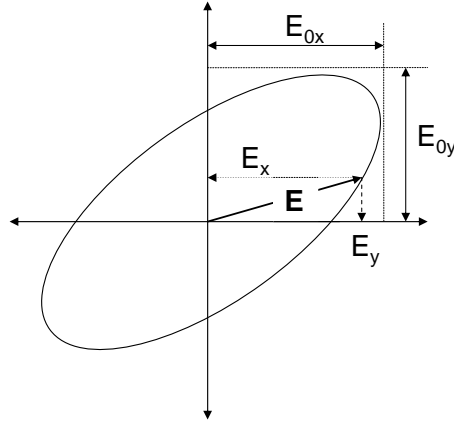


**Figure 2.1.** A polarization ellipse [8]

## 2.2 The Jones Polarization Calculus

Developed by Clark Jones, the polarization calculus is a means of representing polarization in terms of electric field components. Named the Jones vector, the polarized light can be represented as a two-component vector that specifies the magnitude and phase of the  $x$  and  $y$  components of the electric field in the plane

perpendicular to the direction of propagation i.e.,  $z$  plane. It has the form

$$E = \begin{pmatrix} E_x \\ E_y \end{pmatrix} = \begin{pmatrix} E_{0x}e^{i\delta_x} \\ E_{0y}e^{i\delta_y} \end{pmatrix}. \quad (2.4)$$

Usually, the Jones vector is expressed in the normalised form where the components are normalized with respect to the  $x$  or  $y$  component of the electric field. It should be noted that the Jones vector representation is limited to completely polarized light and represents light in terms of electric field rather than optical power. In many cases, the latter can be more easily measured than the former.

### 2.3 Degree of Polarization (DOP)

A light wave can either be polarized or unpolarized. Unpolarized light can be intuitively represented by electric field vectors occupying random orientations in the  $xy$  plane from time to time. Even the polarization of a fully polarized lightwave can be scrambled at a high enough rate for it to appear unpolarized. This condition can occur due to bandwidth limitations of optical instrumentation.

In general, the extent of polarization of a light wave describes its uses and challenges based on an application. The extent of polarization of a light wave is defined by the term *Degree of Polarization* (DOP), which is the ratio of polarized power to the total power of the signal [8].

$$DOP = \frac{P_{polarized}}{P_{polarized} + P_{unpolarized}} \quad (2.5)$$

Light wave in free space maintains its DOP indefinitely. But its DOP through a nonideal transmission medium or optical components changes due to the dis-

persion properties of the medium or the spectral width of the signal.

## 2.4 Stokes Parameter Representation of Polarization

The Stokes vector contains an array of elements that represent optical power in specific polarization states. The Stokes parameters are described as

$$\begin{pmatrix} S_0 \\ S_1 \\ S_2 \\ S_3 \end{pmatrix}, \quad (2.6)$$

where  $S_0$  represents the total power in the optical signal.  $S_1$  represents the difference in power between the linear horizontal (LH) and the linear vertical (LV) polarizations.  $S_2$  represents the difference in power between the linear +45 deg and the linear -45 deg polarizations.  $S_3$  represents the difference in power between the right hand circular(RHC) and the left hand circular (LHC) polarizations. The polarized part of the optical power using Stokes parameters is given by,

$$P_{polarized} = \sqrt{S_1^2 + S_2^2 + S_3^2}. \quad (2.7)$$

The Stokes parameters can also be represented by normalizing with the total optical power, i.e., $S_0$ . The normalized stokes parameters are

$$\begin{aligned} s_1 &= \frac{S_1}{S_0} \\ s_2 &= \frac{S_2}{S_0} \\ s_3 &= \frac{S_3}{S_0}. \end{aligned} \quad (2.8)$$



The normalized stokes parameters can be represented in an  $xyz$  cartesian coordinate system as shown in figure 2.2.

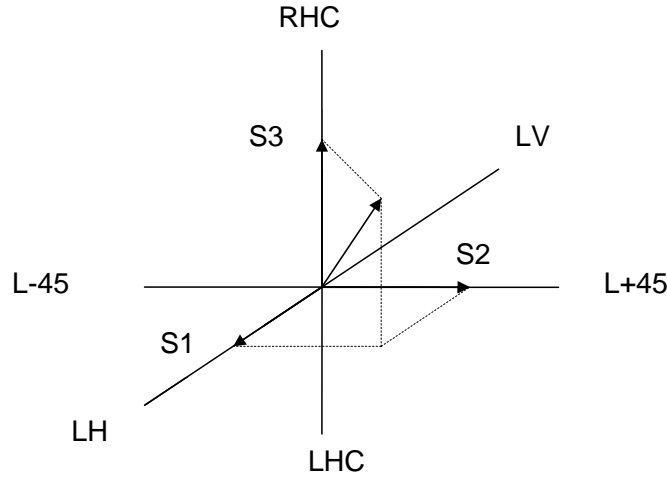


**Figure 2.2.** Cartesian Coordinate representation of the stokes parameters [8]

## 2.5 The Poincare Sphere

The locus of all points described by the polarization equation 2.3 describes a sphere called the Poincare Sphere. The Poincare Sphere shown in figure 2.3 shows the mapping of the normalized stokes parameters. It is a three - dimensional graphical representation of polarization states within a sphere centered on a three - dimensional Cartesian coordinate system. A given point on the sphere represents a unique polarization state of the completely polarized light, i.e., the DOP for the light wave at that polarization state is unity. A partially polarized light wave will describe a sphere whose radius lesser than the radius of the Poincare sphere. Alternatively, the DOP can be represented in terms of the normalised stokes

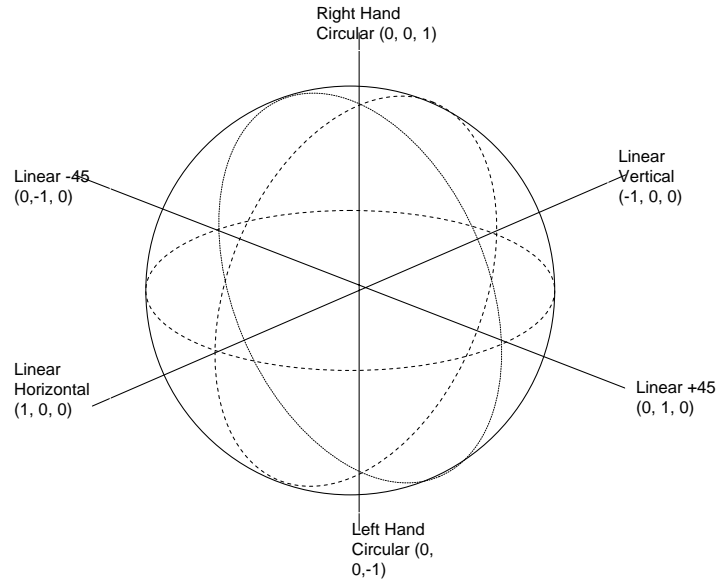


**Figure 2.3.** The Poincare Sphere

parameters as

$$DOP = \sqrt{s_1^2 + s_2^2 + s_3^2} \quad (2.9)$$

As seen in figure 2.3, the circular polarization states occupy the north and south poles of the sphere while the equator represents the linear polarization states. The right(left) hand elliptical states occupy the northern(southern) hemisphere. Two polarization states that are orthogonal to one another are located on the diametrically opposite sides of the Poincare sphere. Hence the Poincare sphere can be used in optics to represent fully polarized light or the polarized part of the partially polarized light.

## 2.6 Polarization Effects in Light Wave Systems

Traditionally, polarization effects have had little impact on development of light wave systems. This is primarily due to the fact that commercial optical

receivers detect the optical power instead of the optical field and are therefore insensitive to polarisation [23]. However, in recent times, polarization effects on light wave systems have gained significance. The advent of optical amplifiers has increased the path lengths of optical fiber and the number of optical elements in an optical link. Moreover, rapid increase of bit rates in digital systems and modulation techniques in analog systems have pushed the capacity of optical fibers to its limit. This has led to the polarization effects such as the polarization mode dispersion (PMD) and polarization-dependent loss (PDL) can accrue to a point where they are detrimental to optical communication at high data rates [18]. The causes and effects of PMD along with its modeling are discussed in the remaining sections of this chapter.

## 2.7 Birefringence and PMD

Ideally, in a single mode fiber, a light wave of arbitrary polarization can be represented as a linear superposition of orthogonally polarized modes. Due to the cylindrical symmetry of the waveguides, the two  $HE_{11}$  modes are degenerate. In reality, owing to manufacturing defects and external stresses acting on the fiber results in loss of symmetry [18]. The asymmetry can be either non circular waveguide geometry or asymmetry in the stress field in the fiber core as shown in figure 2.4.

The asymmetry results in loss of degeneracy, i.e., two distinct  $HE_{11}$  modes with different group and phase velocities. The perturbation that causes degeneracy is called birefringence. Birefringence can be caused by intrinsic or extrinsic factors. Intrinsic factors are due to faults in the fiber manufacturing process such as a non circular core and non symmetrical stress fields around the core. Such

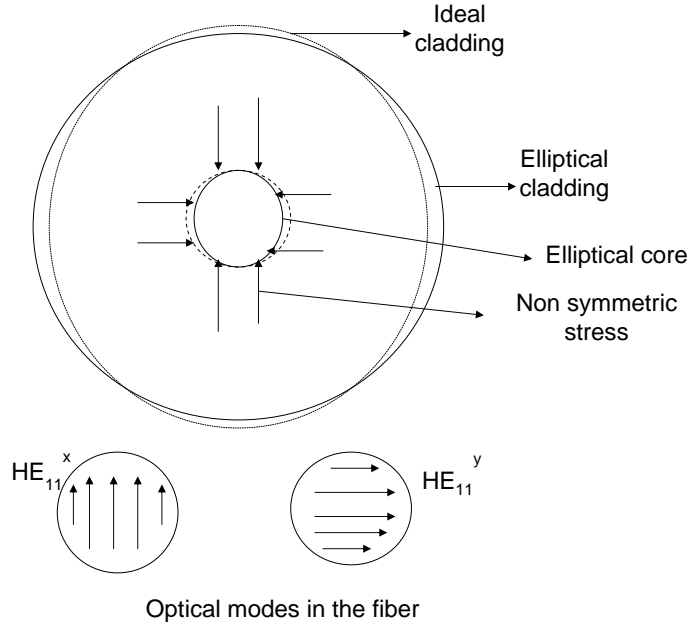


**Figure 2.4.** Optical modes and stresses in a single mode fiber [18].

fibers have PMD of around  $0.5ps/\sqrt{km}$ . These class of fibers are called legacy fibers. Modern manufacturing techniques produce fibers with lesser defects have a very low PMD that is typically lesser than  $0.1ps/\sqrt{km}$  [18]. Factors causing birefringence after the fiber manufacturing process such as cabling of fibers, environmental pressure and temperature are classified as extrinsic factors. The geometric and stress related factors causing birefringence cause an asymmetric change in refractive index of the core. Thus, when a light pulse is input into the asymmetric fiber core, it results in two different modes of propagation with one mode being faster than the other. The mode with lower refractive index and thus with higher velocity is called the fast axis or the extraordinary mode while the mode with higher refractive index and lower velocity is called the slow axis or the ordinary mode.

## 2.8 Polarisation Mode Coupling

Let us consider a significant population of birefringent fibers all subject to the same conditions and thus the same random perturbations. Also consider a light pulse launched into one of these fibers such that only one of two polarization modes is excited. When this launched pulse propagates along a birefringent axis of the fiber, the polarization state of the lightwave evolves with distance along the fiber. Thus a portion of power is coupled from one mode of the fiber to its orthogonal mode and this in turn couples back to the original mode. The power coupled from one mode to another depends on the perturbations which are random along the length of the fiber as shown in figure 2.5. If the average optical power leakage from the fast-axis to the slow axis were calculated, we would find that the power leakage increases with distance until the average power in the two orthogonal polarization modes is the same. In other words, at large distances from the input of the fiber, all polarisation states of the lightwave are equally likely.

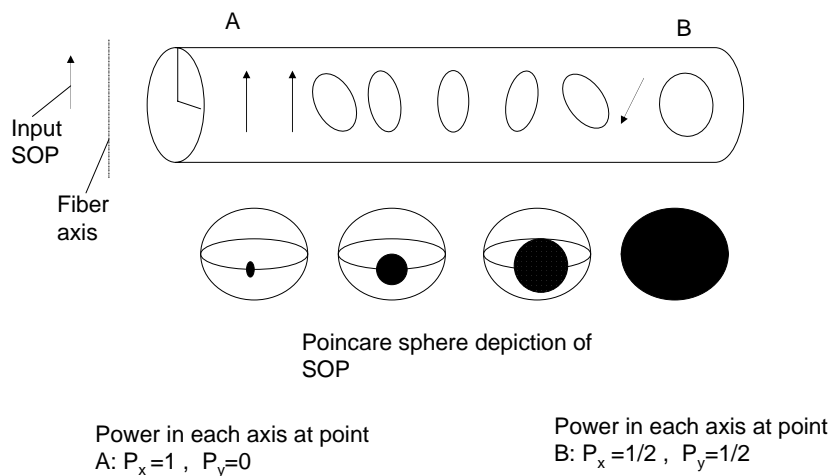


**Figure 2.5.** Evolution of SOP along the length of a single mode fiber due to Polarization mode coupling [18].

The loss of correlation between the polarization at the input and the output of the fiber can be mathematically represented by correlation length,  $l_c$ . The correlation length is defined as the length at which the average power at the orthogonal mode,  $P_{\perp}$ , is within  $1/e^2$  of the power in the originally launched mode,  $P_{\parallel}$ . Typically, correlation lengths vary from tens of meters to a kilometer. Mode coupling further complicates the characteristics of PMD. Typically, the class of fibers whose length ( $l_i$ ) are less compared to the correlation length of the fiber ( $l_i \ll l_c$ ) are called short fibers, and those whose length are long compared to the correlation length ( $l_i \gg l_c$ ) are called long fibers [18].

According to the statistical theory of PMD, the mean square DGD,  $l_c$  and  $l_i$  are related as

$$(\Delta\tau^2) = 2(\Delta\tau_b \frac{l_c}{l_b})^2 (l/l_c + e^{-l/l_c} - 1), \quad (2.10)$$

where  $l_b$  is called the beat length of the fiber. The beat length is defined as the propagation distance for light through a fiber for which a phase difference of  $2\pi$  occurs between the fast axis and the slow axis of the fiber. For short fibers i.e., when  $l \ll l_c$ , the expression simplifies to

$$\sqrt{(\Delta\tau^2)} = \Delta\tau_{rms} = \Delta\tau_b l/l_b \quad (2.11)$$

and for long fibers, i.e., when  $l \gg l_c$ , the expression simplifies to

$$\sqrt{(\Delta\tau^2)} = \Delta\tau_{rms} = (\Delta\tau_b/l_b) \sqrt{2ll_c}. \quad (2.12)$$

The birefringence in a short length fiber can be considered to be uniform [22].

The difference between the propagation constants of the fast axis and slow axis can be given as

$$\Delta\beta = \frac{\omega n_s}{c} - \frac{\omega n_f}{c} = \frac{\omega \Delta n}{c}, \quad (2.13)$$

where  $\omega$  is the angular frequency of the light,  $c$  is the velocity of light and  $\Delta n = n_s - n_f$  is the refractive index difference between the fast axis and slow axis.

## 2.9 Principal States Model

Developed by Poole and Wagner in 1986, the Principal States Model states that for any given length of the fiber and at every frequency of light wave transmission, there exists a pair of input polarization states called the Principal States of Polarization (PSPs) over a small range of frequencies [18]. A PSP is that input polarization state for which the output polarization state is independent of first order changes in frequency. The model provides both time and frequency domain characterisation for PMD. The model assumes that polarization does not affect the optical loss in a fiber span and also that time delay caused by PMD in the span is considerably smaller than transmission bit period. Thus the model applies to low bandwidth pulses only. This is a fair assumption in that all practical high speed fiber optic systems today satisfy this assumption of the model. If we neglect the polarization dependent loss in the fiber (which is negligible in most fiber links), the PSPs are orthogonal. The model implies that for each pair of input PSPs, there is a corresponding orthogonal pair of output PSPs related by

the frequency dependent transmission matrix  $T(\omega)$

$$E_2(\omega) = T(\omega)E_1(\omega), \quad (2.14)$$

where  $E_2(\omega)$  is the complex electric field vector at the output of the fiber and  $E_1(\omega)$  is the field vector at the input of the fiber. Equivalently, in Stokes space, if  $\hat{p}_s$  represents the unit vector of the input PSP while  $\hat{p}$  represents the unit vector of the output PSP then,

$$\hat{p}_s = R\hat{p}, \quad (2.15)$$

where  $R$  is the transmission matrix of the fiber. In the time domain, the model allows us to express any light wave at the input (output) as a vector sum of two components each of which is aligned with one of the input (output) PSPs [22]. As a result the output field vector,  $E_2(t)$  can be represented as

$$E_2(t) = c_+\hat{\epsilon}_+E_1(t + \tau_+) + c_-\hat{\epsilon}_-E_1(t + \tau_-), \quad (2.16)$$

where  $E_1(t)$  is the input field vector,  $\hat{\epsilon}_+$  and  $\hat{\epsilon}_-$  are unit vectors aligned with output PSPs.

For short fibers, because the birefringence is uniform, the PSPs correspond to the polarization modes of the fiber. However, in long fibers, the birefringence and thus the PMD are highly sensitive to ambient changes in temperature and pressure. This leads to the slow change of net PMD of the link as well as the PSPs.



## 2.10 Vector form of PMD

Pure PMD is completely described by the PSPs and the PMD vector [7]. For a given input polarization state, the PMD vector can be represented using the Principal States Model as

$$\frac{d\hat{s}}{d\omega} = \Omega \otimes \hat{s}, \quad (2.17)$$

where  $\hat{s}$  is the unit vector in Stokes space. Here  $\Omega \otimes = R_w R^T$ . Thus, the PMD vector represents a change in the Stokes vector of the output polarization. The PMD vector is expressed as a function of distance, time and optical frequency, i.e., as  $\Omega(z, t, \omega)$  in the Stokes space. From equation 2.17, it is clear that the PMD vector has a length which is the DGD and points in the direction of the fast axis of the fiber about which the output state of polarization (SOP) rotates in the counter clockwise direction as  $\omega$  increases [24]. The PMD vector evolves along the length of the fiber as

$$\frac{d\tau}{dz} = \frac{d\beta}{d\omega} + \beta \times \tau, \quad (2.18)$$

where  $z$  is the position along the direction of propagation of the fiber and  $\beta$  is the three-dimensional local birefringent vector the direction of which is the same as that of  $z$  [18]. The DGD can also be represented as the rate of change of output SOP with respect to optical frequency as

$$\Delta\tau = \frac{\Delta\theta}{\Delta\omega}. \quad (2.19)$$

## 2.11 PMD in short and long fibers

### 2.11.1 Frequency domain behavior of PMD

When a 45 deg linearly polarized light is launched into a short fiber, the state of polarization evolves along the length of the fiber. Also if the polarisation of the light is fixed and the optical frequency is varied, the polarization state at the output of the fiber will evolve in the cyclic fashion [22]. The locus of the output polarization states is a circle on the Poincare Sphere. As we shall see in chapter 3, the frequency domain characteristic of PMD is used by PMD measurement techniques such as Jones Matrix Eigenanalysis method, Poincare Arc method and Fixed Analyzer method.

### 2.11.2 Time domain behavior of PMD

To describe the time domain behavior of PMD, we first define a beat length,  $L_b$  which is the propagation distance for light through a fiber for which a phase difference of  $2\pi$  occurs between the fast axis and the slow axis. Mathematically,

$$L_b = \frac{\lambda}{\Delta n}. \quad (2.20)$$

Telecommunication fibers have beat lengths of approximately 10m. For a short fiber, the DGD,  $\Delta\tau$ , is defined as the difference in group delay between the fast axis and the slow axis. The time domain behavior of PMD in short fibers is shown in figure 2.6.

$\Delta\tau$  can be obtained by the frequency derivative as

$$\frac{\Delta\tau}{L} = \frac{d}{d\omega} \left( \frac{\Delta n\omega}{c} = \frac{\Delta n}{c} + \frac{\omega}{c} \frac{d\Delta n}{d\omega} \right). \quad (2.21)$$

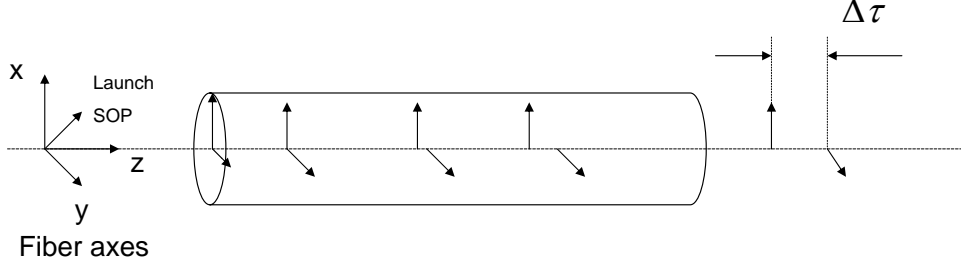


**Figure 2.6.** Time domain behavior of PMD in short fibers [22]

The dispersion of  $\Delta n$  is negligible for a short fiber. Thus, the second term of the above equation can be neglected and the DGD per beat length of a short fiber,  $\Delta\tau_b$ , can be written as

$$\Delta\tau_b = L_b \frac{\Delta n}{c} = \frac{\lambda}{c} = \frac{1}{\nu}. \quad (2.22)$$

As can be seen from the above expression, the DGD per beat length is equal to one optical cycle of the lightwave.

## 2.12 Random behavior of PMD

Since PMD varies randomly with wavelength of transmission and environmental stresses, the statistical distribution of PMD has been studied in some detail. The PMD vector can be decomposed into three orthogonal components along each of the axes of the Poincare sphere. Each component can be described by Gaussian distribution with zero mean. The DGD, which is the magnitude of the PMD vector, can then be given by the square root of the sum of the squares of these orthogonal components. It has been shown that the distribution of DGD of

fibers in long length regime, follows a Maxwellian distribution or a Chi distribution with three degrees of freedom [21]. Thus, if one were to measure the DGD of a fiber over a range of wavelengths at fixed time, or over a long time with a fixed wavelength, and with changing environmental conditions, the distribution of DGD will be Maxwellian. If  $\Delta\tau$  represents the instantaneous DGD of the system, the distribution of  $\Delta\tau$  is given by

$$p(\Delta\tau) = \sqrt{\frac{2}{\pi}} \frac{\Delta\tau^2}{\sigma^3} e^{-\frac{\Delta\tau^2}{2\sigma^2}}, \quad (2.23)$$

where  $\sigma^2$  is the variance of DGD. The mean DGD of the expression above is given by

$$\langle \Delta\tau \rangle = \sigma \sqrt{\frac{8}{\pi}}. \quad (2.24)$$

### 2.13 Effects of PMD

PMD causes pulse broadening and signal distortion and hence, leads to system penalties [20]. The DGD between two pulses propagating in orthogonal polarization modes induces inter-symbol interference (ISI) in digital transmission channels. A system that is designed with penalties for normal conditions with tolerable PMD may be subject to rare occurrences of very high PMD due to rapid changes in environmental conditions. Such rapid fluctuations in PMD cannot be simulated in lab environments and so the power penalties assigned due to the effects of PMD rely heavily on theoretical simulations [22]. In general, the power penalty incurred due to PMD has the form

$$\epsilon(dB) = A \frac{\Delta\tau^2 \gamma (1 - \gamma)}{T^2}, \quad (2.25)$$

where  $\gamma$  is the power splitting ratio between the two orthogonal components, and  $T$  is the full width of the half maximum of the optical pulse. Equation 2.25 shows that the penalties have a quadratic dependence on DGD. In reality, the penalties incurred vary randomly with DGD and  $\gamma$ . It has been established that any penalty over 1dB is unsuitable [1, 15]. Such a condition is called an outage, an analogy to radio systems. The acceptable cumulative outage in a year due to PMD should be less than 30 minutes.

Another effect of PMD is in polarization multiplexed systems such as the polarization interleaved WDM systems. Here the adjacent channels are launched on orthogonal polarization modes to suppress nonlinear effects such as cross phase modulation and four wave mixing. PMD destroys the orthogonality of the polarization states, leading to power leakage between the adjacent channels, thereby inducing coherent cross talk at the receiver end [12, 22].

# Chapter 3

## PMD Measurement Techniques

PMD places limitations on the transmission bandwidth of an optical communication system particularly on very high bit rates. Thus, it becomes very important to measure PMD to characterize a fiber optic link and to design the system in such a way that the effects of PMD in the system are mitigated. Techniques for measuring PMD has been well researched over the last two decades. These techniques measure  $\Delta\tau$ , the time delay differential between the PSPs of the fiber. Traditional PMD measurement techniques focused on measuring PMD on a single mode fiber in the short length regime [8, 19]. With time, however, the need to measure PMD on fibers in the long length regime gained significance, as this is the regime under which modern telecommunication fibers fall. In the long length regime, the PMD behavior is random. Many measurement techniques measure the average or the root-mean-square DGD in a fiber [27]. For a given fiber, the average values can be obtained by either varying the optical wavelength or by measuring DGD over varying external factors such as ambient temperature.

In general, the techniques can be classified based on the behaviour of PMD used. The two main categories of PMD measurement techniques are, time-domain

and frequency domain [13]. The time domain techniques sense pulse delays between the PSPs, while the frequency domain methods detect changes in SOPs with change in optical frequency.

### 3.1 Time-domain measurement techniques

#### 3.1.1 Pulse delay technique

The pulse delay technique is conceptually the simplest method to measure PMD. This technique involves launching short pulses into the fiber, varying the input polarization state to measure the maximum differential time of flight between output PSPs. The differential time is measured using an oscilloscope synchronized with the input pulses by the same clock source as shown in figure 3.1.

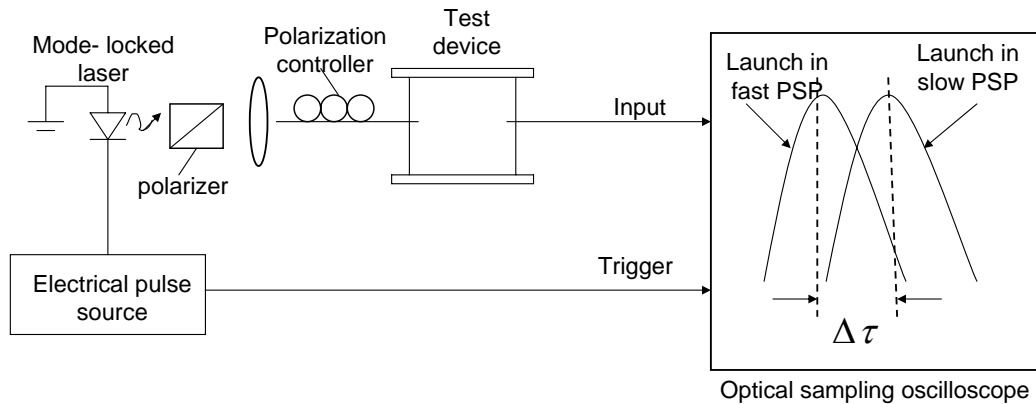


**Figure 3.1.** The pulse delay technique for measuring DGD [19]

The duration of pulses places a limit on sensitivity of PMD measurement, i.e., pulses with extremely short duration are required for measuring low DGD. In general, this method provides best results for measuring high DGD [8]. A disadvantage is the need to sweep through input polarization states to find the

two input PSPs. Hence, the pulse delay method is best suited for measuring instantaneous DGD at a specific wavelength and not for measuring the average DGD.

### 3.1.2 The interferometric method

The interferometric method is based on the basic Michelson interferometer and is applicable to optical components with uniform birefringence or well-defined Eigen modes as well as fibers with random PMD in the long length regime. The principle behind this technique is based on measuring the mutual coherence of the electric fields of two signal generated from a wideband source [8]. This method, like the pulse delay method, directly measures the time delay of the two signals.

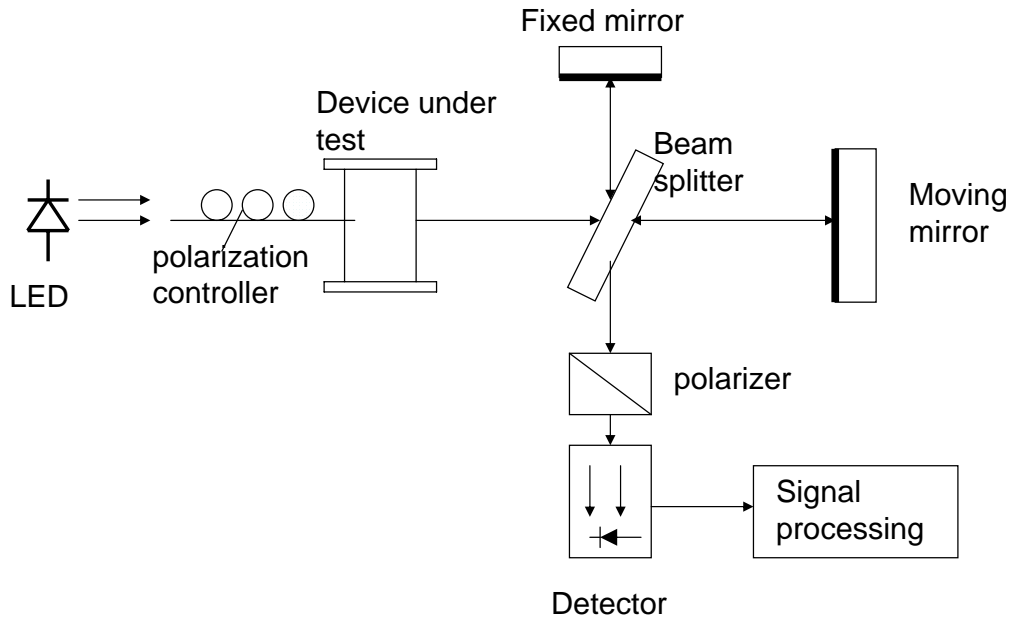


**Figure 3.2.** The interferometric technique for measuring DGD [8]

Light from the LED source is coupled into the arms of the interferometer and at the detector, light from the fixed and moving mirrors are superimposed. When



the length of the arms is less than the coherence length of the source, interference occurs. The width of the response is inversely proportional to the spectral width of the source. If  $\Delta x$  is the distance of the mirror from the point where the interferometric paths are of equal length, then the time delay  $\Delta t$  of the two pulses is given by,  $\Delta t = 2\Delta x/c$ . An experimental setup for the interferometric method to measure DGD is shown in figure 3.2. Two polarizers, one at the source and the other at the photodetector (called the analyzer), are required. The arms of the interferometer are orthogonally polarized with respect to one another. The analyzer only allows the interference caused by the coupling of two output Eigen modes of the test device onto the photodetector [8]. The two Eigen modes share a common polarization. In the case of devices with uniform birefringence with no mode coupling, the central peak occurs when the path lengths of the interferometric arms are of equal length. The outlying peaks occur when the mirrors introduce a delay equal to the DGD of the device under test. The two outlying peaks correspond to the interference between slow (fast) mode light in the fixed mirror path and the delayed fast (slow) mode of the moving mirror.

For fibers with mode coupling, and DGD greater than the coherent time of the source, the fringe pattern becomes complex, with the photocurrent envelope taking a Gaussian form with a width that is determined by the DGD of the device under test. The DGD in this case can be determined either by Gaussian fitting or by computation of the second order moment [8]. It has been proved that, in the case of an ideal set, the mean DGD is related to the Gaussian fit as

$$\langle \Delta\tau \rangle = \sqrt{\frac{2}{\pi}}\sigma. \quad (3.1)$$

Although the interferometric method applies both to fibers in the short and

long length regimes, it can only measure PMD for wideband devices. As such, a drawback of the method is that it cannot be used to measure PMD in narrow band WDM optical components.

### 3.1.3 The modulation phase-shift method

The experimental setup is shown in figure 3.3

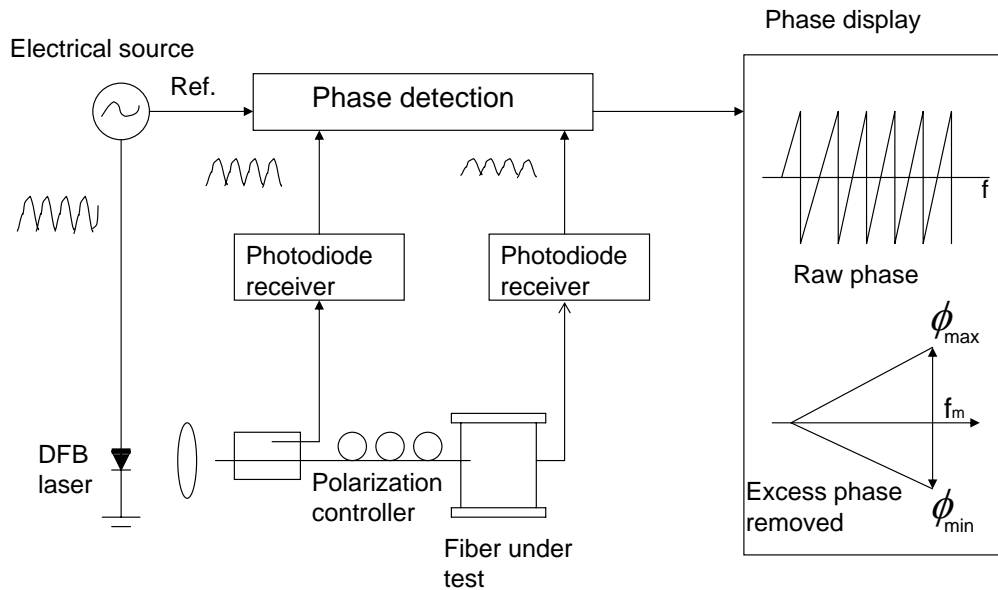


**Figure 3.3.** The modulation phase-shift method [8]

As the name suggests, the modulation phase-shift method measures DGD by measuring the difference in modulation phase between the PSPs. An intensity modulated light wave is launched into the fiber. The modulation phase of the output signal in the detector is measured with respect to an electrical source using a network analyzer that provides the source, phase detection and normalization capabilities. Then, the input polarization of the lightwave is varied to detect the minimum and maximum excursions of phase at which the polarization is aligned

with the input PSPs of the device under test. The DGD of the device under test at a given modulation frequency can be computed as

$$\Delta\tau = \frac{\phi_{max} - \phi_{min}}{360 \times f_m}. \quad (3.2)$$

Like the pulse delay method, the modulation phase-shift method requires the user to experimentally determine the PSPs of the fiber by varying the input SOP. This method requires a stable operating temperature and thus, is unsuitable for field measurements of PMD in fiber optic links.

## 3.2 Frequency domain techniques

### 3.2.1 The Fixed Analyzer method

In the Fixed Analyzer method, the mean DGD is calculated statistically from the number of peaks and valleys of the output optical power as the wavelength is scanned. For this reason, this method is also called the wavelength-scanning method. The experimental set up for this method for narrowband as well as broadband devices is shown in figure 3.4.

In the case of uniform birefringence, the output SOPs of the device under test trace out a circle as we sweep through the wavelengths. The size of the circle depends on the ratio of power in the PSPs. At the PSPs, the diameter of the circle is zero. In other words, at the PSPs the output SOPs do not change with the wavelength. For long fibers with random mode coupling, the path described by the output SOPs on the Poincare Sphere is no longer a circle; but at a specific wavelength, a pair of PSPs exists about which the output SOPs will rotate over

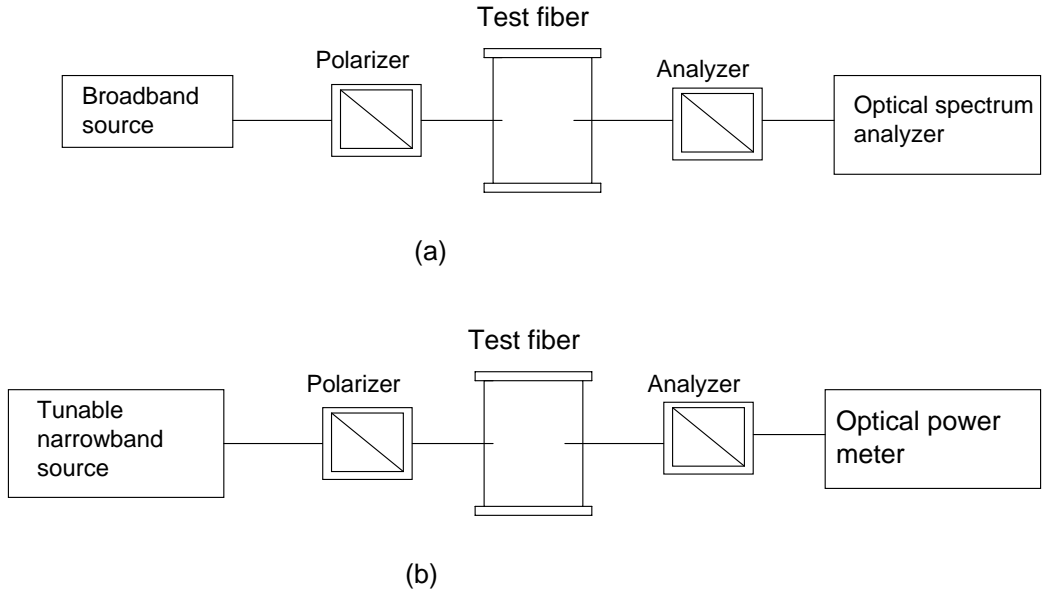


**Figure 3.4.** The Fixed Analyzer technique using (a) a broadband source and (b) a narrowband laser [8]

a small wavelength range. As seen earlier, the DGD can be calculated as

$$\Delta\tau = \frac{\Delta\theta}{\Delta\omega}. \quad (3.3)$$

Thus, the fixed analyzer is based on the same principle as the Poincare arc method. The rate of rotation of the output Stokes vector in this case is calculated by the rapid change in peaks and valleys in the transmission through the polarizer. The mean DGD can be calculated using several methods. One such method is called extrema counting. In this method, the DGD can be found using the relation

$$\langle \Delta\tau \rangle_\lambda = \frac{kN_e\lambda_{start}\lambda_{stop}}{2(\lambda_{stop} - \lambda_{start})c}, \quad (3.4)$$

where  $c$  is the speed of light,  $\lambda_{start}$  and  $\lambda_{stop}$  are start and stop wavelengths of the scan in meters,  $N_e$  is the number of peaks and valleys across the scan. The

dependence of PSPs on wavelength is accounted for by the constant  $k$ . The value of  $k$  has been experimentally determined to be 0.824 for fibers with random mode coupling and unity for devices and short fibers with no mode coupling.

As seen from the equation, mean DGD of a fiber is determined over a range of wavelengths and as such this method cannot measure the instantaneous DGD. However, this method is simple and mean DGD can be found by an uncomplicated data analysis. When a broadband source is used, transmitter and receiver can operate independently for measuring DGD and hence, this method can be used for field measurements of DGD.

### **3.2.2 The Poincare Arc method**

As for the Fixed Analyzer method, DGD is computed from the equation (3.3). The traces for the output SOP are generated by light from a narrowband optical source into each of the input PSPs of the device under test. Then, wavelength is incremented, resulting in an arc on the Poincare Sphere perpendicular to the principal axis of the device. As in the Fixed Analyzer method, the Poincare Arc method is applicable to devices with simple birefringence as well as to long fibers. Since the PSPs are wavelength dependent, the launch polarization should be varied so that a reasonable ratio of power is maintained in the PSPs of the device.

### **3.2.3 The Jones-Matrix Eigenanalysis (JME) method**

The JME method directly measures the DGD between the PSPs as a function of wavelength and is based on the transmission matrix of the device under test. It is applicable to measurement of linear time invariant (LTI) devices. In other

words, the polarization transformation of the device should be constant over the time of measurement. As seen in section 2.3, the Jones vector completely describes the amplitude and polarization of a signal. The transmission characteristics of the device are described by a two-by-two Jones matrix [14]. The JME requires that three known polarization states be applied to the device under test. Usually, these are the three linear polarization states oriented at 0, 45 and 90 degrees. The transmission matrix can then be computed from the relationship of measured output states to the known input states. The derived Jones matrix then describes the polarization transformation characteristic of the device under test.

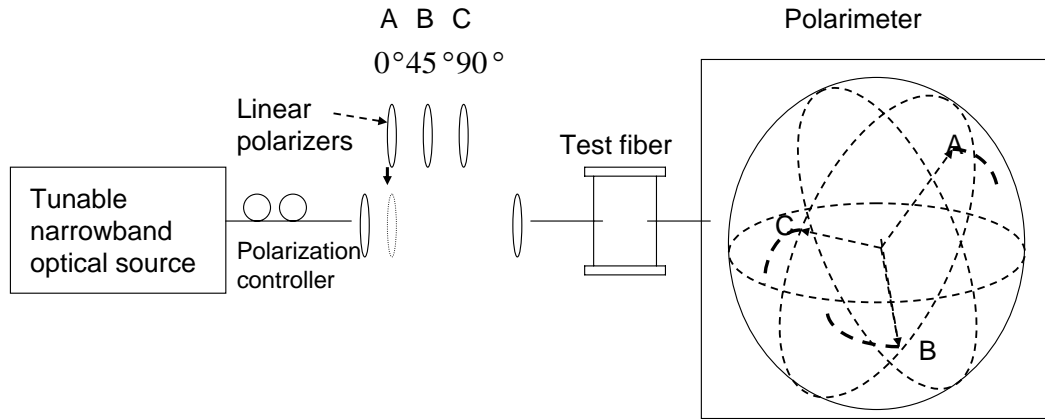


**Figure 3.5.** The Jones-Matrix Eigenanalysis technique [8]

The experimental setup for the JME is shown in figure 3.5. The setup consists of a tunable narrowband optical source, a switchable polarizer for generating the linear polarization states, the device under test and a fast polarimeter. A computer is used to process the measured data and compute the DGD. The source is adjusted to be circularly polarized to allow transmission through each polarizer. Then, for a series of wavelengths, the Jones matrix of the path between polariz-

ers and polarimeter is calculated [8, 19]. The DGD at a given wavelength,  $\lambda_i$  is calculated using the following expression

$$\Delta\tau = \left\| \frac{\text{Arg} \left( \frac{\rho_1}{\rho_2} \right)}{\Delta\omega} \right\|, \quad (3.5)$$

where  $\rho_1$  and  $\rho_2$  are the Eigenvalues of the expression involving the Jones matrix, T. The JME can be easily automated to measure DGD over a range of wavelengths. The JME also requires a feedback loop to coordinate the transmitter and the receiver. Also, the accuracy of the JME is dependent on test path stability, polarimeter accuracy and stray birefringences in the test path.

### 3.3 Summary of PMD measurement techniques

A short summary of PMD measurement techniques and their characteristics is given in figure 3.6. For devices with simple birefringence and no mode coupling, the measurement techniques discussed in this chapter agree with each other very closely. But for fiber in long length regime, the error is about 20 percent for these techniques. This is due to a number of reasons. First and foremost, PMD in long fibers is random and is subjected to variation in temperature and mechanical stresses. As such using long fibers to compare the performance of different measurement techniques is not ideal. Another reason is the orientation of polarization of the source and output lightwave with respect to the PSPs of the fiber. For instance, in the fixed analyzer method, adjusting the fiber pigtailed of the test fiber can transform the orientation of polarizations and cause a change in number of peaks and valleys [11]. Thirdly, the measurement techniques vary in their design and algorithms used for computing the DGD. Also, the wavelength range of these

measurements is limited by the bandwidth of the optical instrumentation used in the test setup. Finally, the strong wavelength dependence of the PSPs is another factor for disagreement between the measurement techniques.



Measurement method	Pulse delay	The interferometer method	Modulation phase shift method	Poincare arc method	Fixed analyzer method	JME
DGD is determined from...	Sampling oscilloscope that determines the time difference in flight between pulses in the two PSPs	An interferogram obtained by placing the test device in low coherence interferometer	The pulse change of an intensity modulation enveloped between the two PSPs	The rate of rotation of output SOP about the PSP axis	Random evolution of output SOP as the wave-length is scanned	The changes in Jones matrix across wave-length intervals.
Domain (Time or frequency)	Time	Time	Time	Frequency	Frequency	Frequency
Source	Chirp free laser	Broadband	Chirp free laser	Tunable	Broadband or tunable laser	Tunable
Measures(mean/instantaneous DGD)	instantaneous	Mean	Both	Both	Mean	Both
Measures higher order PMD?	No	No	No	Yes	No	Yes
Measurement range(ps)	~10->100	~0.002-100	~25->1000	~0.002->1000	~0.1-100	~0.002->1000
Sensitive to launch SOP?	Yes	Yes	Yes	Yes	No	No
Sensitive to fiber motion	Yes	No	Yes	Yes	Yes	Yes
Measurement accuracy(ps)	>~20	>~0.003		>~0.05	>~0.05	>~0.025

Figure 3.6. Summary of PMD measurement techniques [8, 19].

# Chapter 4

## In situ PMD monitoring

### 4.1 Need for in-situ PMD measurement techniques

Traditional PMD measurements discussed in chapter 3 require access to both ends of the fiber. In a long haul fiber optic link, the transmitter and receiver are located far away from each other and are not accessible at the same time. Moreover, the links carry traffic all the time which means using the traditional measurement techniques to measure PMD would require disrupting the data traffic carried by these fibers. As a result, there arises a need for developing a measurement technique that does not block the traffic carried by the links and has no need for accessing both ends of the fiber. An in-situ measurement technique is necessary for conducting PMD measurements on traffic carrying signals so that PMD in fiber optic links can be characterized. Several techniques were proposed for in - situ measurement of PMD using the traffic carrying signal as the probing signal [5,6].A nonintrusive technique using a heterodyne polarimeter with an RF spectrum analyzer was used to estimate the PMD-induced system penalty by measuring the 'string' length of the state of polarization [4]. A similar method

was also proposed for greater measurement speed [26]. The method uses direct detection with a high resolution optical spectrum analyzer consisting of an In-GaAs line-scan camera and a virtually imaged phase array was also proposed for greater measurement speed. Researchers also proposed a novel method for measuring PMD using four wave mixing where the possibility of in-situ measurement of PMD was discussed [25]. In this chapter, a nonblocking and nondestructive PMD monitoring technique developed by the light wave laboratory at the University of Kansas is discussed. This is followed by a detailed discussion of PMD measurement algorithms, namely, polarization scrambling and polarization tracking. The implementation of these two algorithms is also discussed here and a comparison of their performances is discussed in chapter 5.

## **4.2 The coherent PMD monitor**

### **4.2.1 Block diagram of the coherent heterodyne detector**

The block diagram in figure 4.1 shows a coherent heterodyne detection used for PMD monitoring. In this setup, a small portion of the optical signal is tapped from the transmission fiber optic link in a WDM system. A tunable laser, which chooses a channel on the International Telecommunication Union (ITU) grid acts a local oscillator. A polarization scrambler is used to randomly scramble the output polarization of the local oscillator. The two optical signals are combined using a 3 dB coupler and the output is incident on a wideband photodiode. The beating of the signals at the diode converts the optical domain signal to its equivalent RF spectrum. The detected spectrum is amplified before two RF bandpass filters of bandwidth 1 GHz and center frequencies at 15 and 25 GHz are used to select two different frequency components from the signal spectrum. An RF envelope

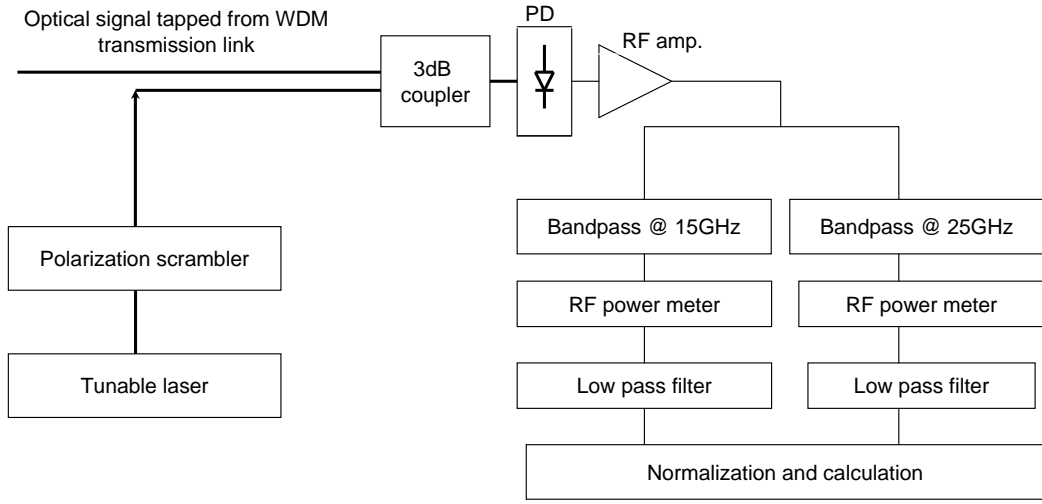


**Figure 4.1.** A coherent heterodyne detection setup for PMD monitoring

detector is used to measure the RF power variation at the output of each bandpass filter. The RF detectors' output is then recorded using AD converters. It has been shown that the first order DGD of the optical signal can be measured from the differential polarization walk off between the two frequency components [10, 16]. This implies that the corresponding angular walk off can be measured and that the DGD value can be calculated. Figure 4.2 illustrates a Poincare arc described by the optical signal when its state of polarization changes from point A to point B, where the points represent the polarization of the frequency components selected by the banpass filters.

#### 4.2.2 The theory of PMD measurement

The photocurrent of the photodiode,  $i$  due to the interference term of the coherent heterodyne detection, is given by

$$i = 2\eta_D \sqrt{TP_S P_L} \cos \frac{\phi}{2} \cos(\omega_{IF}t + \theta), \quad (4.1)$$

where the proportionality constant,  $\eta_D$  includes the effects of the responsivity of the photodiode and the coupling coefficient of optical 3 dB coupler.  $P_L$  and  $P_S$  are the optical power of the Local Oscillator (LO) and the transmission signal.  $\phi$  is the angle between the SOP of the local oscillator and the optical signal in the Poincare Sphere,  $T$  is the transmission coefficient of the fiber optic link and  $\theta$  is the phase difference between transmission signal and the LO.

Then, the RF power at the photodiode is given by

$$P_{in} = i^2 R = 4\eta^2 R T P_L P_S \cos^2 \frac{\phi}{2} = k_p T \cos^2 \frac{\phi}{2}, \quad (4.2)$$

where  $R$  is the load resistance and  $k_p = 4\eta^2 R P_L P_S$ . After RF signal processing, output voltage at the RF detector is proportional to RF power at the input of the RF amplifier.

$$V = k_v P_{in} = k T \cos^2 \frac{\phi}{2}, \quad (4.3)$$

where  $k_v$  includes the effects of the bandwidth of the RF bandpass filters, the RF amplifier and the efficiency of the RF detector. It can be shown that output voltage at point A is

$$V_A = k T \cos^2 \frac{\phi_A}{2} \quad (4.4)$$

and output at point B can be written as

$$V_B = k T \cos^2 \frac{\phi_A + \Delta\alpha}{2}, \quad (4.5)$$

where  $\phi_B = \phi_A + \Delta\alpha$ . Here  $\Delta\alpha$  is the angular polarization walk off between the two frequency selected components as shown in figure 4.2.

Now, if we were to let the SOP of the optical signal at point A be aligned with

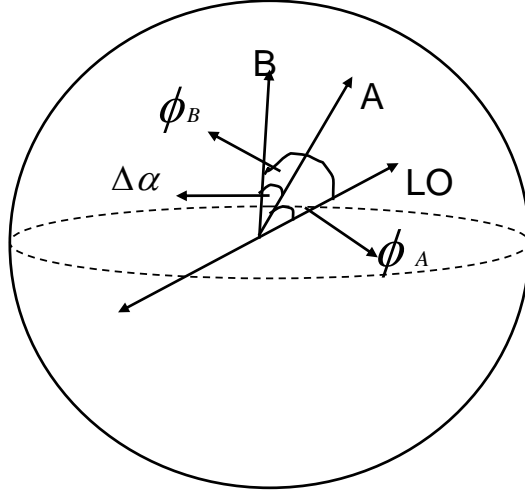


**Figure 4.2.** An illustration of polarization walk off between the two frequency selected components  $f_1$ , point A and  $f_2$ , point B

the SOP of the LO, i.e.,  $\phi = 0$ , then the output voltage from point A is

$$V_A = kT, \quad (4.6)$$

and the output voltage from point B is given as

$$V_B = kT \cos^2(\Delta\alpha/2). \quad (4.7)$$

Thus, the angular walk off between points A and B on the Poincare Sphere can be extracted from equations 4.6 and 4.7. The true DGD of the transmitted signal is represented by the equation

$$\Delta\tau_{true} = \frac{\Delta\theta}{\Delta\omega}, \quad (4.8)$$

where  $\Delta\theta$  is the separation between the azimuth angles of points A and B with

the PMD vector  $\vec{\Omega}$  as shown in figure 4.3. The SOP of the input signal is not adjustable and hence, it is not feasible to measure the true DGD. However, as illustrated above, the differential walk off  $\Delta\alpha$  between the frequency selected components can be measured and the DGD as seen by the probing signal is given by

$$\Delta\tau_{\text{apparent}} = \frac{\Delta\alpha}{\Delta\omega}. \quad (4.9)$$

To correctly interpret the results of the PMD monitoring equipment, an understanding of the relationship between  $\Delta\alpha$  and  $\Delta\theta$  is essential. From figure 4.3,  $\Delta\alpha$

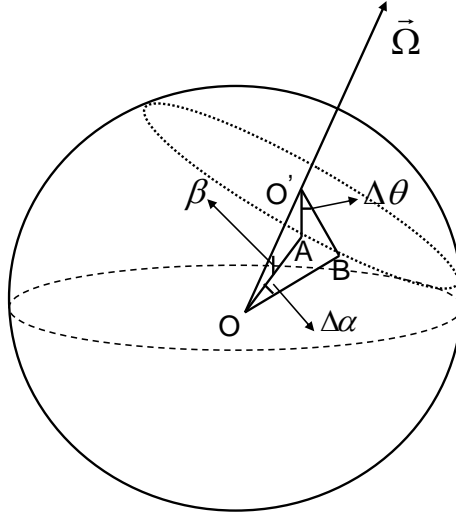


**Figure 4.3.** An illustration of polarization states of frequency components and their relative orientations with the PMD vector of a long fiber

and  $\Delta\theta$  are related as

$$\sin\left(\frac{\Delta\alpha}{2}\right) = \sin\left(\frac{\Delta\theta}{2}\right) \sin\beta, \quad (4.10)$$

where  $\beta$  is the angle between point A and PMD vector,  $\vec{\Omega}$ .  $\Delta\theta$  can be made small by choosing the appropriate frequency difference  $\Delta\omega$ . As a result, the

equation 4.10 simplifies to

$$\Delta\alpha = \Delta\theta \sin\beta. \quad (4.11)$$

Using the principal states model discussed in section 2.9, a fiber in the long - length regime can be regarded as a waveplate with time retardation equal to the DGD of the fiber whose principle axis is aligned with the slow axis of the PMD vector. Thus  $\beta$  can be equivalently viewed as the angle between the input polarization state of the signal  $\vec{S}_{in}$  and the PMD vector of the fiber,  $\vec{\Omega}$ . Hence,  $\beta$  can be expressed as

$$\cos\beta = \frac{\vec{\Omega} \cdot \vec{S}_{in}}{\|\vec{\Omega}\| \|\vec{S}_{in}\|}. \quad (4.12)$$

The PMD vector,  $\vec{\Omega}$ , can be represented in the cartesian coordinate system by decomposing it into its three orthogonal components as,  $\vec{\Omega} = \vec{a}_x\Omega_1 + \vec{a}_y\Omega_2 + \vec{a}_z\Omega_3$ , where  $\vec{a}_x$ ,  $\vec{a}_y$  and  $\vec{a}_z$  are unit vectors and  $\|\vec{\Omega}\| = \sqrt{\Omega_1^2 + \Omega_2^2 + \Omega_3^2}$ . As discussed earlier in section 2.12, when each orthogonal component follows an independent Gaussian distribution with zero mean and the same variance  $q^2$ , the statistics of the PMD vector follows a Maxwellian distribution [2] represented as,

$$p_3(x) = \sqrt{\frac{2}{\pi}} \frac{x^2}{q^3} e^{-\frac{x^2}{2q^2}}, \quad (4.13)$$

where the mean of the Maxwellian p.d.f described can be given as [3],

$$\mu_3 = E(x) = q\sqrt{\frac{8}{\pi}}. \quad (4.14)$$

The SOP of the input optical signal is determined by the laser in the transmitter of the fiber optic link. As a result, the SOP of the probing signal used for the coherent PMD monitor is stable. In other words, we can conceptually assume



that  $\vec{S}_{in}$  is aligned with one of the three orthogonal components, for instance,  $\Omega_1$  of the PMD vector, i.e.,

$$\vec{S}_{in} = (1, 0, 0). \quad (4.15)$$

Substituting equation 4.15 into 4.12 we get

$$\Omega_1 = \|\vec{\Omega}\| \cos \beta. \quad (4.16)$$

Combining equations 4.16 and 4.11 yields,

$$\Delta\alpha = \Delta\theta \frac{\sqrt{\Omega_2^2 + \Omega_3^2}}{\|\Omega\|}, \quad (4.17)$$

which results in

$$\tau_{apparent} = \frac{\Delta\alpha}{\Delta\omega} = \sqrt{\Omega_2^2 + \Omega_3^2}. \quad (4.18)$$

It should be noted that equation 4.18 describes the apparent PMD as measured by the probing signal. The apparent PMD is related to only two of the three independent orthogonal components, while it has been shown here and by previous works that the true PMD of the fiber is related to all three independent components of the PMD vector. Therefore, the true PMD follows a Maxwellian distribution or a Chi distribution with three degrees of freedom. Hence, we can conclude that the statistics of the apparent PMD measured by the probing signal in our work should follow the Chi distribution with two degrees of freedom otherwise called the Rayleigh distribution. The p.d.f of the Rayleigh distribution can be given as

$$p_2(x) = \sqrt{\frac{2}{\pi}} \frac{x}{q^2} e^{-\frac{x^2}{2q^2}}, \quad (4.19)$$

whose mean value is given by

$$\mu_2 = E(x) = q\sqrt{\frac{\pi}{2}}. \quad (4.20)$$

The relationship between the mean value of the true and apparent DGD can now be expressed by the relationship between  $\mu_2$  and  $\mu_3$  as

$$\mu_3 = 4\mu_2/\pi. \quad (4.21)$$

Equation 4.21 implies that the true DGD is always greater than the DGD measured by the probing signal.

### 4.3 Polarization Scrambling

The techniques that are presented in this report differ in the algorithm that is used to maximize the output power of one of the frequency selected components. Briefly, the idea behind scrambling is that the SOP of the LO is scrambled in such a way that all the possible states of polarization of the LO are covered at least once in every measurement period as shown in the figure 4.20. As described in section 4.2.2, the maximum value of the frequency component  $f_1$  occurs when its SOP is aligned with the SOP of the local oscillator. The relative output power of the other component gives a measure of DGD of the probing signal. When the

output power of channel A is maximum, we have

$$\begin{aligned}
 V_A &= kT \\
 V_B &= kT \cos^2(\Delta\alpha) \\
 \Delta\alpha &= \arccos \sqrt{\frac{V_B}{V_A}}.
 \end{aligned} \tag{4.22}$$

Now the DGD measured by the probing signal can be given as

$$DGD = \frac{\Delta\alpha}{\Delta\omega}, \tag{4.23}$$

where  $\Delta\omega = 2\pi\Delta f$  and  $\Delta f$  is the frequency of separation between the two frequency components. In our experiment,  $\Delta f$  is 10 GHz. Polarization scrambling is the simplest algorithm used for the purpose of maximising the output power of one of the two frequency selected components. The output data for a measurement period is processed to obtain the maximum voltage of each component and the relative voltage of the other component at that instant. Once these voltage levels have been attained, the DGD can be calculated by the following equations,

$$\begin{aligned}
 \beta_1 &= \frac{V_2 - V_{min2}}{V_{max1} - V_{min1}} \\
 \beta_2 &= \frac{V_1 - V_{min1}}{V_{max2} - V_{min2}} \\
 \beta &= \arccos(0.5(\sqrt{\beta_1} + \sqrt{\beta_2})) \\
 DGD &= \frac{\beta}{\pi * \Delta f}.
 \end{aligned} \tag{4.24}$$

$V_{max1}$ ,  $V_{min1}$ ,  $V_{max2}$ ,  $V_{min2}$  are the maximum and minimum voltages of frequency components where the subscript 1 represents the voltage of component  $f_1$  and the subscript 2 represents voltage values of  $f_2$ .  $V_1$  is the voltage of  $f_1$  at  $V_{max2}$  and

$V_2$  is the voltage of  $f_1$  at  $V_{max1}$ . The details of hardware used for implementation and the data acquisition algorithm used for implementing polarization scrambling is discussed in this section.

### 4.3.1 The hardware for implementing polarization scrambling

The earlier implementation for PMD monitoring using coherent detection and polarization scrambling [16] shown in figure 4.1 is bulky and tedious to set up at each test site. Therefore, the need arose for using smaller and more compact hardware for the measurement trials. Figure 4.4 shows the hardware used for field measurements of the PMD and figure 4.5 shows a picture of the equipment developed for this research. The RF signal processing hardware has already been described in the previous sections of this chapter. This section looks at the characteristics of other blocks used in the equipment.

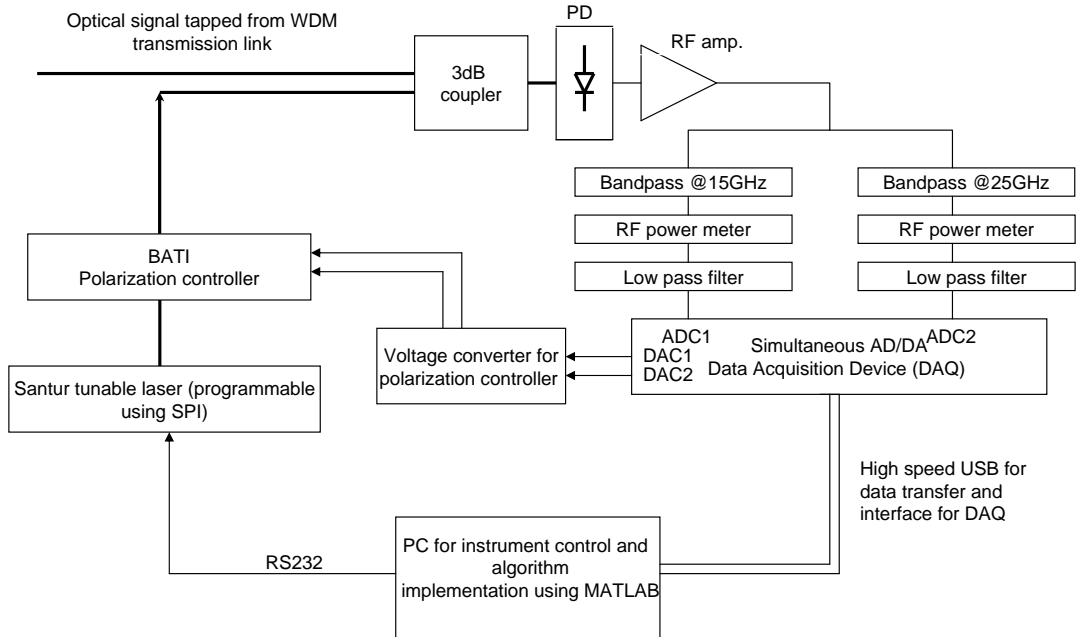


**Figure 4.4.** Hardware implementation for PMD monitoring using polarization scrambling technique

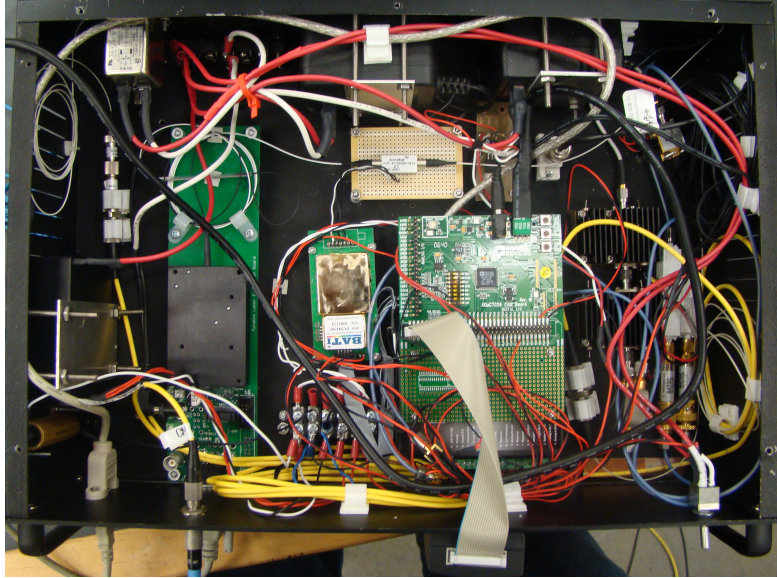


**Figure 4.5.** A picture of the hardware used for our reserach

#### **4.3.1.1 The Local Oscillator(LO)**

The Agilent 8164A tunable laser is replaced by a much smaller MEMS based tunable laser from Santur Corporation. The polarization maintaining (PM) fiber at the output of the LO means that the output SOP of the LO is stable. The LO outputs light at a constant power of 10 dBm. The tuning grid of the LO output is 25 GHz with a frequency resolution of 0.1 GHz made possible via off-grid tuning. The wavelength of the laser can be controlled via an RS232 serial port interface. A simple software such as the Hyperterminal in WindowsXP can be used to tune the wavelength of the LO with appropriate RS232 settings.

#### **4.3.1.2 The polarization controller**

The ceramic based polarization controller with two retardation plates (cells) is used for polarization control of the LO output. The important characteristics of the polarization controller are given in table 4.1. By applying a high voltage

Attributes	Performance
Insertion Loss	0.6 dB
Polarization dependent loss	0.1 dB
Polarization mode dispersion	0.01 ps
Input power	2.7 W
Speed	30 $\mu s$
Power consumption	600 mW
Dimensions	22.3*11*7.8 mm
Input voltage range for driver	1 to 4 V
Output voltage range of driver	0 to 383 V
Supply current	0.7 A
Supply voltage	5 V

**Table 4.1.** Characteristics of polarization controller

(in the range of 100 to 300 volts) to either of the cells, the SOP at the input of the polarization controller can be transformed to any SOP at the output of the controller. The input PM fiber pigtail of the polarization controller is aligned at 45 deg to the first cell, while the second cell is aligned at 45 deg with respect to the first cell as shown in figure 4.6.

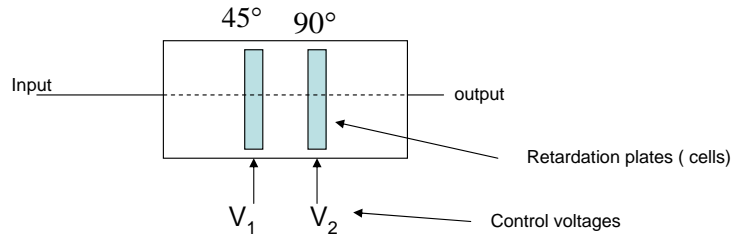


**Figure 4.6.** The BATI polarization controller

Thus the SOP transformation of the first cell is orthogonal to the transformation of the second cell as shown in figure 4.7. This is due to the equal splitting of energy between the two PSPs of the fiber which results in a circular polarization at the input of the first cell. Similarly, varying the electric voltage applied to the second cell, takes the SOP of the LO through the linear polarization states in the

Poincare Sphere. Thus by a combination of applied voltages to the polarization

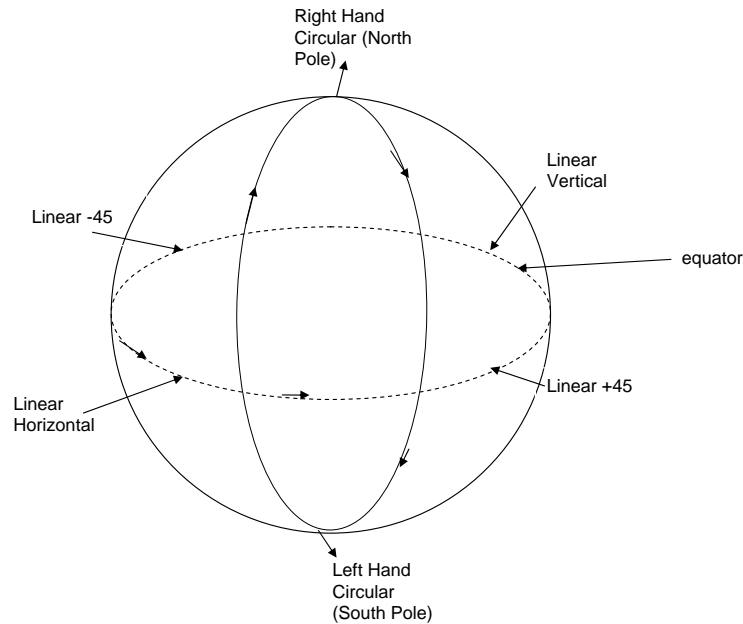


**Figure 4.7.** Polarization control of the SOP of the local oscillator using two retardation plates

controller’s control inputs, the input SOP of the LO can be transformed to any polarization state at the output of the polarization controller. It is important to note that the angular separation on the Poincare Sphere is twice that of the actual separation between the two frequency selected components. For instance, the right hand circular and left hand circular polarizations that are 90 deg apart are located at the north and south poles of the Poincare Sphere which are 180 deg apart.

#### 4.3.1.3 The Driver circuitry for the polarization controller

The driver circuitry for the polarization controller is an voltage transformer circuit that transforms a low DC voltage in the range of 1 – 4 V to a high voltage in the range of 82 – 380 V. The low voltage input is supplied to the polarization

control driver by a DAC. The DAC input voltage that is required to transform the input SOP of the LO by 180 degrees or equivalently 360 degrees in the Poincare sphere is termed  $V_\pi$ . Varying the input voltage to the driver from 1V to 4V transforms the SOP of the LO by  $4\pi$  on the Poincare sphere. It should be noted that the transformation function from low to high voltage of the driver is quadratic. Thus, for the purpose of polarization scrambling, a fairly linear portion of the function that corresponds to the input voltage range of 2.2 V to 3.35 V is used. This voltage range corresponds to more than  $2\pi$  radians on the Poincare Sphere. The additional voltage is used to allow for a weak dependence of  $V_{pi}$  on the temperature. Refer table 4.2 for characteristics.

Attributes	Performance
Input voltage range for driver	1 to 4 V
Output voltage range of driver	0 to 383 V
Supply current	0.7 A
Supply voltage	5 V
No of inputs and outputs	4
Repetition rate	1 KHz
Speed	30 $\mu s$

**Table 4.2.** Characteristics of polarization controller driver.

#### 4.3.1.4 The Data Acquisition Device (DAQ)

The input voltage for the driver circuitry is supplied from a high speed DAQ with simultaneous DA converters. The DAQ also has two AD converters to sample and digitize the output of the RF power meters for normalization and calculation. The DAQ can be programmed using the data acquisition tool box provided by Matlab. The DA converter output rate is set at 10 KHz. The AD converter sample rate is set at 20KHz. The input range of the AD converter is from -10 V to +10 V. A triangular waveform is generated on two DA output channels. The



number of sample points per period of the DA waveform is determined by the resolution required for the polarization scrambling. For instance, if a precision of 1 deg per point is required on the Poincare sphere, then a triangular waveform with 360 equally spaced values from 2.2 to 2.35 V is generated for one half of the time period is used. For the other half of the time period, another 360 values equally spaced between 3.35 to 2.2V are generated. One of the vital characteristic required for AD converter of the DAQ is the simultaneous sampling of the two channels which ensures that any sample pair acquired by the DAQ occur at the same instant in time. This is made possible by a dedicated clock source for each of the AD converter channels. Characteristics of the DAQ are given in table 4.3

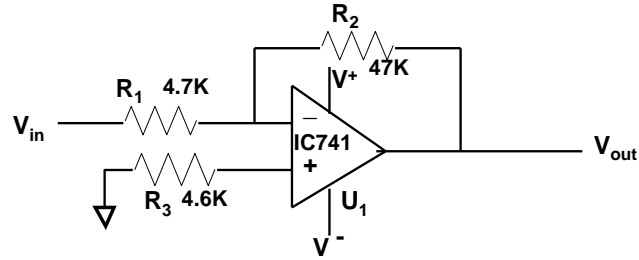
Attributes	Performance
AD sampling Rate	20 KHz
No. of AD channels	2
Resolution	12 bits
AD input voltage range	-10 to +10 V
DA waveform frequency	10 KHz
No. of DA channels	4
Resolution	12 bits
DA output voltage range	2.2 to 3.37 V
Simultaneous AD and DA	Yes
Trigger	Software trigger

**Table 4.3.** Characteristics of DT9832 DAQ

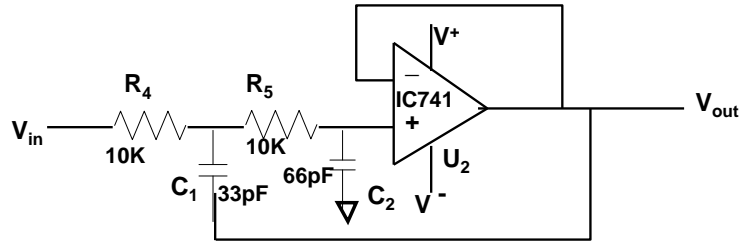
#### 4.3.1.5 Low pass filter-amplifier

The filtering operation after the RF power meter is carried out by a two pole sallen key low pass filter as shown in figure 4.8. Also the signal level is boosted using two stages of a simple amplifier circuit using an IC741 operational amplifier. The first stage used before the filter is an inverting amplifier because the voltage output at the RF power meter is negative. The second stage is used so that a

considerable portion of the AD converter input voltage range is occupied, resulting in better resolution. The amplifier and filter operations on the two channels are identical as a photodiode, whose response at 15 GHz and 25 GHz is fairly similar, is used. In the circuit the values are chosen such that,  $R_1 = R_2 = mR$ ,  $C_1 = nC$



(a) Non Inverting amplifier section



(b) Sallen-Key Low pass filter section

**Figure 4.8.** Amplifier and filter circuits used for reducing the effects of noise

and  $C_2 = C$  where  $R = 100$  Kohm and  $C = 66$  pF and  $m$  and  $n$  are integers multiplication factors that determine the Q factor given in equation 4.26. Also, choosing  $R_1 = 100$  Kohm,  $R_2 = 100$  Kohm,  $C_1 = 132$  pF and  $C_2 = 66$  pF implies that  $m = 1$  and  $n = 2$ . The cut-off frequency of the low pass filter is found using the formula

$$f_c = \frac{1}{2\pi\sqrt{2}RC}, \quad (4.25)$$

where the value of  $Q$  is given by

$$Q = \frac{\sqrt{mn}}{m+1}. \quad (4.26)$$

Using the values of  $m$  and  $n$ , the low pass filter is designed to have a  $f_c$  of 15 KHz and a  $Q$  value of 0.707 for maximally flat response.

### 4.3.2 Data acquisition algorithm for polarization scrambling

The basic idea of measuring PMD by polarization scrambling is to ensure that all points in the Poincare Sphere are covered at least once during a measurement period. The measurement period can be defined as the average time required to extract one DGD value. One of the means of achieving the full coverage on the Poincare sphere is to concatenate two polarization Scramblers [16].

In our system, the polarization controller can be used to achieve the same result. The algorithm for acquiring the data after polarization scrambling is shown in figure 4.9. The total number of points covered in a measurement period is determined by the number of points generated for the DA. With a precision of 3 deg for every point, there are 120 points generated for the second cell per step increment for the first cell. The DAC waveform generated for the control voltage input of the polarization controller is shown in figure 4.10.

## 4.4 Polarization tracking

One of the disadvantages of using polarization scrambling is its low speed of measurement. Also, high memory requirements for data storage and data processing make it tedious for long time PMD monitoring in field measurements.

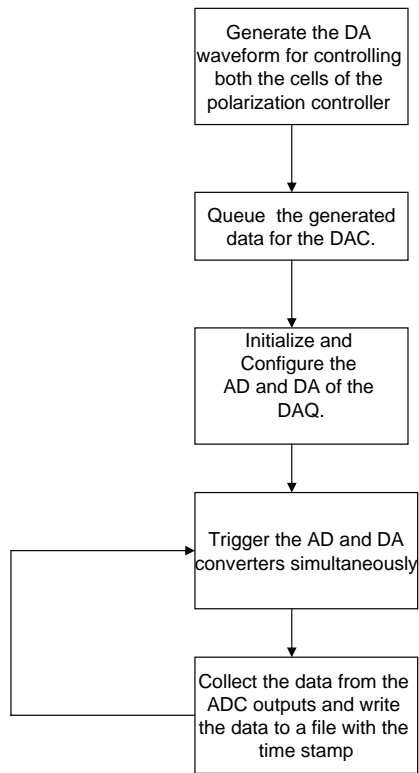


**Figure 4.9.** Data Acquisition algorithm for polarization scrambling

Additionally, using scrambling, it would require huge memory resources to calculate DGD in real time. For this reason, we have come up with a polarization tracking algorithm to monitor the DGD in a fiber optic link. The basic idea behind tracking is that each of the retardation cells of the polarization controller can be controlled such that the optimized voltage value of a frequency component can be attained. This generally involves a decision feedback loop that searches for the maximum voltage of the frequency component being monitored. In this way, polarization of the LO can be made to continuously track the changes in SOP of the incoming signal so that the frequency component is always maximized. The voltage value of the other frequency component gives a measure of DGD. In our

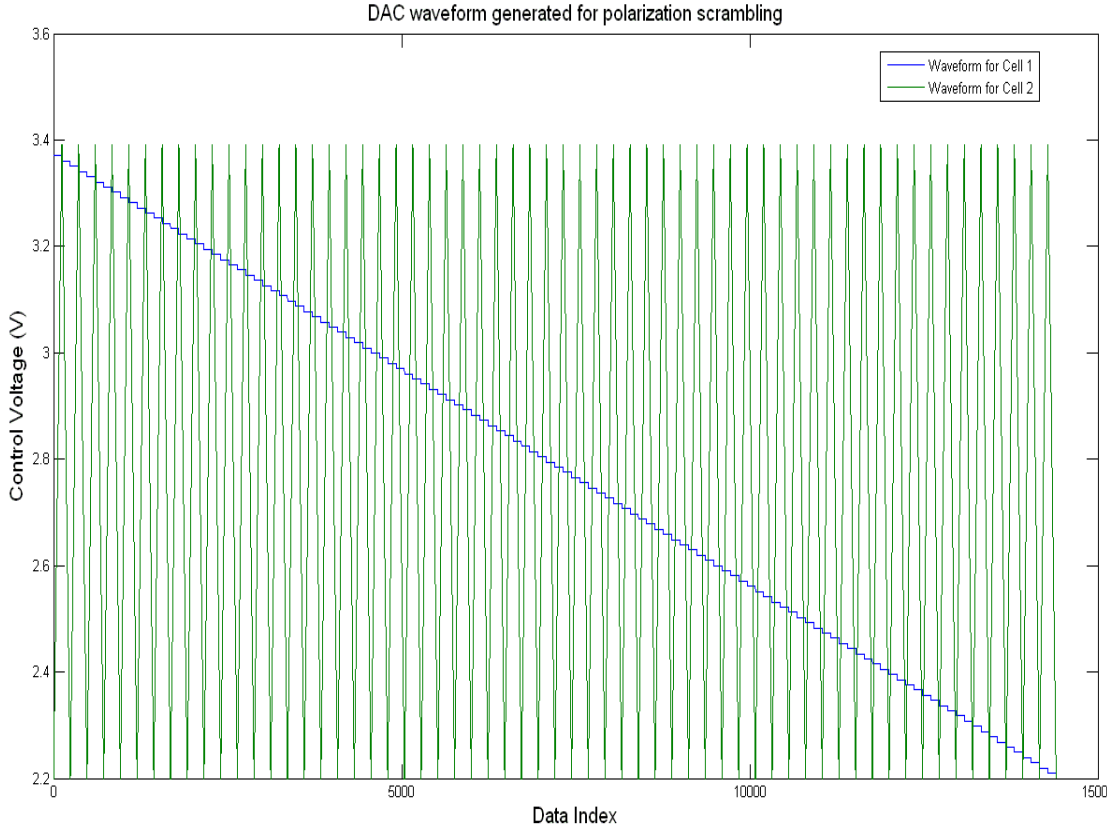


**Figure 4.10.** The DAC waveform generated for polarization controller driver

report, for validating the tracking algorithm and also to reduce the effects of noise in the system, we maximize and minimize both the components alternatively. As a result one full measurement cycle of the algorithm will consist of four voltage value pairs. After normalizing the voltage components, we can obtain four values of DGD in a tracking period. It will be asserted in the subsequent sections that the tracking period is shorter than the scrambling period for a given hardware implementation. But in our tests, for comparison purposes of scrambling and tracking algorithms, the four DGD values obtained have been averaged to have the same number of DGD samples. The search and track algorithms used for polarization tracking, along with its hardware implementation, are discussed in

this section.

#### 4.4.1 Hardware implementation for polarization tracking

The hardware setup for polarization tracking is shown in figure 4.11. The

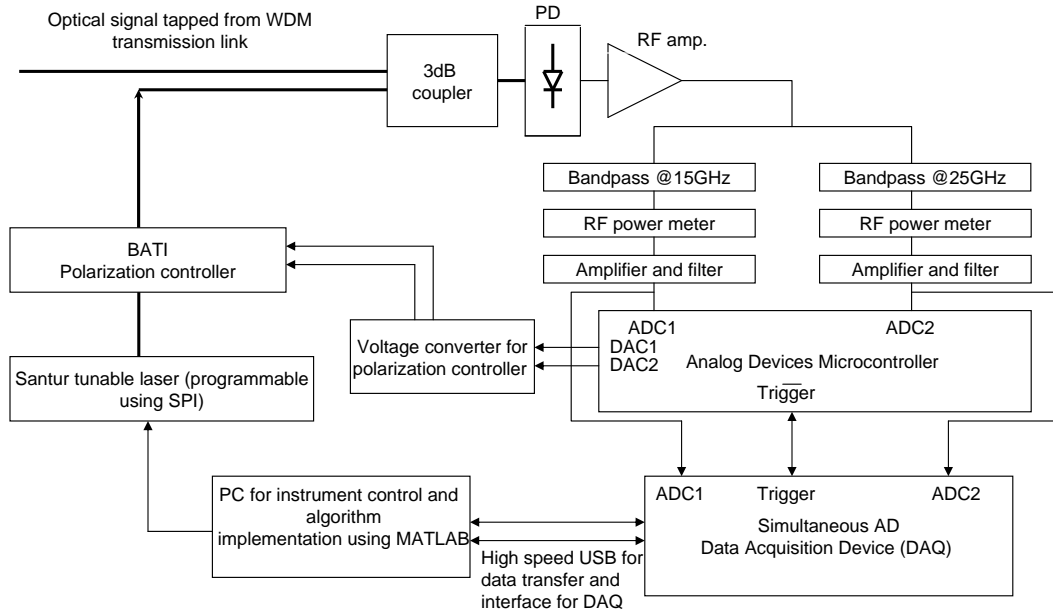


**Figure 4.11.** Hardware implementation for polarization tracking

optical and RF blocks remain the same as those used in scrambling, while the maximum search is performed using a feedback loop by a microcontroller from Analog Devices. Also, a wideband amplifier with very low input offset voltage (40 pV) is used to amplify the RF output.

##### 4.4.1.1 Microcontroller Unit

The microcontroller used for feedback is equipped with high speed AD and DA. The important characteristics that highlight its usefulness for our implementation is given in Table 4.4.

Attributes	Performance
AD sampling Rate	1 MHz
No of AD channels	12
Resolution	12 bits
Single ended mode voltage range	0 to 2.5 V
DA output settlign time	10 $\mu$ s
No of DA channels	4
Resolution	12 bits
DA voltage range	0 to 3.3 V
Clock rate	41.78 MHz

**Table 4.4.** Characteristics of ADuC7026 microcontroller

#### 4.4.2 Algorithm used for polarization tracking

Two algorithms are implemented with MCU to increase DGD measurement rate and to reduce the memory size required to store acquired data using polarization scrambling. First, a coarse search algorithm is used to find a voltage which is close to the maximum voltage. Then, a fine search algorithm with a smaller step size is used to reach the maximum voltage corresponding to the alignment of the SOP of the LO with the frequency selected component that is being tracked. Finally, a tracking algorithm is used to monitor the voltage output. If the output voltage falls below a specified threshold, then the coarse and fine search algorithms are repeated until the maximum output voltage is reached. The coarse search algorithm is implemented in the following steps.

1. Intialize the step size for coarse search and set maximum AD value to be zero. Also set corresponding DA value as zero.
2. Search the first cell for the maximum output voltage by scanning through all possible control voltage values as allowed by the step size
3. For each value of j from 2.2 to 3.35 in increments of step size, where j is the

control voltage for the cell which is being scanned

- (a) Set control voltage for cell 1, i.e., DAC equal to  $j$ .
  - (b) Read ADC input.
  - (c) If ADC value  $>$  maximum, then update the maximum = ADC value and record corresponding DA value =  $j$ .
4. Search the second cell for the maximum output voltage by repeating step 3 with the control voltage for the first cell that corresponds to the maximum output voltage.

The two dimensional fine search algorithm is different from the coarse search in that the smallest possible step size is used and a grid pattern of variable radius is used for the search. The algorithm for fine search can be described as:

1. Initialize the smallest possible step size for fine search and set maximum AD value to be the value found using coarse search. Also set corresponding DA value for the first and the second cell as those found in coarse search.
2. For each value of  $i$  from (DA value - gridlength) to (DA value + gridlength) in cell 1.
  - (a) Set DAC for cell 1 equal to  $i$ .
  - (b) Set DAC for cell 2 equal to  $j$ .
  - (c) Read ADC input.
3. For each value of  $j$  from (DA value - gridlength) to (DA value + gridlength) in cell 2.
  - (a) Set DAC for cell 1 equal to  $i$ .
  - (b) Set DAC for cell 2 equal to  $j$ .
  - (c) Read ADC input.



- (d) If  $\text{ADC value} > \text{maximum}$ , then  $\text{maximum} = \text{ADC value}$  and corresponding DA value = j.
4. Search the second cell for the maximum output voltage by repeating step 3 with the DA value for the first cell that corresponds to the maximum output voltage.

After the coarse and fine search algorithms, the output voltage is continuously monitored. When the voltage drops below a specified threshold, the fine search algorithm is repeated again with varying grid size until the maximum output voltage is found. The complete algorithm for polarization tracking is described by the flowchart in figure 4.12. It is important to note that, the magnitude of the output voltage for the two channels in most cases are not equal. As a result, a normalization procedure is required. This is done by tracking the maximum output voltage of the two channels successively. Also a minimum search can also be performed instead of the maximum search for the two cells.

## **4.5 Time-interleaved implementation of polarization scrambling and tracking**

In this section, the implementation of polarization scrambling and tracking using the same hardware and data acquisition algorithm is discussed. For a detailed analysis of the performance and a comparison of the measurement techniques, a time interleaved implementation of the two techniques is needed. The hardware implementation of tracking is sufficient for this purpose. With minor adjustments in the data acquisition algorithm and micro controller embedded C programming code, a time synchronised version of polarization scrambling and tracking can be

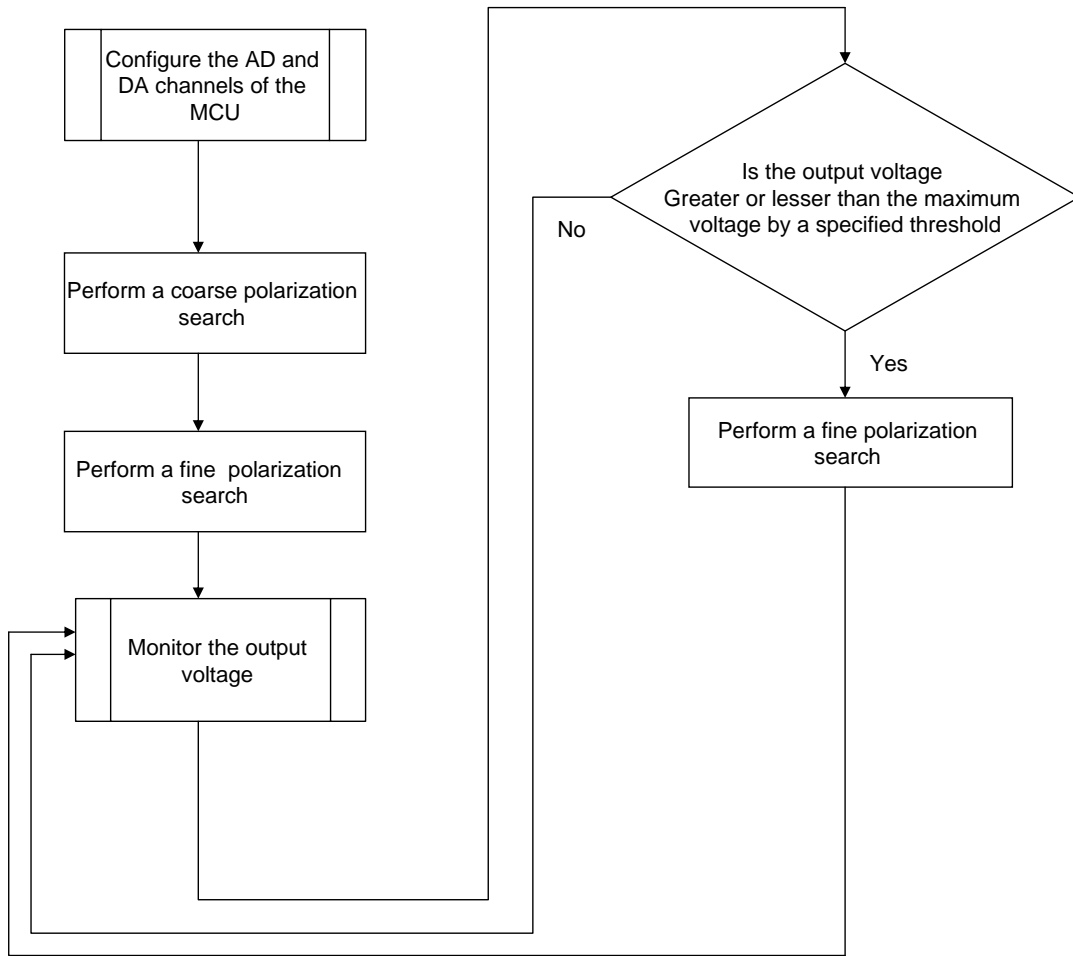


**Figure 4.12.** Algorithm for polarization tracking

implemented. The software required for this implementation will be discussed in this section.

#### 4.5.1 The Microcontroller algorithm

The high speed DA of the MCU makes it possible to implement the polarization scrambling algorithm described in section 4.3.2. The microcontroller algorithm for implementing scrambling and tracking with time interleaving is given by the flowchart in the figure 4.13.

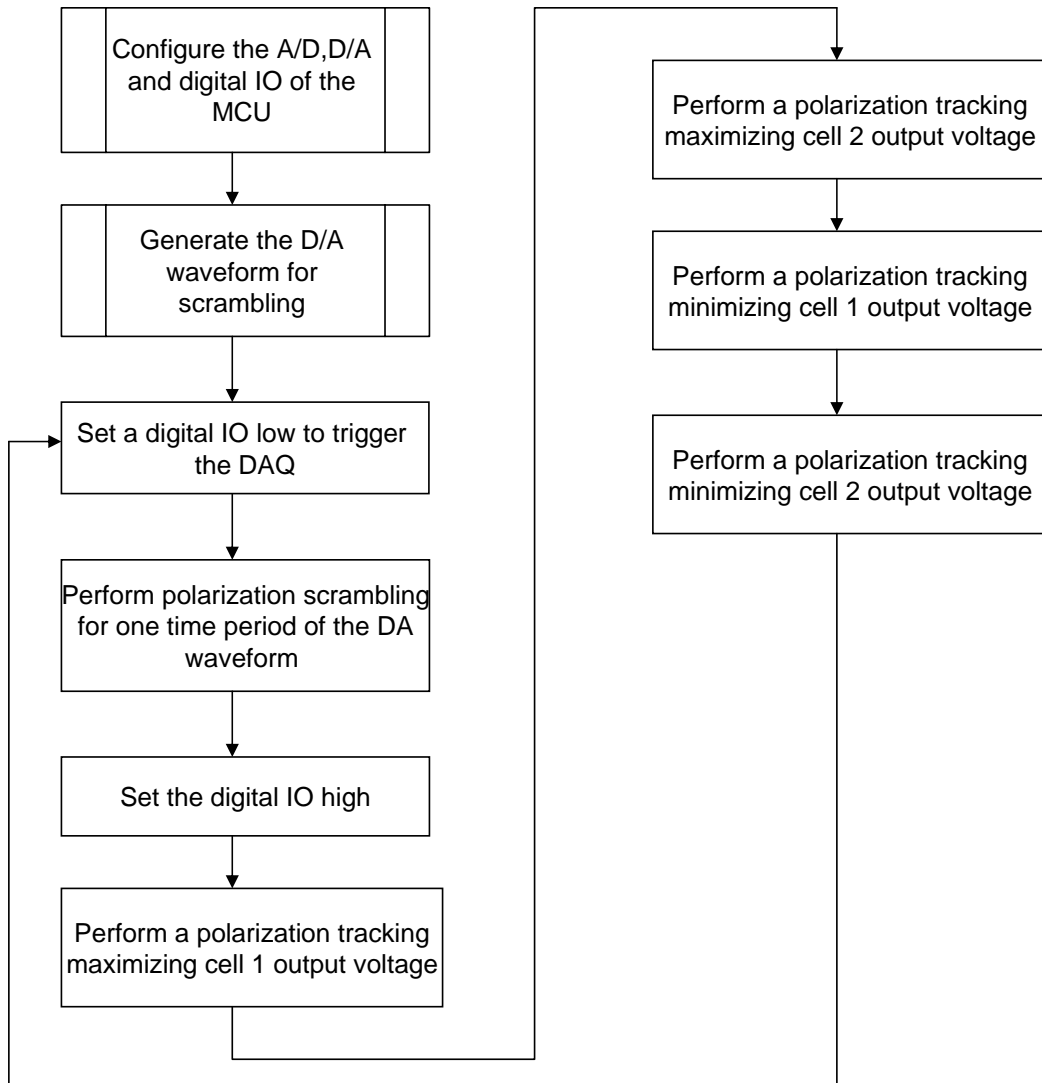


**Figure 4.13.** Microcontroller algorithm to implement time inter-leaved implementation of scrambling and tracking

### 4.5.2 The Data Acquisition algorithm

The data acquisition algorithm is shown in figure 4.14. The DT9836 simultaneous DAQ is triggered using the digital IO of the microcontroller. Since the number of points in scrambling and tracking can be pre-determined, the time slots for scrambling and tracking are fixed. As a result the DAQ can be programmed to collect a fixed number of data points when the falling edge trigger is detected by the DAQ.

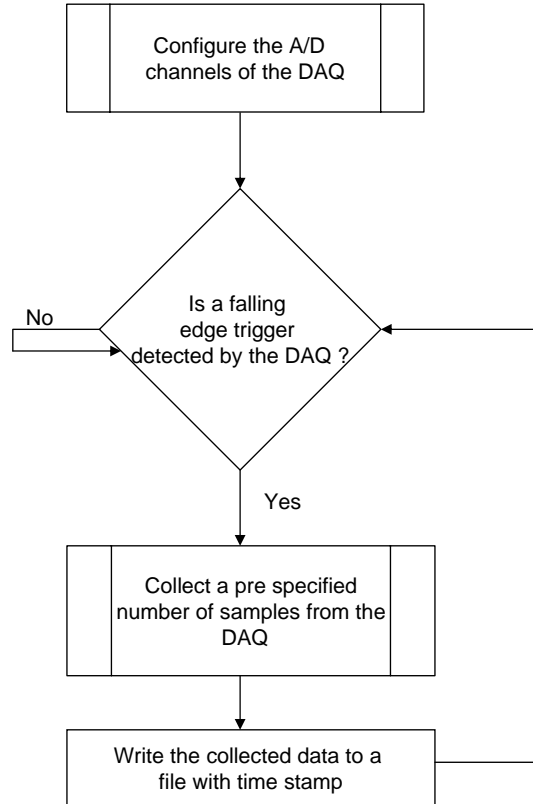


**Figure 4.14.** Data acquisition algorithm for time interleaved implementation of scrambling and tracking

## 4.6 Algorithm for extracting DGD information from the acquired data

The data file acquired from PMD monitor is processed by a separate signal processing algorithm that extracts the portion of the data that represents polarization scrambling or tracking. The implementation consists of one full cycle of polarization scrambling and four cycles of polarization tracking as shown in figure 4.15. So one can expect, one DGD value per second using polarization scrambling and 4 values using polarization tracking given ideal conditions. However when the SOP of the incoming signal changes, the voltage obtained from the tracking algorithm may not always reflect the maximum output voltage. This section discusses the signal processing algorithms used to extract DGD information from scrambling and tracking.

### 4.6.1 Extracting DGD information from polarization tracking

The output waveform for polarization tracking is shown in figure 4.16. The polarization tracking algorithm consists of a maximum search and a minimum search for each frequency component. As shown in figure 4.16, while the length of the polarization search for the global maximum of the two cells is fixed, the length of the fine search algorithm can vary. As a result, a stable portion of the tracking waveform should be extracted for DGD calculation. For this purpose, the tracking algorithm is made to last 20 ms. With a DAQ sample rate of 50 KHz, this amounts to 1000 samples. The maximum length of fine search is calculated to be around 500 samples. So using the constant length of the coarse search algorithm, the exact data locations that correspond to tracking algorithm can be found. Allowing for the worst case, the last 500 of the 1000 samples are extracted for

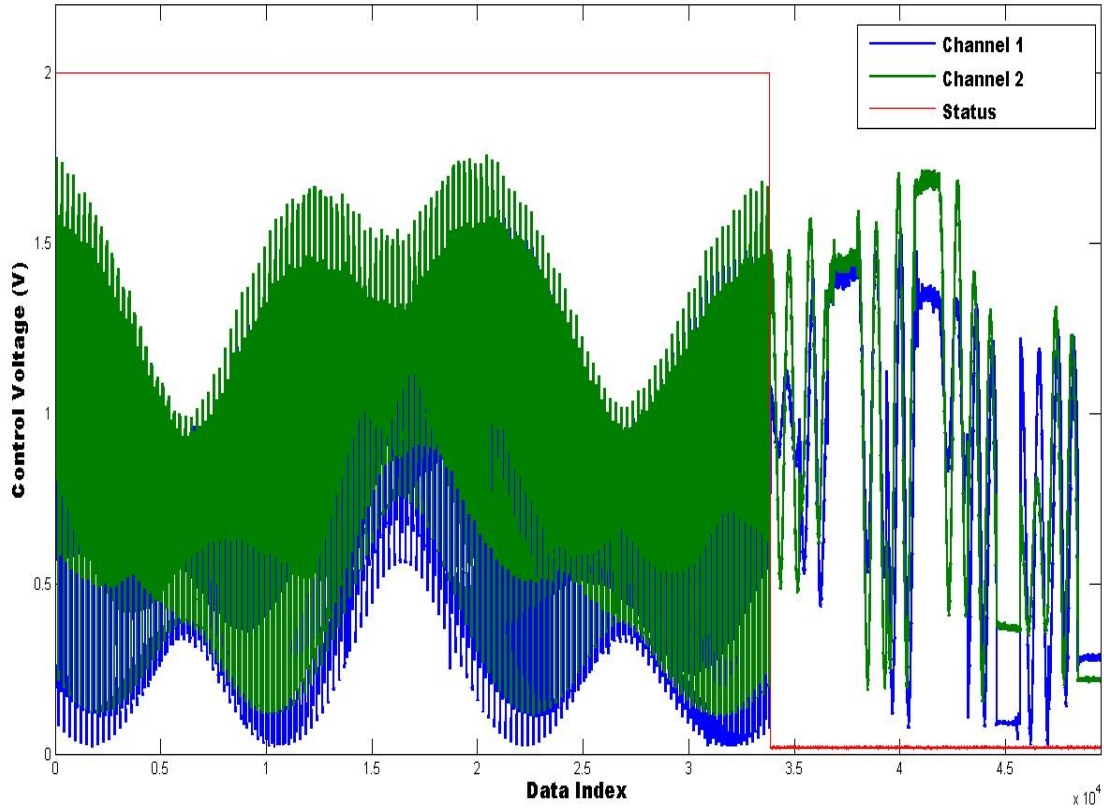


**Figure 4.15.** Data acquisition algorithm for time interleaved implementation of scrambling and tracking

DGD calculation. These samples are then filtered using a 4 point moving average filter. For a stable maximum or minimum, two conditions should be satisfied. First, the standard deviation of the samples should be lesser than the threshold specified for tracking. Secondly, the polarization scrambling algorithm yields the reference global maximum (or minimum). The global maximum (or minimum) found by polarization tracking should be no lesser than 98 *percent* of the reference global maximum (or minimum). This is done to ensure that polarization tracking always yields a global maximum(or minimum) rather than a local maximum (or minimum). If and only if the two conditions are met, the samples are extracted. Then the mean values of the samples are used as voltages that represent the DGD

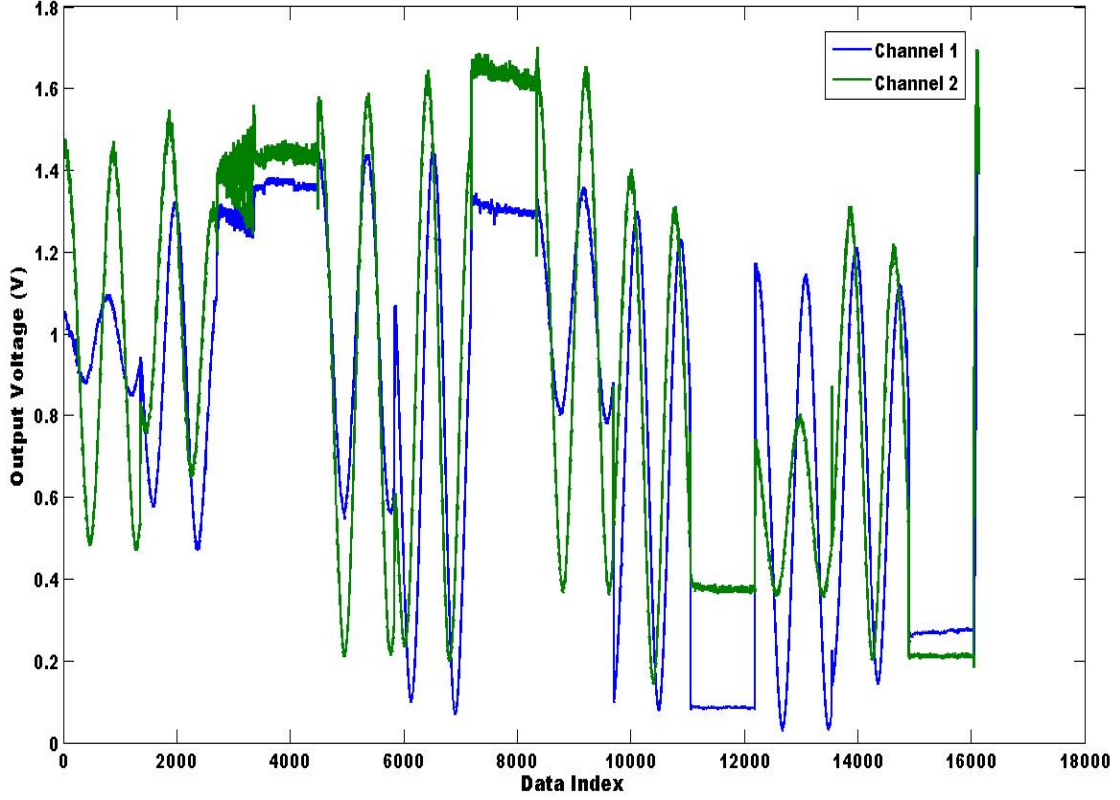
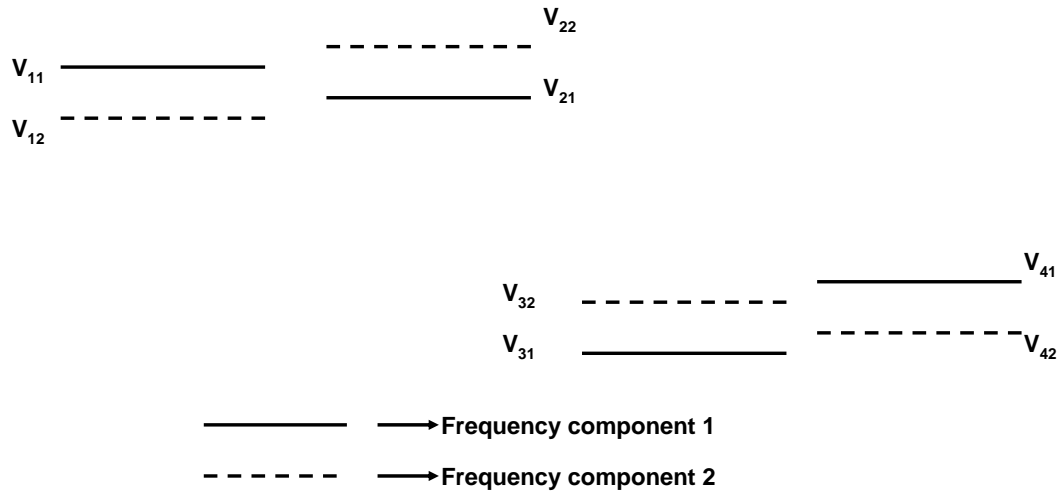


Figure 4.16. Output waveform for polarization tracking

information in the signal. Figure 4.17 shows the voltage values obtained after the data extraction. The DGD values can then be extracted by normalizing the voltages using the equations described by 4.27.

$$\begin{aligned}
 dgd_1 &= \frac{\arccos\left(\sqrt{\frac{V_{21}-V_{13}}{V_{11}-V_{13}}}\right)}{\pi * 10^{10}} \\
 dgd_2 &= \frac{\arccos\left(\sqrt{\frac{V_{12}-V_{24}}{V_{22}-V_{24}}}\right)}{\pi * 10^{10}} \\
 dgd_3 &= \frac{\arcsin\left(\sqrt{\frac{V_{14}-V_{13}}{V_{11}-V_{13}}}\right)}{\pi * 10^{10}} \\
 dgd_4 &= \frac{\arcsin\left(\sqrt{\frac{V_{23}-V_{24}}{V_{22}-V_{24}}}\right)}{\pi * 10^{10}}, \tag{4.27}
 \end{aligned}$$



**Figure 4.17.** Voltage values obtained data processing and DGD extraction

where  $10GHz$  is the frequency separation between the two components,  $V_{11}$  is the mean voltage obtained by maximizing the frequency component  $f_1$ ,  $V_{22}$  is the mean voltage obtained by maximizing the frequency component  $f_2$ ,  $V_{13}$  is the mean voltage obtained by minimizing the frequency component  $f_1$ ,  $V_{24}$  is the mean voltage obtained by minimizing the frequency component  $f_2$ .  $V_{21}$ ,  $V_{12}$ ,  $V_{23}$  and  $V_{24}$  are the corresponding mean voltages of the other frequency component at the maximized or minimized voltages. The matlab code for DGD extraction is given in appendix C.

#### 4.6.2 Extracting DGD information from polarization scrambling

The algorithm for extracting DGD from the scrambling waveform is fairly simple. The output waveform for polarization scrambling is shown in figure 4.18. The output waveform is filtered using a digital low pass filter with cutoff frequency of  $100Hz$ . Then the maximum and minimum values of the two waveform are found and the DGD value can be extracted in the same procedure as the one used for



polarization tracking.

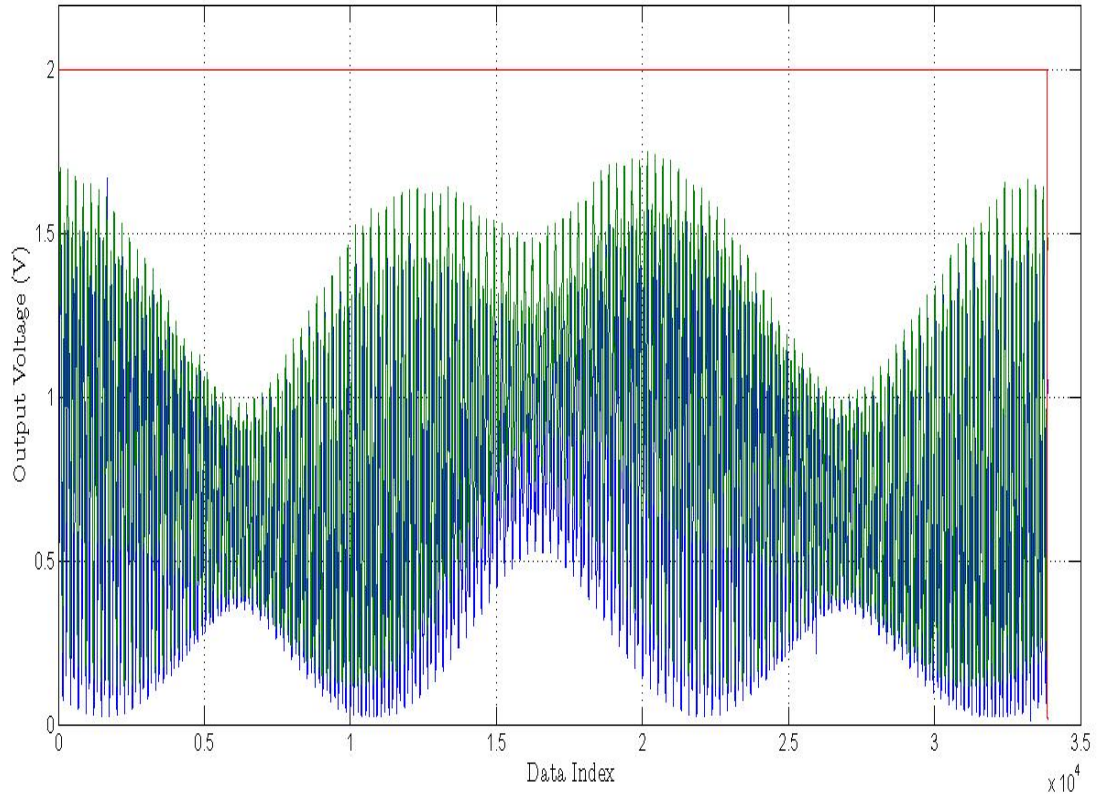


**Figure 4.18.** Output waveform for polarization scrambling

## 4.7 Performance analysis of polarization scrambling and polarization tracking

A number of factors influence the characteristics of the PMD monitor and as a result, the algorithms implemented to measure DGD using the PMD monitor. In this section such factors are discussed qualitatively and quantitatively.

#### 4.7.1 Range of DGD measured by the PMD monitor

The PMD monitor measures the DGD based on the angular walk off between two frequency selected components. As such the range of DGD value that can be measured by the PMD monitor is limited. Assuming ideal conditions, when the two frequency components are aligned with each other in the Poincare sphere, the DGD is given by the equation

$$DGD = \left( \frac{0}{\pi * 1e10} \right) = 0ps, \quad (4.28)$$

and when they are farthest apart in the Poincare Sphere, the DGD is

$$DGD = \left( \frac{\frac{90\pi}{180}}{\pi * 1e10} \right) = 50ps. \quad (4.29)$$

So, DGD values from 0 ps to 50 ps can be measured by the PMD monitor. It should be noted that the angular separation on the Poincare Sphere is twice that of the actual angular separation between the two components.

#### 4.7.2 Measurement speed

The step size used for polarization tracking and scrambling determine the measurement speed of the respective algorithms. Using the same step size for both algorithms, their measurement speed can be calculated. The number of DAC samples required for a scrambling is given by the product of number of points for the first cell,  $N_{DAC1}$  and number of points for the second cell,  $N_{DAC2}$ . If  $f_{DAC}$  is the DAC sample rate, then the measurement speed is

$$Speed_{scrambling} = (N_{DAC1} * N_{DAC2}) / f_{DAC}. \quad (4.30)$$

For polarization scrambling, the total number of points is 14400. With a DAC sample rate of  $21.7\text{KHz}$  for the microcontroller, the measurement speed is about 680 ms. This means that one DGD data can be extracted from scrambling every 680 ms. It should be noted that a delay of  $30\ \mu\text{s}$  is introduced by the polarization controller's response time. For polarization tracking, the measurement speed is given by

$$Speed_{tracking} = (2 * N_{DAC}) / f_{DAC}. \quad (4.31)$$

which yields a measurement speed of 11 ms. However, using a delay of  $20\ \mu\text{s}$  for every DAC sample in addition to the response time of the polarization controller, the length of a polarization tracking cycle is about 64 ms. This is done in order to reduce the jitter caused due to step size. Adding the worst case fine search algorithm time of 20 ms, the total length of polarization tracking cycle is 84 ms. This means that 12 DGD values can be extracted every second for the polarization tracking implementation. Though the complexity of the polarization tracking algorithm is  $2 * n$  as compared to the polarization scrambling which is  $n^2$ , the hardware used for the research has placed restriction on the measurement speed of polarization tracking. Use of better hardware, such as a faster polarization controller and high speed AD and DA converters the measurement speed of polarization tracking can be increased further.

### 4.7.3 Accuracy of the measurement

#### 4.7.3.1 Step size used by the DA converter

For optimum performance, keeping in mind the measurement period required for the PMD monitor, a step size should be decided. If the step size is too small it would mean a longer measurement period, and if it is too large, lesser accuracy.

So, a compromise between speed and accuracy is made. For this purpose, the step size for the DA converter dedicated to each cell of the polarization controller is set at 3 deg. In other words, for the purpose of scrambling, the Poincare Sphere can be visualised as being partitioned into grids whose corners are 3 degrees apart from each other with respect to the origin of the sphere. This inherently introduces an error of

$$DGD = \left( \frac{\left( \frac{1.5\pi}{180} \right)}{(\pi * 1e10)} \right) = 0.8333ps. \quad (4.32)$$

#### 4.7.3.2 Threshold used for validation of polarization tracking

As seen in section 4.4.2, a threshold is used to verify whether the tracking achieves a maximum (or minimum) that is close to the reference maximum(or minimum) found by scrambling. This threshold used for validation introduces an error in the DGD measurement. The error is proportional to the DGD that is being measured. A simulation is carried out to find the error in measurement for DGD values that can be measured by the PMD monitor. The results of the simulation is shown in the figure 4.19. As expected the magnitude of error decreases with increase in the DGD value being measured. This can be understood by analyzing the arc cosine function which is steep near one and flat around zero. So to minimize the measurement error, a 98 percent threshold is used in the microcontroller C code.

#### 4.7.4 Dead zone of the polarization controller

When the input fiber pigtail is aligned at 45 deg to the first cell of the polarization controller given that the second cell is aligned at 45 deg with respect to the first cell, the polarization controller can transform a given incoming SOP

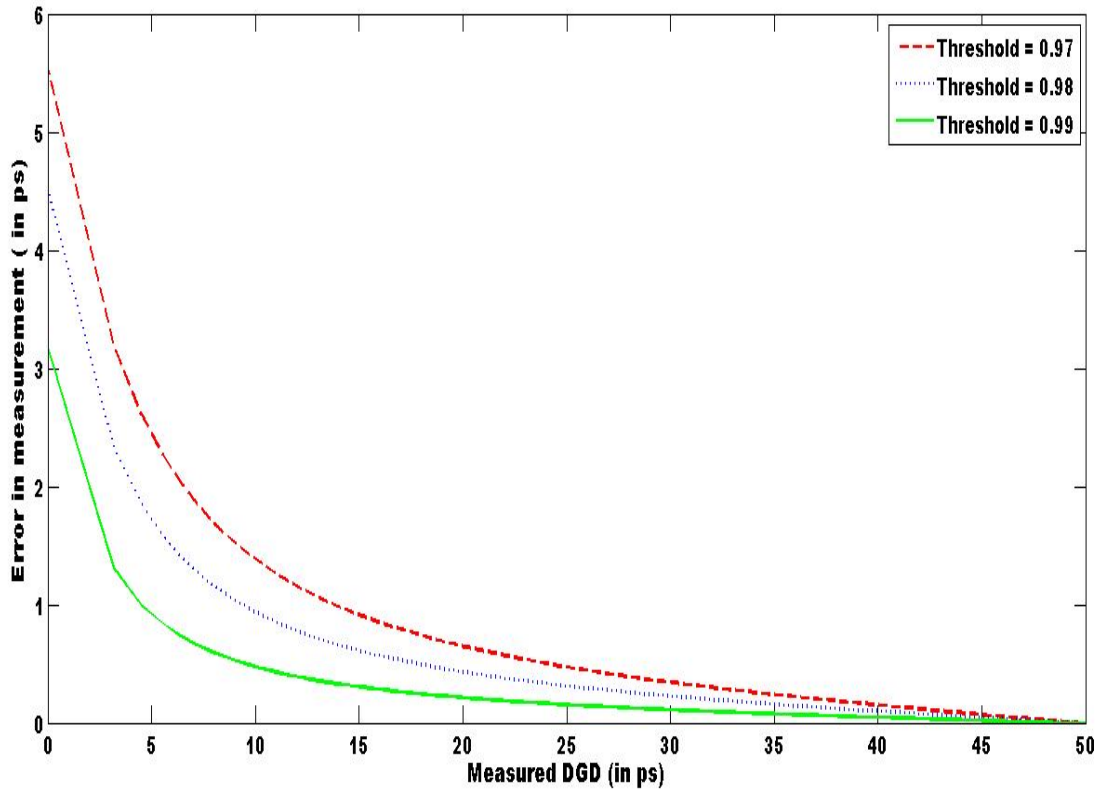


**Figure 4.19.** Simulation results for error in the DGD measurement due to threshold used for validating polarization tracking

of the incoming signal to any outgoing SOP in the Poincare sphere. But when there is an alignment error, i.e., the first cell is not 45 deg to the fiber input, there exists a portion of the Poincare sphere that is left uncovered by the polarization controller. This unreachable region in the Poincare sphere as shown in figure 4.20 is called the dead zone.

As a result, one or both of the frequency selected component may lie in the dead zone. Since the alignment of fiber pigtail with the first cell is fixed, the area of the dead zone is fixed. For the polarization controller used in the PMD monitor, the diametrically opposite points of the dead zone of the polarization controller subtend an angle of 15 deg with the origin of the Poincare sphere. The worst case

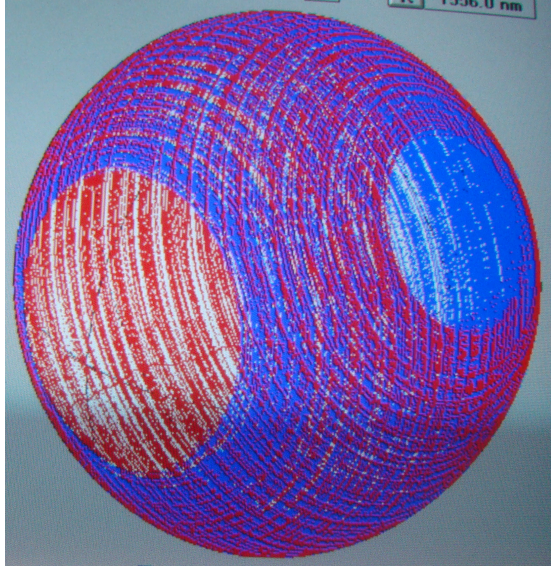


**Figure 4.20.** The dead zone of the polarization controller

error occurs when the frequency component being tracked is located at the center of the dead zone. For the given example, the worst case error in measurement would be

$$DGD_{error} = \left( \frac{\left( \frac{3.75\pi}{180} \right)}{(\pi * 1e10)} \right) = 2.08ps. \quad (4.33)$$

#### 4.7.5 Measurement period and Statistics of data collected for extracting DGD

The amount of time required to extract one DGD data from the coherent PMD monitor is called a measurement period. For polarization scrambling, a measurement period is the time of one full DA waveform cycle shown in figure 4.10. In our experiment, a data file consists of 4 seconds of measurement. Every second of data consists of one full cycle of polarization scrambling and a maximum and minimum search for each of the two frequency components. As described in section 4.6.1, although four values of DGD can be extracted from tracking, for comparative analysis of polarization scrambling and polarization tracking, one value of DGD

is extracted by averaging the four values obtained by the normalization in polarization tracking. This yields two DGD values (one each for scrambling and tracking) per second of data collected. Allowing two seconds for writing the data file after every four seconds, 80 DGD values can be extracted per minute.

#### 4.7.6 Noise characteristics

The noise from optical sources present in the PMD monitor can be classified into two categories; the shot noise due to coherent detection in the photodiode and the relative intensity noise (RIN) from the laser diode of the local oscillator output. Shot noise in fiber optic systems is caused by random generation of electron hole pairs in the photodiode [1]. Mathematically, the photodiode current can be written as

$$I(t) = I_p + i_s(t), \quad (4.34)$$

where  $I_p$  is the average current and  $i_s(t)$  is the current fluctuation contributed by the shot noise. Generally, the electron hole pair generation is modelled as a Poisson process. But for simplicity shot noise can be described as a white noise with constant power spectral density using the Gaussian approximation. Then, the variance of the shot noise can be calculated as

$$\sigma_s^2 = \int S_s(f)df = 2qI_p\Delta B, \quad (4.35)$$

where  $\Delta B$  is the effective noise bandwidth of the receiver. The input signal level,  $P_s$  is  $-15dBm$  and the LO output power is  $-2dBm$  approximately. The output

power,  $P_o$  at 3dB coupler is given by

$$P_o = \frac{P_s + P_L}{2} = \frac{631 + 31}{2} = 330.5\mu W.$$

The responsivity of the photodiode with a 40GHz bandwidth is  $0.5A/W$ , so the average photocurrent at the photodiode output,  $I_{ph}$  is  $330.5 * 0.5 = 160.25\mu A$ . Now the root mean square shot noise at 40 GHz bandwidth can be given as

$$\sigma_s^2 = 2 * 1.6 * 10^{-19} * 160.25 * 10^{-6} * 40 * 10^9 = 2.05pW, \quad (4.36)$$

and the output current at the photodiode  $I_o$ , of the coherently detected output at the photodiode with responsivity,  $\rho$ , is given by,

$$I_o = 2 * \rho * \sqrt{(P_s * P_L)} = 2 * 0.5 * \sqrt{(631 * 31 * 10^{-12})} = 139\mu A. \quad (4.37)$$

The equation 4.36 shows that noise power due to shot noise is proportional to the bandwidth. When the optical spectrum is down converted to the RF spectrum of 1GHz bandwidth, the contribution from shot noise is reduced. At 1 GHz bandwidth, we can assume that the signal spectrum is assumed to be flat in the bandwidth of interest of the signal. The signal power at 1GHz is  $1/20th$  of the total signal power since the signal bandwidth is 20GHz. Then the output current can be given as

$$I_o = 139/20\mu A = 6.45\mu A.$$



After the sallen key low pass filter whose bandwidth is of the order of 15KHz, the noise contribution due to shot noise is

$$\sigma_s^2 = 2 * 1.6 * 10^{-19} * 160.25 * 10^{-6} * 15 * 10^3 = 7.9 * 10^{-19}W. \quad (4.38)$$

Also, it should be noted that the thermal noise places a lower limit on the LO output power. The lowest signal power at which the thermal noise power dominates the signal is when the signal power equal noise power i.e., when SNR due to thermal noise is unity. The thermal noise for a room temperature of 300 K at bandwidth  $\Delta B$  of 40 GHz is given by,

$$E[n(t)^2] = 4kT\Delta B/R_L = 4*1.38*10^{-23}*300*40*10^9/50 = 1.3*10^{-11}W = -78.6dBm.$$

Here  $R_L$  is the load resistance of the photodiode. For high speed optical systems, the photodiode's load resistance is generally 50 ohms. The RF signal power of coherent detection is

$$P_{sig} = 20\log(160.25 * 10^{-6}) = -47dBm.$$

So the signal level is atleast 30dBm more than the thermal noise limit. At the output of the low pass filter, the noise contribution at bandwidth  $\Delta B$  of 15KHz due to the thermal noise can be calculated as

$$\sigma_{th}^2 = 4 * 1.38 * 10^{-23} * 300 * 15 * 10^3/50 = 4.96 * 10^{-18}W. \quad (4.39)$$

The relative intensity noise (RIN) occurs due to intensity fluctuations of a semiconductor laser. It can either be due to internal factors such as modal instabilities

or due to extrinsic factors such as near end and far end reflections. Generally at very high frequencies, the RIN due to intrinsic factors is not significant as the laser will not be able to respond to such fluctuations. Only the extrinsic RIN affect the LO. The near end reflections at the fiber interface can be reduced by antireflection coating while the far end reflections result in peaks in the noise power spectrum. From the manufacturer's datasheet for the Laser, we have found that the RIN from the laser is about  $-137$  dB/Hz. The RIN is defined for frequencies from 0.5MHz to 10 GHz as shown in figure 4.21.

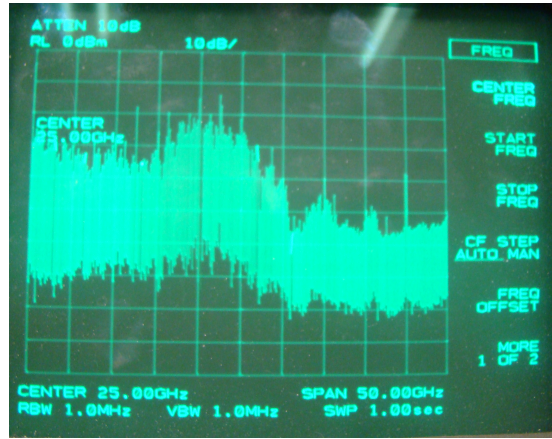


**Figure 4.21.** The RF spectrum at the output of the RF amplifier without attenuating the LO output

A 15 dB attenuator is used to reduce the effect of RIN at high output power of the LO. The RF spectrum at the RF amplifier's output with attenuation of the LO output is shown in the figure 4.22.

The RIN at the frequency range of interest, i.e., for 40GHz bandwidth can be calculated as

$$\sigma_{RIN}^2 = RIN * \Delta B * P_L^2 * \rho^2 = 2\epsilon^{-14} * 40 * 10^9 * (631 * 10^{-6})^2 = 7.963 * 10^{-11} W. \quad (4.40)$$

At the output of the low pass filter, the noise contribution at bandwidth  $\Delta B$  of

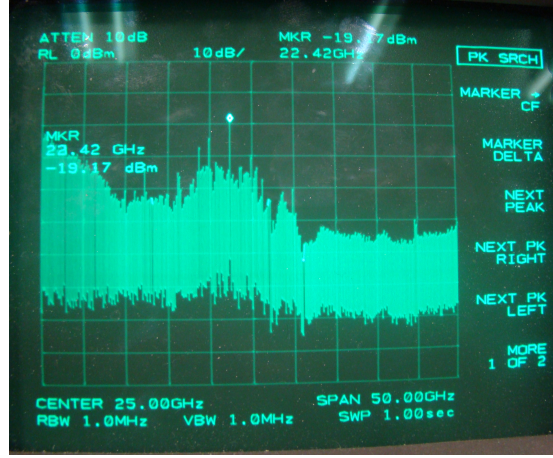


**Figure 4.22.** The RF spectrum at the output of the RF amplifier with attenuation of the LO output

15KHz due to RIN is

$$\sigma_{RIN}^2 = 2\epsilon^{-14} * 15 * 10^3 * (631 * 10^{-6})^2 = 3 * 10^{-17}W. \quad (4.41)$$

The RF detector calculates the total signal power in 1GHz bandwidth and also the wideband noise at 1GHz. Therefore the RF equivalent signal power at the output of the low pass filter is

$$S_o = (6.45 * 10^{-6})^2W = -73.8dBm. \quad (4.42)$$

Further more, the RIN, shot noise and the thermal noise add together at the input of the filter. By central limit theorem, it is reasonable to assume that the noise at the input of the filter is Gaussian. From equations 4.38, 4.39, 4.41, the total noise power can be calculated as the sum of the noise powers. Therefore, the SNR at the output of the low pass filter is

$$SNR = 10\log(4.16 * 10^{-11}/(3.58 * 10^{-17})) = 60.65dB. \quad (4.43)$$

Therefore, we can conclude the noise contributions due to the optical sources is negligible. However, the RF noise from the high speed RF amplifiers used in the signal processing circuitry must be taken into account. Adding the Johnson noise limit for the input of the RF amplifier to the optical noise contributions the total noise power is,

$$\sigma_{total}^2 = 3.58 * 10^{-17} + 4kT\Delta f/R_s = 3.65 * 10^{-17}W$$

where  $R_s$  is the load resistance of the source and  $\Delta f$  is 15KHz. Therefore the total SNR at the input of the RF amplifier is

$$SNR_{RFinput} = 10\log(4.16 * 10^{-11}/(3.65 * 10^{-17})) = 60.5dB.$$

At the output of the first amplifier the signal power is  $S_o = -53.8dBm$ . With a noise figure of 7 dB, the output noise power is given by  $N_o = F.G.N_i$  where  $F$  is the noise figure of the RF amplifier,  $G$  is its gain and  $N_i$  is the noise input power at the RF amplifier. The noise power at the output of the first RF amplifier is

$$N_o = 10\log(3.65 * 10^{-17} * 10^7 * 5.011) = -117.377dBm. \quad (4.44)$$

At the output of the second RF amplifier, the noise power can be calculated as

$$N_o = 10\log(1.82 * 10^{-12} * 10^7 * 5.011) = -74.8dBm. \quad (4.45)$$

Therefore the SNR at the output of the bandpass filters is  $-33.8 - (-74.8)$  i.e., 41.5 dB. Hence the noise at the output of the low pass filter due to optical and RF sources is very low.

## 4.8 Advantage of polarization tracking over polarization scrambling

In this chapter, we have seen that polarization tracking has some important advantages over scrambling. Firstly, the measurement period of polarization tracking implementation is around 12 DGD values per second. This is many times faster than scrambling which would yield one DGD value in two seconds. Secondly, the amount of data collected and stored for DGD extraction is very large for scrambling. For instance, about 144 Gigabytes of hard disk space is required for an hour of data. For tracking, the memory requirement reduces to about 13.4 Megabytes of data in a hour when samples are collected for averaging. If the averaging can be carried out in the hardware, only 1.4 Megabytes of disk space is required. A closely related and more significant advantage of tracking is that the DGD value can be processed in real time. In other words, the DGD can be extracted as the data is being collected. This is not possible in scrambling as filtering and search operations are to be carried out for every data file that is collected. The real time implementation of tracking requires change of hardware or software that has been used thus far, at the lightwave laboratory. As a result, with the available hardware, a test has been conducted to prove the advantages of polarization tracking over polarization scrambling. Using the OC192 transmission test set and the PM fiber to generate an unknown but fixed DGD in the probing signal, the PMD monitor has been used to extract the DGD information real time. This has been made possible by the use of RS232 serial communication between the microcontroller and the computer. The results of the test with details of hardware and data processing algorithms are discussed in section 5.

# Chapter 5

## Experiments and Results

### 5.1 Measuring the DGD of a PM fiber

In this test, a polarization maintaining fiber was used as a link from a OC192-10GHz transmission test kit to the PMD monitor as shown in figure 5.1. The data is collected and stored in time-stamped files. An optical spectrum analyzer (OSA) is used to locate the frequency at which the peak optical power occurs. For proper coherent detection, the optical signal power from the test kit should be lesser than -15dB so that the wideband photodiode is not saturated. The local oscillator output is attenuated to reduce the relative intensity noise from the LO of the PMD monitor. Then the local oscillator frequency is changed to be within 25GHz of the optical signal frequency so that the IF terms lie within the spectrum of commercially available bandpass filters.

Though the relative orientation of the PSPs of the PM fiber is unknown, they are fixed with respect to the fiber axis. As a result, this test serves as a measure of repeatability for the PMD monitor. This experiment can be considered an ideal experiment where the SOP change is negligible. The PM also has a

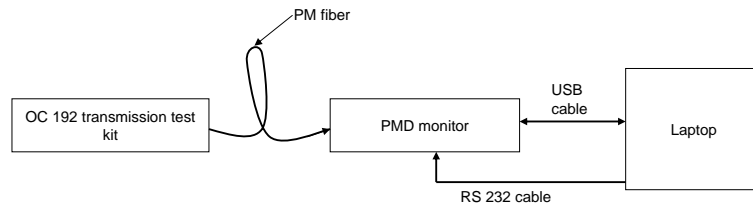


**Figure 5.1.** Experimental setup for the PM fiber experiment

constant but unknown DGD. The figure 5.2 shows the plot for the DGD measured from the fiber using polarization scrambling. The data is collected for about

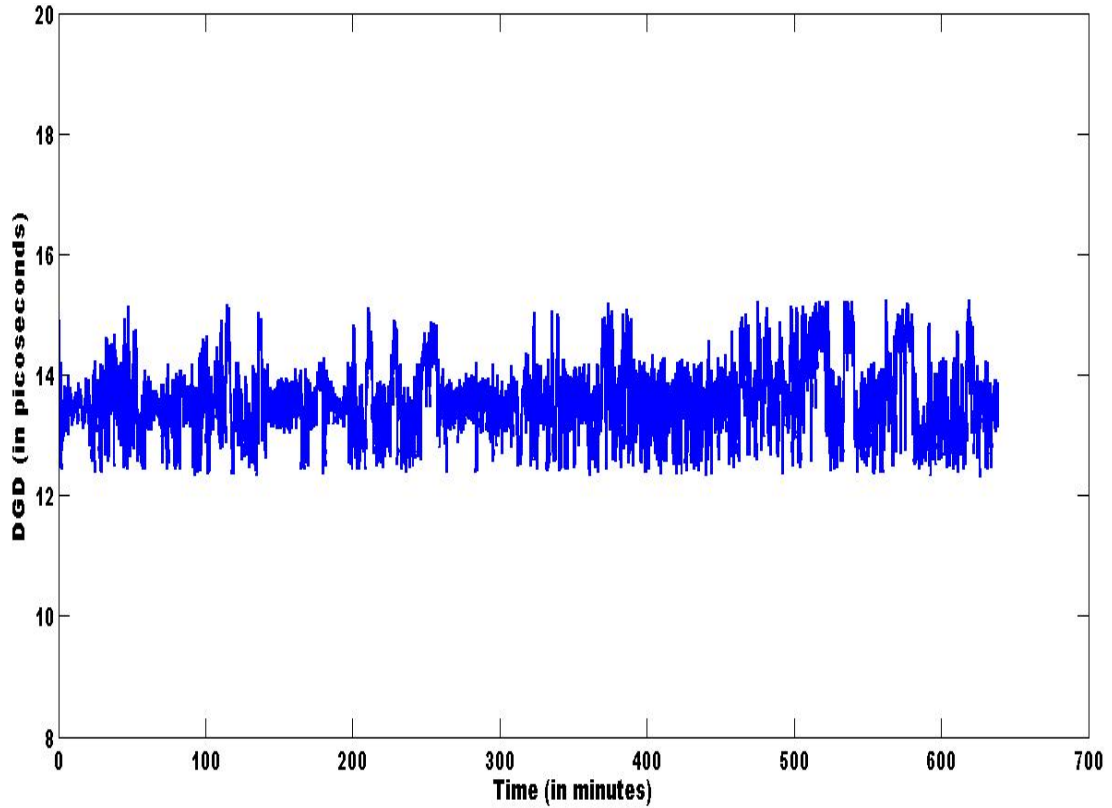


**Figure 5.2.** Plot for DGD calculated by the PMD monitor using polarization scrambling for the PM fiber experiment

10.5 hrs. The histogram of the DGD is shown in figure 5.3. As can be inferred from the figure, the total width of the distribution is about 2.5ps for a mean DGD of 13.53ps. Ideally one is expected to measure a constant DGD and as

a result a narrower distribution. But limitations on the hardware used for the measurement, lead to errors in the measurement. It should be noted that DGD is a random quantity depending on factors ranging from the instrumentation to the ambient temperature. A detailed error analysis is discussed in the later chapters. Literature suggests there is atleast a 15 to 20 percent of error margins between different measurement techniques [13]. The DGD measured using polarization

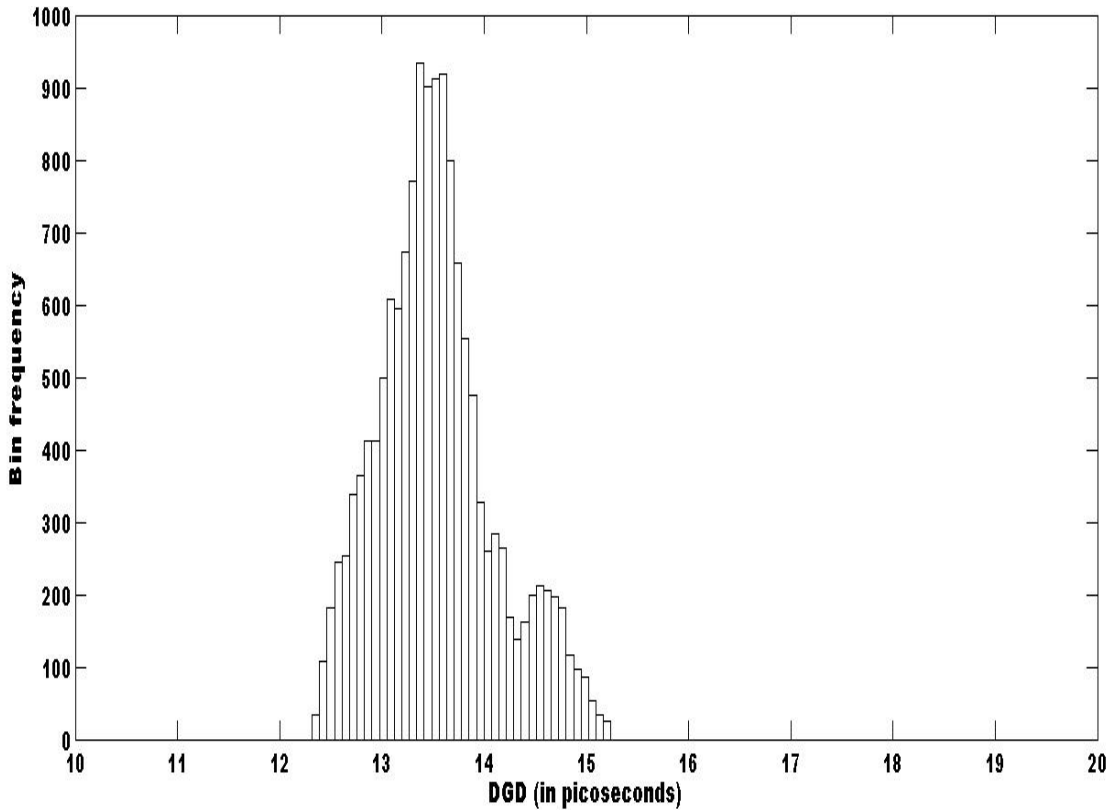


**Figure 5.3.** Histogram for DGD calculated by the PMD monitor using polarization scrambling for the PM fiber experiment

tracking is given in figure 5.4. The total width of the distribution is about 3 ps, which is slightly wider than that of scrambling. This is expected as the threshold for the global maximum in tracking is 98 percent of the reference global maximum in scrambling. For instance, using a 98 percent threshold to measure a mean DGD



of 13.5 ps would give a mean DGD of 14.1 ps with polarization tracking. The mean DGD of the measurement using tracking is 13.94ps. As a result there is 7 percent error between the DGD measured by the two algorithms. The histogram for the

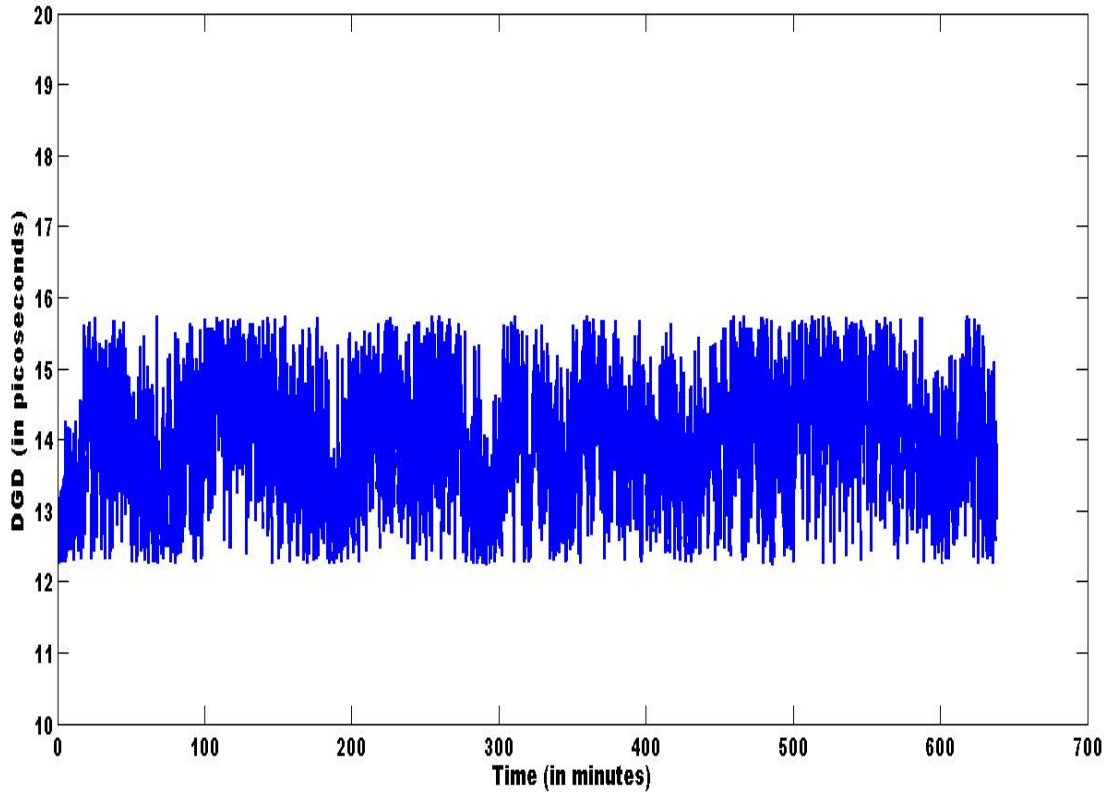


**Figure 5.4.** Plot for DGD calculated by the PMD monitor using polarization tracking for the PM fiber experiment

DGD measured by polarization tracking is given in figure 5.5. The summary of the DGD statistics measured using polarization scrambling and polarization tracking is given in Table 5.1.

## 5.2 Measuring the DGD of a PMD emulator

For the purpose of verifying how accurately the PMD monitor measures a known DGD value, a PMD emulator is used to introduce a known DGD in the

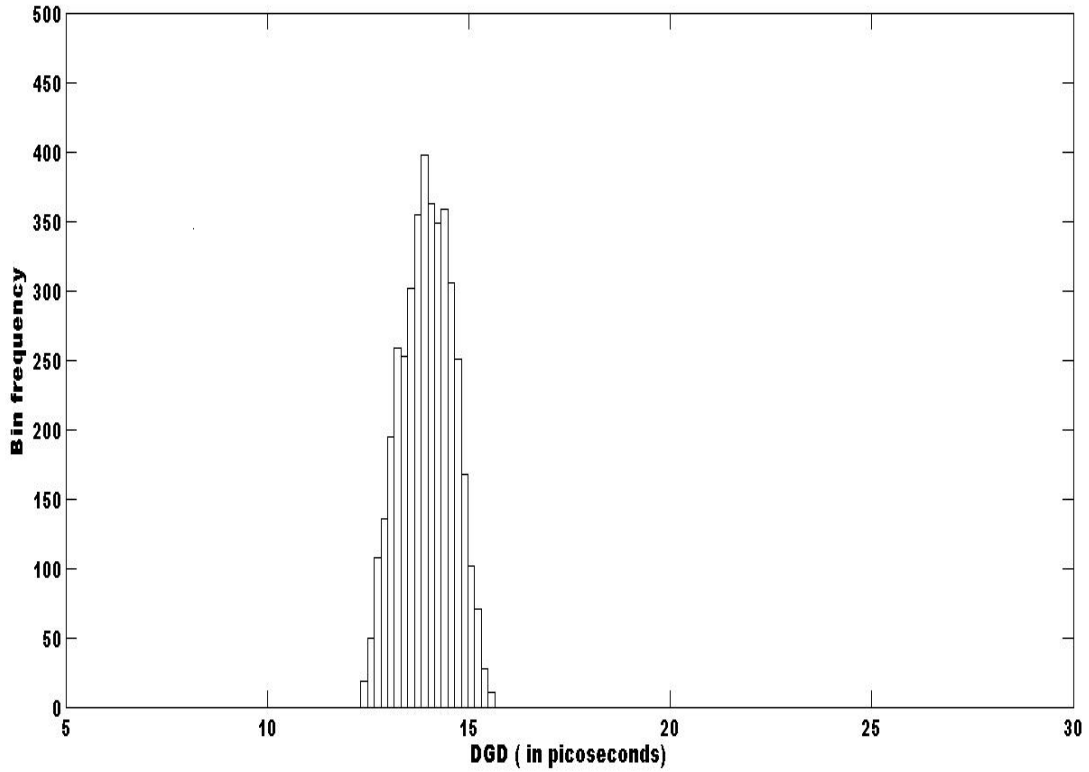


**Figure 5.5.** Histogram for DGD calculated by the PMD monitor using polarization tracking for the PM fiber experiment

Attributes	Polarization scrambling	Polarization tracking
Measurement time	630 minutes	630 minutes
No of samples	14,748	12,220
Mean value of DGD	13.52 ps	13.94 ps
Standard deviation of DGD	0.54 ps	0.73 ps
Width of the distribution	2.56 ps	3.23 ps

**Table 5.1.** DGD statistics for the PM fiber experiment.

optical signal. The experimental set up for the PMD emulator test is shown in the figure 5.6. The optical signal is fed as an input to the PMD emulator in

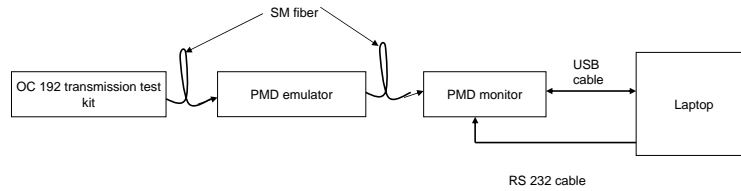


**Figure 5.6.** Experimental setup for the PMD emulator experiment

such a way that optical power is equally divided between the two axes of the fiber. The output from the PMD emulator is then input into the coherent PMD montior. The PMD emulator can be used to introduce DGD ranging from 0 to

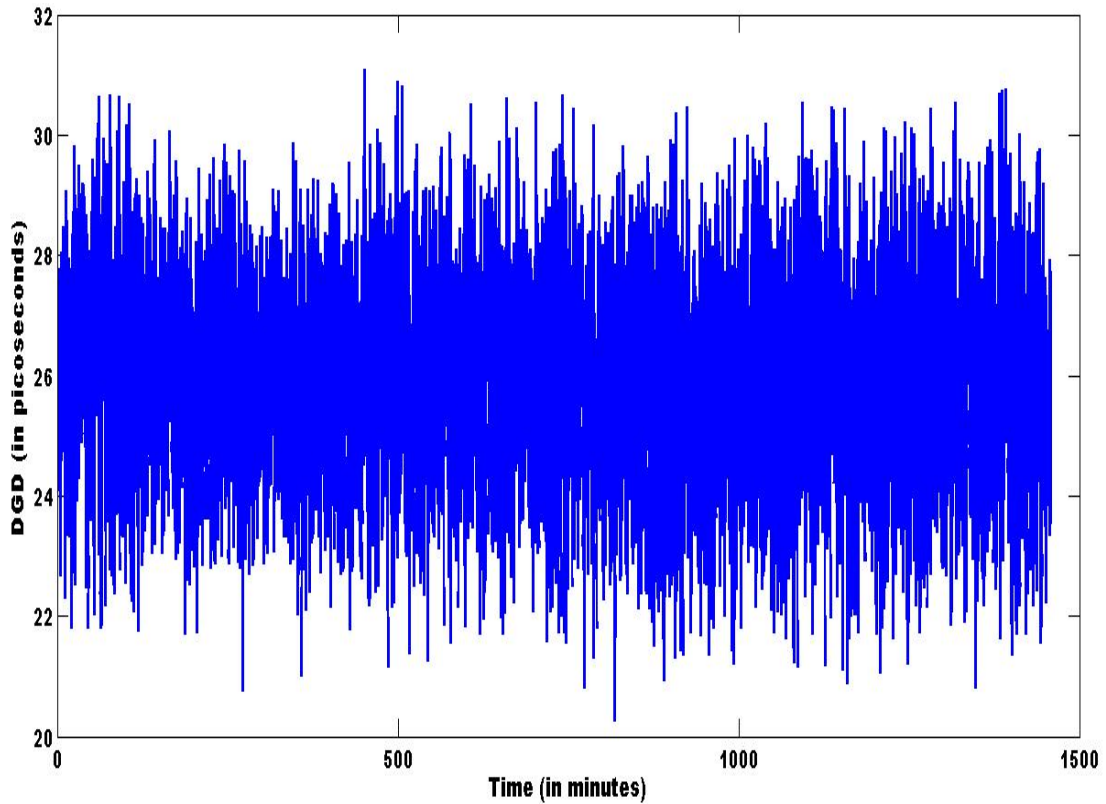


**Figure 5.7.** Plot for DGD calculated by the PMD montior using polarization scrambling for the PMD emulator experiment

1000 ps. However, as proved earlier, a maximum of 50 ps can be measured using the PMD monitor. The PMD emulator in our experiment introduces a DGD of 25 ps. Figure 5.7 shows the plot for the measured using polarization scrambling. The histogram of the DGD is shown in figure 5.8. The mean value of the DGD is 25.3ps. Since the DGD introduced by the emulator is based on mechanical vibrations and these vibrations change slowly in a lab environment we expect to see a narrower distribution than a Rayleigh or a Maxwellian distribution. The  $3\sigma$  width of the distribution is 10 ps. The DGD measured using polarization tracking

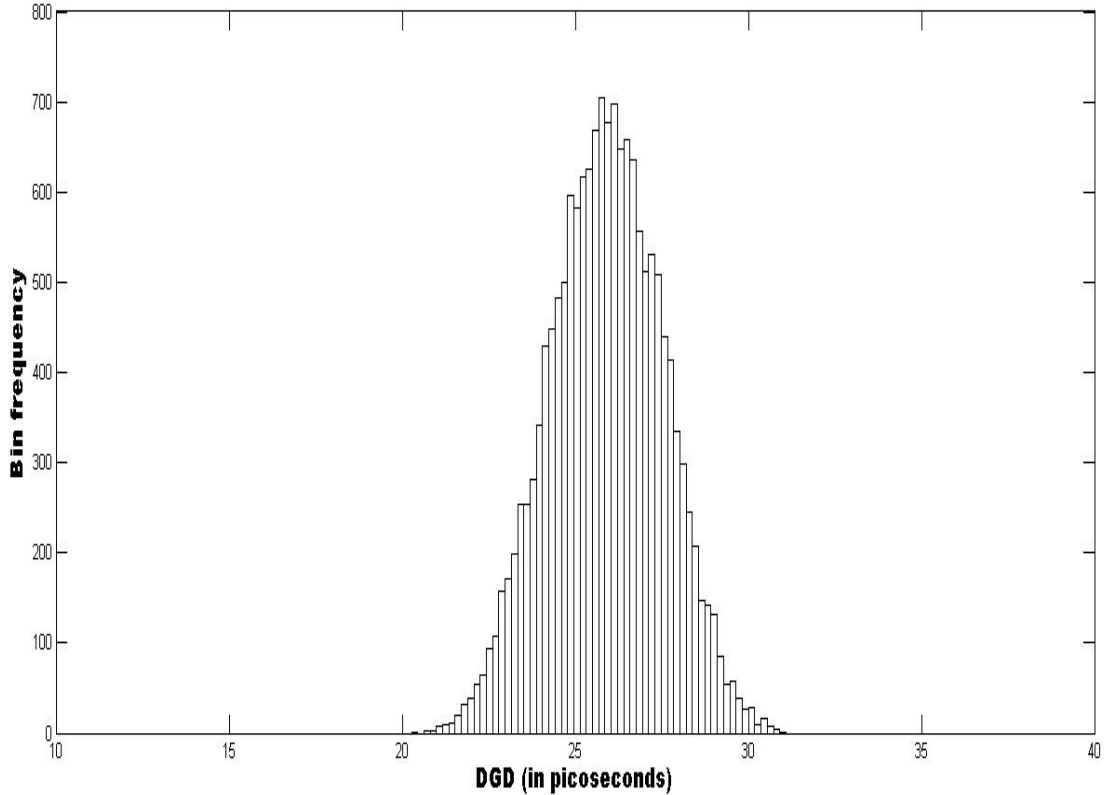


**Figure 5.8.** Histogram for DGD calculated by the PMD monitor using polarization scrambling for the PMD emulator experiment

is given in figure 5.9. We observe a wider distribution for tracking than that of scrambling due to the fact that the SOP is not stable. However, the mean value of

DGD measured by scrambling and tracking differ from each other by 9.7 percent. The normalization procedure used for DGD calculation in tracking assumes that the SOP does not change for one full tracking cycle. This is not the case for a PMD emulator. So even a slow change in the SOP during the polarization tracking

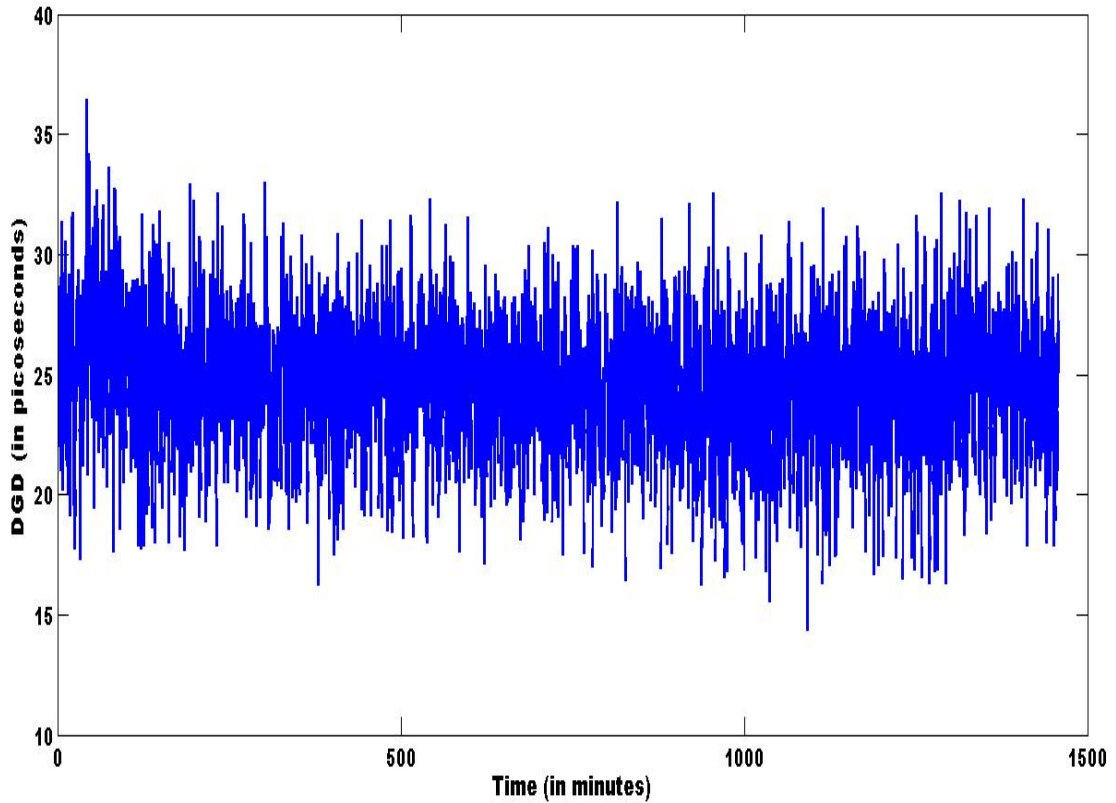


**Figure 5.9.** Plot for DGD calculated by the PMD monitor using polarization tracking for the PMD emulator experiment

cycle will introduce errors in the DGD extracted from the data. In general, the faster the SOP in a link changes the less accurate is the polarization tracking for measuring DGD in the link. The histogram for the DGD measured by polarization tracking is given in figure 5.10. The  $3\sigma$  width for polarization tracking is found to be 15ps. The summary of the DGD statistics measured using polarization scrambling and polarization tracking is given in Table 5.2. It should be noted

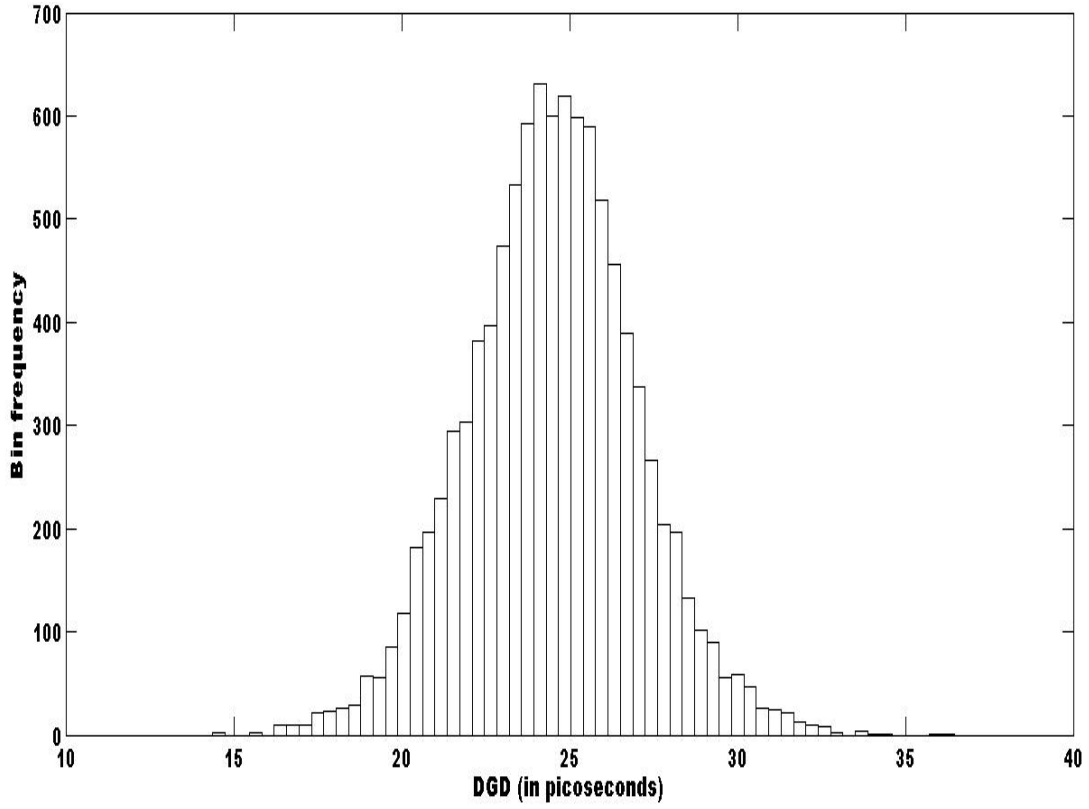


**Figure 5.10.** Histogram for DGD calculated by the PMD monitor using polarization tracking for the PMD emulator experiment

that the number of DGD samples extracted from tracking is considerably lesser than scrambling because of changes in SOP during a measurement cycle.

Attributes	Polarization scrambling	Polarization tracking
Measurement time	730 minutes	730 minutes
Mean value of DGD	25.8 ps	25.2 ps
Standard deviation of DGD	1.62 ps	2.5 ps
Width of the distribution	9.7 ps	15.3 ps

**Table 5.2.** DGD statistics for the PMD emulator experiment.

## 5.3 PMD monitor in field measurement trial

The coherent PMD monitor was used to measure DGD in optical switch stations in Kansas City, Kansas and Sprint laboratories in San Francisco, California. This section discusses the results of the field trials.

### 5.3.1 Trials in optical switch station for polarization scrambling

The field tests were conducted from the 11<sup>th</sup> to the 23<sup>rd</sup> June, 2008, in the optical switch station at Kansas City, Kansas. The DGD was measured on the fiber optic link from Kansas City to Chicago, IL. In the field test, the channel for which DGD is to be monitored is chosen using a tunable filter which selects only the frequency region of interest. Then a portion of signal is tapped from the live traffic and an erbium doped fiber amplifier (EDFA) is used to boost the optical signal power to -15 dB. Then the signal is fed to the PMD monitor. The frequency of the LO is tuned so that the center frequency of the LO is offset by 25GHz to the peak frequency of the channel. Data is then collected for a period of 1 to 10 days. Then DGD values are extracted by post processing. The histogram for the DGD data measured by the PMD monitor is given in figure 5.11 As proved theoretically, the expected distribution of the measured DGD using our measurement technique is Rayleigh and not Maxwellian. From the figure 5.11, it can be inferred that the measured distribution is closer to a Rayleigh distribution. The mean value of the DGD measured by the PMD monitor is 8.83 ps. This is the apparent DGD of the probing signal. The true DGD of the fiber is 11.42 ps which is as a result of the multiplication factor  $4/\pi$  relating the true and apparent DGD of the fiber. The plot for the DGD collected is shown in figure 5.12. Numerical simulation have been carried out by others for PMD induced system impairments and the

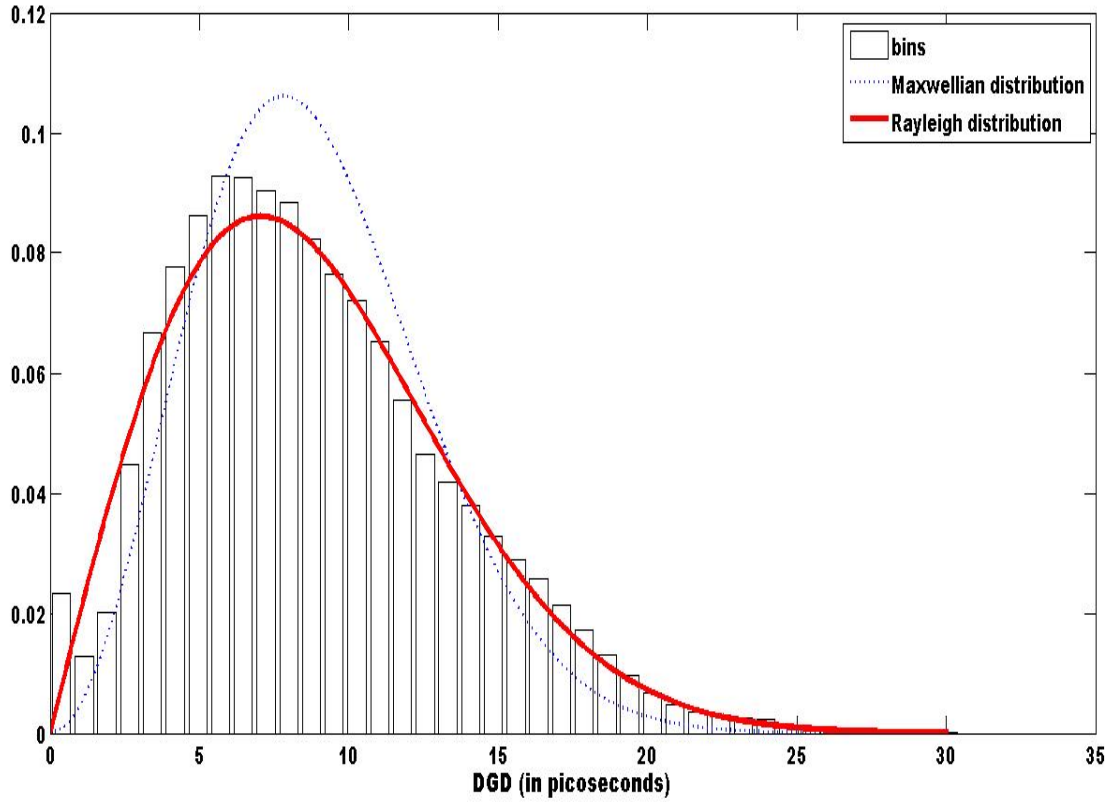


**Figure 5.11.** Histogram for DGD calculated by the PMD monitor using polarization scrambling for the KC-Chicago fiber optic link

result in [9] are very similar to the results in figure 5.11. The DGD statistics of the measured data are given in the table 5.3

Statistics	Values
No of samples	606380
Measurement speed	1 DGD value in 2 seconds
Mean of the measured DGD	8.83 ps
Mean of the true DGD	11.42 ps
Minimum value of DGD	0 ps
Maximum value of DGD	30.43ps
Correlation time of the data	28 minutes

**Table 5.3.** DGD statistics for the measurement trial with polarization scrambling



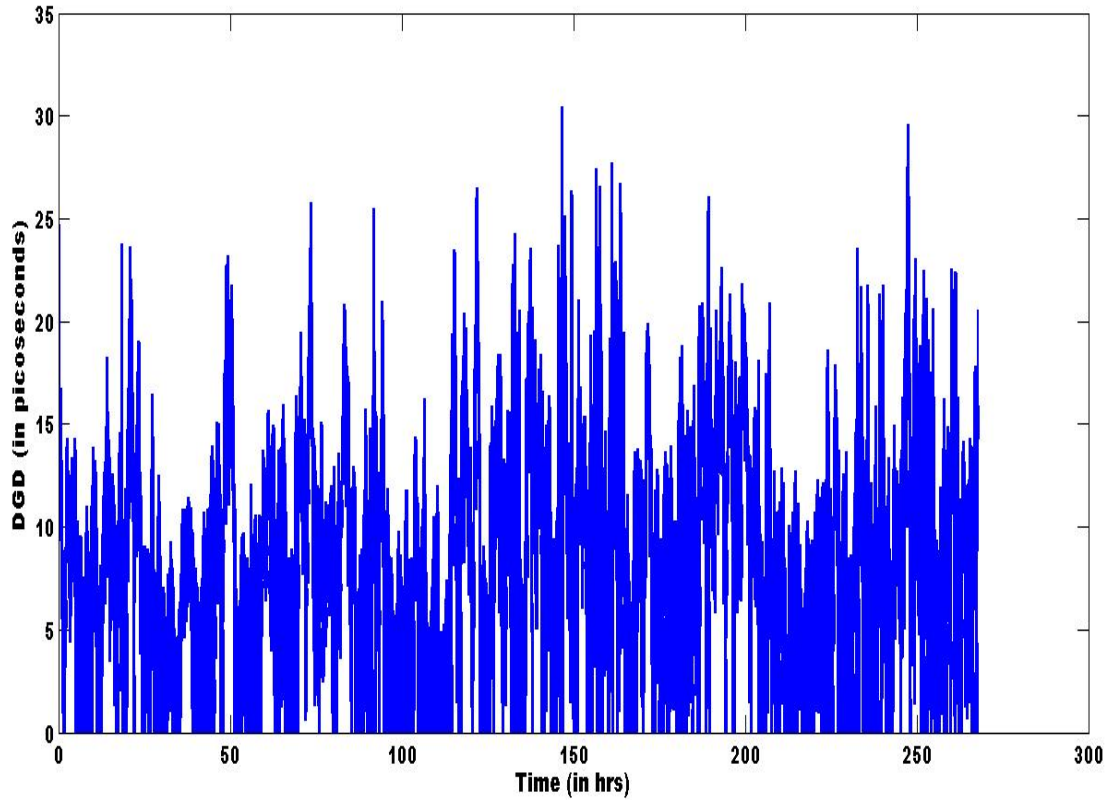


**Figure 5.12.** Plot for DGD calculated by the PMD monitor using polarization scrambling for the KC-Chicago fiber optic link

### 5.3.2 Field trial results of polarization tracking

A laboratory test with fiber spools of 700 km length was conducted in the Sprint research laboratories in San Francisco, CA. The time interleaved implementation of polarization scrambling and tracking was used to measure DGD in this case. The histogram for DGD data measured by the PMD monitor is given in the figure 5.13 From the figure, the distribution of the measured DGD is closer to a Rayleigh distribution than the Maxwellian distribution. The mean value of DGD measured by the PMD monitor is 2.9 ps. This is the apparent DGD of the probing signal. The true DGD of the fiber is 3.82ps. The plot for DGD data collected for close to 14 hrs is shown in the figure 5.12 The correlation time for

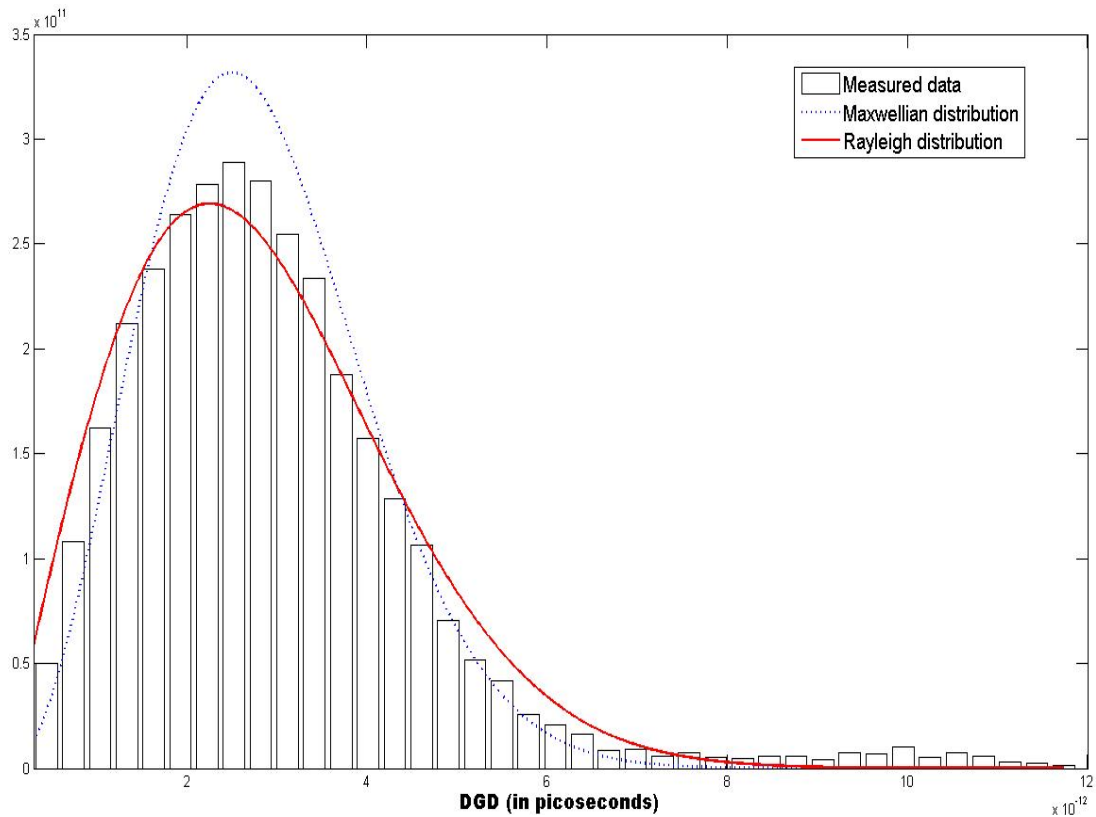


**Figure 5.13.** Histogram for DGD calculated by the PMD monitor using polarization tracking

the measured data is found to be 7 minutes. Since the time for which the data is collected is much greater than the correlation time of the measured data, a fairly accurate distribution is achieved inside a day. Table 5.4 presents the statistics of DGD data for the measurement trial.

## 5.4 DGD measurement of a scrambled input signal

In this test, the incoming signal from the WDM system is fed to a PMD emulator that introduces a DGD of 40 ps. Also the input signal is polarization scrambled at the rate of a few Hz. Then, this signal is launched into a fiber spool of length of a few hundred kilometers. Thus the input signal whose DGD

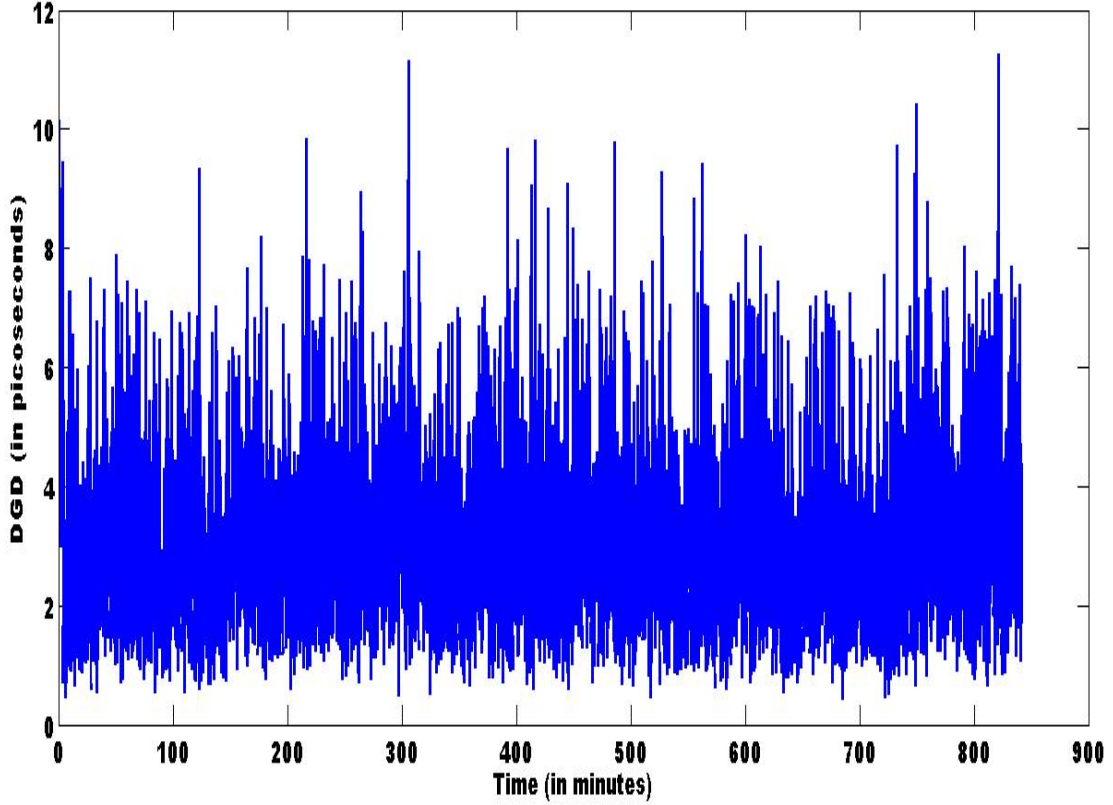


**Figure 5.14.** Plot for DGD calculated by the PMD monitor using polarization tracking

Statistics	Values
No of samples	26213
Measurement speed (Average)	3 DGD values/second
Mean of the measured DGD	2.9 ps
Mean of the true DGD	3.83 ps
Minimum value of DGD	0 ps
Maximum value of DGD	12.1ps
Correlation time of the data	17 minutes

**Table 5.4.** DGD statistics for the measurement trial with polarization tracking

is to be measured is unstable. So the DGD measured by the coherent PMD monitor is the root mean square DGD and not the average DGD. The rms DGD is proportional to DGD with the proportionality constant being the cosine square function. As a result the mean DGD measured by the PMD monitor is the average of the rms DGD which is equal to the true DGD divided  $\sqrt{2}$ . Hence we should measure a mean DGD of around  $40/\sqrt{2}$  which is 28.2ps. Figure 5.15 shows the DGD measured by the PMD monitor using scrambling and the figure 5.16 shows the DGD plot for the same experiment whose DGD is measured by tracking. Though, the test was conducted only for a period of 15 minutes, the mean DGD measured using scrambling is 27.9ps. Hence, this test serves as another validation of both polarization scrambling and polarization tracking. The mean value of the polarization tracking measurement is 27.8ps. The correlation time for this measurement is 2 seconds.

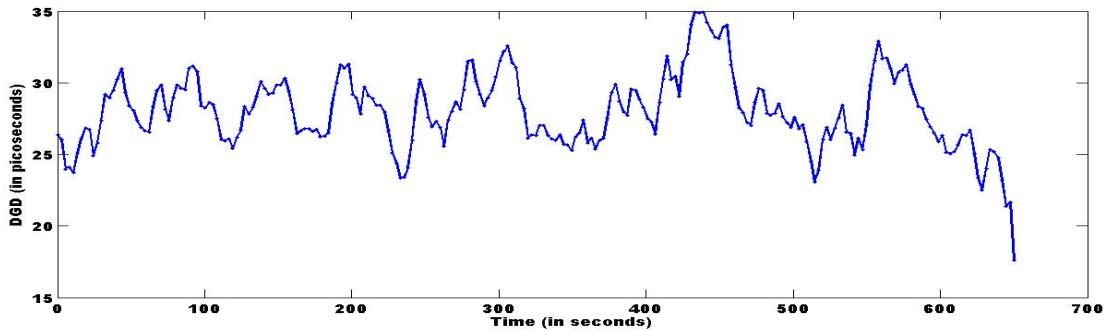


**Figure 5.15.** Plot for DGD calculated by the PMD monitor using polarization scrambling for an unstable probing signal

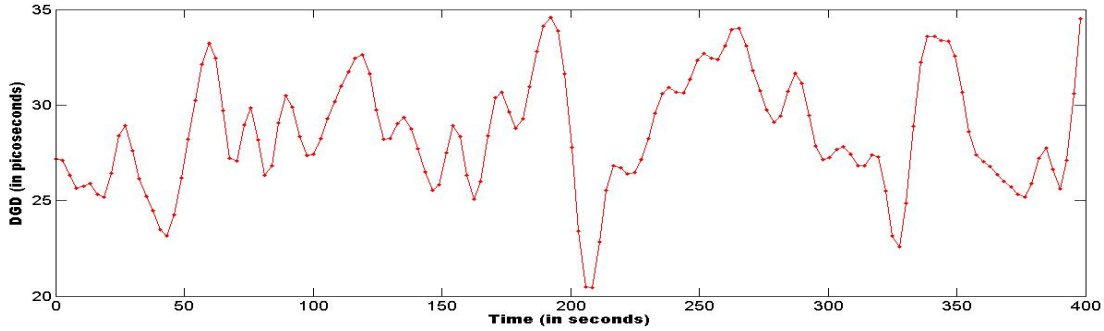


**Figure 5.16.** Plot for DGD calculated by the PMD monitor using polarization tracking for an unstable probing signal

## 5.5 Run time implementation of polarization tracking

### 5.5.1 Hardware and Software used for real time DGD calculation

The need for real time data processing to extract DGD data was already emphasized. A run time implementation will reduce the memory requirements greatly. The hardware for implementing the polarization tracking real time is the same as the one used for polarization tracking with the exception that the DAQ is not required. The microcontroller is used to sample the two channels once a global maximum is reached after the tracking algorithm. The data is sent through a RS 232 serial port interface between the microcontroller and the serial port of the computer. Due to the limitations of the microcontroller data transfer protocol (RS232), the number of samples that can be acquired for a stable global maximum is lower than when using a faster transfer protocol like the USB in the case of DAQ board. So, three samples per acquisition are averaged per tracking cycle. The DGD extraction algorithm is the same as the one described in section 4.6.1. The algorithm for acquiring the data from the microcontroller and DGD calculation is given by the flowchart in figure 5.17.

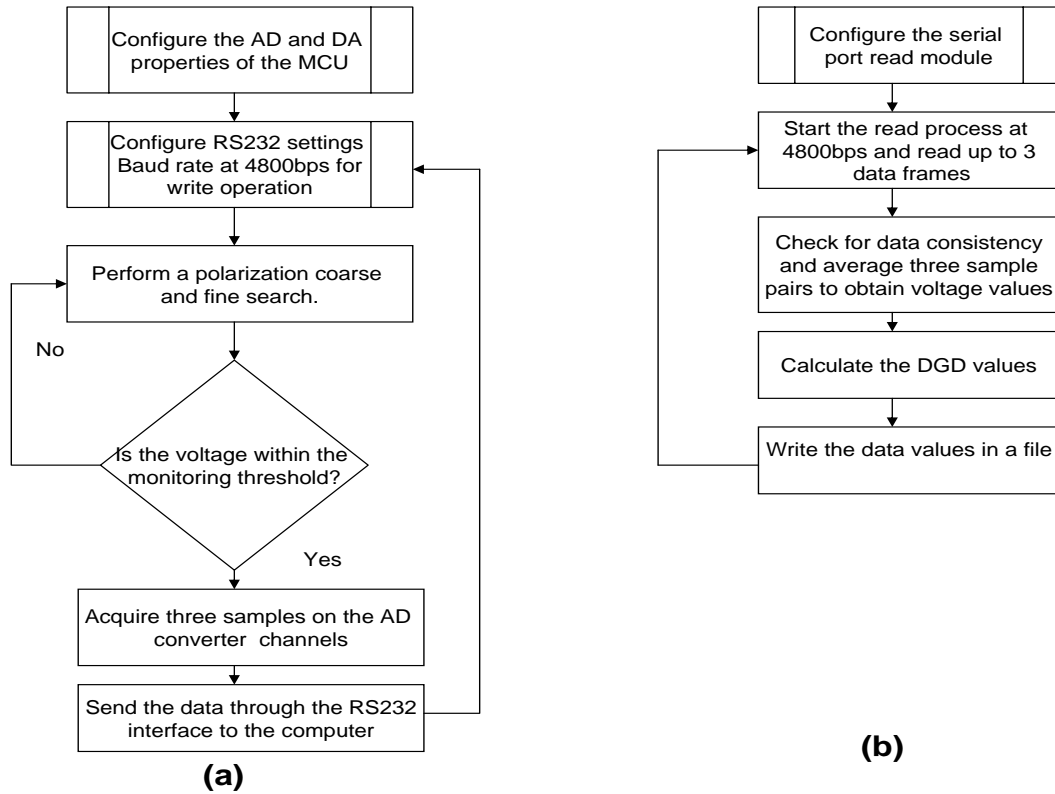


**Figure 5.17.** Algorithm for run time extraction of DGD (a) The MCU algorithm for tracking and (b)The software algorithm for DGD calculation in run time

### 5.5.2 Test for real time implementation using polarization tracking

The run time implementation using polarization tracking has already been described. In this section, its obvious advantages come to view. The test was conducted for a period of 880 minutes. The histogram of the measurement is given in figure 5.18. We can observe that the loss of the ability to average the samples has in fact led to a less accurate DGD measurement of the PMD monitor. Though the mean DGD of the PM fiber agrees with the time interleaved implementation of scrambling and tracking and distribution is still close to a normal distribution, the  $3\sigma$  width is larger and this might lead to more error in the DGD measurement

in field trials. The statistics of the DGD data collected is shown in the table 5.5.

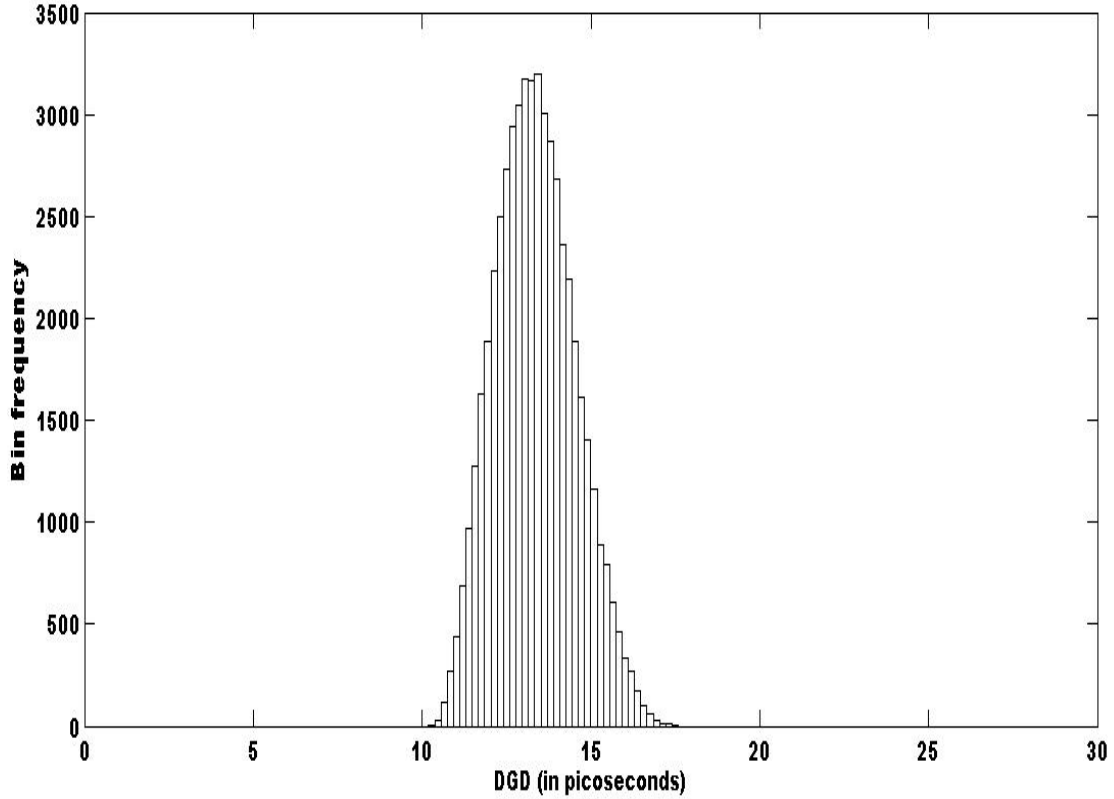


**Figure 5.18.** Histogram for DGD calculated real time by the PMD monitor using polarization tracking

Statistics	Values
No of samples	262,566
Mean of the measured DGD	13.5ps
Measurement speed	4 values/second
Minimum value of DGD	11.1ps
Maximum value of DGD	17ps
Standard deviation	1.1 ps
Width of the distribution	4.2 ps

**Table 5.5.** DGD statistics for the run time implementation of the PMD monitoring with polarization tracking

# Chapter 6

## Summary

### 6.1 Conclusion

An in - situ PMD measurement technique has been proposed and two algorithms have been implemented to measure the DGD of fiber optic links. Experiments have been conducted to characterize the PMD monitor and the effectiveness of the two algorithms in measuring PMD in different conditions has been presented. It has also been established through analysis that DGD measured by the PMD monitor is the apparent DGD as measured by the probing signal. An expression for the relationship between the true DGD and the apparent DGD of the fiber is derived. It has also been proven that the distribution of the apparent DGD is Rayleigh unlike the true DGD which follows a Maxwellian distribution. The theoretical analysis agree well wwith the measured DGD data for both the algorithms. It has also been established by theory and analysis that the polarization tracking is more advantageous than polarization scrambling in terms of speed and ease of data processing. For slow changes in DGD, it has been proven experimentally that the two algorithms agree with each other closely. As dis-



cussed in the PMD emulator experiment, the tracking algorithm is less accurate than scrambling for faster changes in SOP or DGD of the incoming signal. This report also presents a detailed discussion on polarization in lightwave systems, the origin, causes and effects of PMD, an overview of PMD measurement techniques and their relative effectiveness and limitations.

## 6.2 Future work

It should be noted that although the use of polarization tracking has been validated by experiments and field trials, the limitations of the hardware and software used for research have restricted the run-time implementation of the polarization tracking for PMD monitoring in traffic carrying fibers. Herein lies the scope for future work. The use of high speed hardware and software with multi threading capabilities will allow the run time implementation and will further increase the speed of DGD measurements for field trials. For instance, the use of a faster polarization controller will allow higher loop bandwidth for tracking algorithms. Although the tracking algorithm can yield a DGD value every 11 ms, the repetition rate of polarization controller used here is limited to 1 KHz. Using a polarization controller with faster repetition rate and response time can greatly increase the loop bandwidth. These upgrades would make the coherent PMD monitor suitable for field measurements of links with faster DGD changes.

# References

- [1] G. Agrawal. *Fiber-Optic Communication Systems*. Wiley-Interscience, 2002.
- [2] C. Allen. PMD Characterization on an Active Fiber Link: Final Report.
- [3] C. Allen, P. Kondamuri, D. Richards, and D. Hague. Measured temporal and spectral PMD characteristics and their implications for network-level mitigation approaches. *Lightwave Technology, Journal of*, 21(1):79–86, 2003.
- [4] M. Boroditsky, M. Brodsky, N. Frigo, P. Magill, and J. Evankow. Estimation of eye penalty and PMD from frequency-resolved in-situ SOP measurements. *Lasers and Electro-Optics Society, 2004. LEOS 2004. The 17th Annual Meeting of the IEEE*, 1, 2004.
- [5] M. Boroditsky, M. Brodsky, N. Frigo, P. Magill, and L. Raddatz. In-service measurements of polarization-mode dispersion and correlation to bit-error rate. *Photonics Technology Letters, IEEE*, 15(4):572–574, 2003.
- [6] M. Boroditsky, M. Brodsky, N. Frigo, P. Magill, and L. Raddatz. Technique for in-situ measurements of polarization mode dispersion. *Optical Fiber Communications Conference, 2003. OFC 2003*, pages 224–225, 2003.
- [7] J. Damask. *Polarization Optics In Telecommunications*. Springer, 2005.
- [8] D. Derickson. Fiber optic test and measurement. *Fiber optic test and measurement/edited by Dennis Derickson. Upper Saddle River, NJ: Prentice Hall, c1998.*, 1998.

- [9] J. Elbers, C. Glingener, M. Duser, and E. Voges. Modelling of polarisation mode dispersion in singlemode fibres. *Electronics Letters*, 33(22):1894–1895, 1997.
- [10] B. Fu and R. Hui. Fiber chromatic dispersion and polarization-mode dispersion monitoring using coherent detection. *Photonics Technology Letters, IEEE*, 17(7):1561–1563, 2005.
- [11] N. Gisin, R. Passy, and J. Von der Weid. Definitions and measurements of polarization mode dispersion: interferometric versus fixed analyzer methods. *Photonics Technology Letters, IEEE*, 6(6):730–732, 1994.
- [12] J. Hansryd, H. Sunnerud, P. Andrekson, and M. Karlsson. Impact of PMD on four-wave-mixing-induced crosstalk in WDM systems. *Photonics Technology Letters, IEEE*, 12(9):1261–1263, 2000.
- [13] B. Heffner. PMD measurement techniques—a consistent comparison. *Optical Fiber Communications, 1996. OFC’96*, pages 292–293.
- [14] B. Heffner. Automated measurement of polarization mode dispersion using Jones-matrix eigenanalysis. *Photonics Technology Letters, IEEE*, 4(9):1066–1069, 1992.
- [15] F. Heismann. Tutorial: Polarization mode dispersion: Fundamentals and impact on optical communication systems. *Optical Communication, 1998. 24th European Conference on*, 2, 1998.
- [16] R. Hui, R. Saunders, B. Heffner, D. Richards, B. Fu, and P. Adany. Non-blocking PMD monitoring in live optical systems. *Electronics Letters*, 43(1):53–54, 2007.
- [17] R. Jopson, L. Nelson, and H. Kogelnik. Measurement of second-order polarization-mode dispersion vectors in optical fibers. *Photonics Technology Letters, IEEE*, 11(9):1153–1155, 1999.
- [18] I. Kaminow and T. Koch. *Optical Fiber Telecommunications III*. Academic Press, 1997.
- [19] I. Kaminow and T. Li. *Optical Fiber Telecommunications IV-A: Components*. Academic Press, 2002.

- [20] M. Karlsson. Polarization mode dispersion induced pulse broadening in optical fibers. *Optics Letters*, 23(9):688–690, 1998.
- [21] M. Karlsson. Probability density functions of the differential group delay in optical fiber communication systems. *Lightwave Technology, Journal of*, 19(3):324–331, 2001.
- [22] H. Kogelnik, R. Jopson, and L. Nelson. Polarization-mode dispersion. *Optical Fiber Telecommunications IV B*, pages 725–861.
- [23] C. Poole and J. Nagel. Polarization Effects in. *Optical Fiber Telecommunications III*, 1997.
- [24] C. Poole and R. Wagner. Phenomenological approach to polarisation dispersion in long single-mode fibres. *Electronics Letters*, 22:1029, 1986.
- [25] S. Song, C. Allen, K. Demarest, and R. Hui. A novel method for measuring polarization-mode dispersion using four-wave mixing. *Lightwave Technology, Journal of*, 17(12):2530–2533, 1999.
- [26] S. Wang, A. Weiner, M. Boroditsky, and M. Brodsky. Non-intrusive estimation of PMD-induced penalty via high speed, high resolution spectral polarimeter. *Optical Fiber Communication Conference, 2006 and the 2006 National Fiber Optic Engineers Conference*, page 3, 2006.
- [27] P. Williams. PMD measurement techniques-avoiding measurement pitfalls. *Venice Summer School on Polarization Mode Dispersion, Venice, Italy, June*, pages 24–26, 2002.

# Appendix A

## Microcontroller code for polarization tracking and scrambling

```
/* **** */
/* Program for polarisation tracking algorithm */
/* Sathyanarayanan Sundhararajan , Lightwave laboratory ,ITTC KU */
/* **** */
#define START 0x0800
#define STOP 0x0FFF
#define DELAY 100
#define DELAY1 100
#define DELAY2 20
#define TRACKSTEPSIZE 0x005
#define SCRSTEPSIZE 0x010
#define SCRSTEPSIZE1 0x010
int poscell0,poscell1,poscell0min,poscell1min;
int globalmaximum1,globalminimum1;
#include <aduc7026.h>
void ADCpoweron(int);
void delay(int);
void initialize_AD_DA_channels();
```

```

void initialize_UART(void);
void senddata(short);
char hex2ascii(char);
int findmax(int *,int);
int polscramble(int);
float getdata(int);
int poltracking(int);
int poltrackingmin(int);
void sendserialdata(int);
int monitor(void);
void initialize_AD_DA_channels()
{

/* INITIALISES AD AND DA CONVERTERS ON THE ADUC7026 MCU */

ADCpoweron(20000); // power on ADC
GP4DAT = 0x04000000;
REFCON = 0x01; // internal 2.5V reference
DAC0CON = 0x13;
DAC1CON= 0x13; // configuring DAC0,DAC1, DAC2, DAC3
DAC2CON= 0x13;
DAC3CON= 0x13;
}

void initialize_UART()
{

GP0CON = 0x100000; // Enable ADCbusy on P0.5
GP1CON = 0x011; // Setup tx & rx pins on P1.0 and P1.1

// Setting up UART at 9600 (CD=0)

COMCON0 = 0x80; // Setting DLAB
COMDIV0 = 0x44;
COMDIV1 = 0x00;
COMCON0 = 0x07; // Clearing DLAB
}

void ADCpoweron(int time)
{

```

```

ADCCON = 0x620;    // power-on the ADC
while (time >=0)   // wait for ADC to be fully powered on
    time--;
}

void delay (int length)
{
while (length >=0)
    length--;
}

void senddata(short to_send)
{

while(!(0x020==(COMSTAO & 0x020))){}
COMTX = 0xA;
while(!(0x020==(COMSTAO & 0x020))){}
COMTX = 0xD;

while(!(0x020==(COMSTAO & 0x020))){}
COMTX = hex2ascii ((to_send >> 8) & 0x0F);
while(!(0x020==(COMSTAO & 0x020))){}
COMTX = hex2ascii ((to_send >> 4) & 0x0F);
while(!(0x020==(COMSTAO & 0x020))){}
COMTX = hex2ascii (to_send & 0x0F);

}
char hex2ascii(char toconv)
{
if (toconv<0x0A)
{
toconv += 0x30;
}
else
{
toconv += 0x37;
}

return (toconv);
}

int polscramble(int k)

```

```

{
int i,j,max=0,flag=1,data=0;
GP4DAT = 0x04040000;
GP4DAT = 0x04000000;
//GP2DAT = 0x04040000;
if (k%2==1)
{
for (i=START;i<=STOP;i+=SCRSTEPSIZE)
{
if(i%2==1)
flag=1;
else
flag=0;
DACODAT=(i<<16);
delay(20);
if (flag==1)
{
for(j=START;j<=STOP;j+=SCRSTEPSIZE1)
{
DAC1DAT=(j<<16);
delay(DELAY1);
}
}
if (flag==0)
{
for(j=STOP;j>=START;j-=SCRSTEPSIZE1)
{
DAC1DAT=(j<<16);
delay(DELAY1);
}
}
}
}
if (k%2==0)
{
for (i=STOP;i>=START;i-=SCRSTEPSIZE)
{
if(i%2==1)
flag=1;
else
flag=0;
DACODAT=(i<<16);
}
}
}

```



```

delay(20);
if (flag==1)
{
    for(j=START;j<=STOP;j+=SCRSTEPSIZE1)
    {
        DAC1DAT=(j<<16);
        delay(DELAY1);
    }
}
if (flag==0)
{
    for(j=STOP;j>=START;j-=SCRSTEPSIZE1)
    {
        DAC1DAT=(j<<16);
        delay(DELAY1);
    }
}
}
return 0;
}
float getdata(int a)
{
    int i;
    float sum=0;
    for(i=0;i<a;i++)
    {
        while(!ADCSTA){}
        sum=sum+(ADCDAT>>16);
    }
    sum=sum/a;
    return(sum);
}
int poltracking(int adchan)
{
    int i,j,max0=0,max1=0,maxpos1=0,maxpos0=0,data0,data1;
    ADCCP=adchan;
    delay(100);
    for(i=START;i<=STOP;i+=TRACKSTEPSIZE)
    {
        DACODAT=(i<<16);
        delay(DELAY);
    }
}

```

```

data0=getdata(1);
if (data0 > max0)
{
max0=data0;
maxpos0=i;
}
}
DACODAT=(maxpos0<<16);
for(j=START;j<=STOP;j+=TRACKSTEPSIZE)
{
DAC1DAT=(j<<16);
delay(DELAY);
data1=getdata(1);
if (data1 > max1)
{
max1=data1;
maxpos1=j;
}
}
DACODAT=(maxpos0<<16);
DAC1DAT=(maxpos1<<16);
poscell0=maxpos0;
poscell1=maxpos1;
globalmaximum1=max1;
return(max1);
}
int poltrackingmin(int adchan)
{
int i,j,max0=STOP,max1=STOP,maxpos1=0,maxpos0=0,data0,data1;
ADCCP=adchan;
delay(100);
for(i=START;i<=STOP;i+=TRACKSTEPSIZE)
{
DACODAT=(i<<16);
delay(DELAY);
data0=getdata(1);
if (data0 <= max0)
{
max0=data0;
maxpos0=i;
}
}
}

```

```

DACODAT=(maxpos0<<16);
for(j=START;j<=STOP;j+=TRACKSTEPSIZE)
{
DAC1DAT=(j<<16);
delay(DELAY);
data1=getdata(1);
if (data1 <= max1)
{
max1=data1;
maxpos1=j;
}
}
DACODAT=(maxpos0<<16);
DAC1DAT=(maxpos1<<16);
poscell0min=maxpos0;
poscell1min=maxpos1;
globalminimum1=max1;
return(max1);
}
int finetrack(int ad){
int x,i,j,k,l,threshold=0x020,a,range,flag=1,flg1=1,prevrange,z;
k = poscell0;
l = poscell1;
range=0x04;
ADCCP=ad;
delay(100);
while (range<0x40)
{
for (i=(poscell0-range); i<=(poscell0+range);i+=0x001)
{
if(i>(poscell0-prevrange) && i < (poscell0+prevrange))
{ i = poscell0+prevrange; }
DACODAT=(i<<16);
delay(DELAY);
while(!ADCSTA){}
if(globalmaximum1<=(ADCDAT>>16))
{
globalmaximum1=(ADCDAT>>16);
k=i;
DACODAT=(k<<16);
delay(30);
}
}
}

```

```

}
poscell0=k;
DAC0DAT=(poscell0<<16);
for (j=(poscell1-range); j<=(poscell1+range);j+=0x001)
{
if(j>(poscell1-prevrage))
{ j = poscell1+prevrage; }
DAC1DAT=(j<<16);
delay(DELAY);
while(!ADCSTA){}
if(globalmaximum1<=(ADCDAT>>16))
{
globalmaximum1=(ADCDAT>>16);
l=j;
DAC1DAT=(l<<16);
delay(30);
}
}
poscell1=l;
DAC1DAT=(poscell1<<16);
while (!ADCSTA){}
x=(ADCDAT>>16);
if (!(x < (globalmaximum1 - threshold)))
{
ADCCP=0;
while(!ADCSTA){}
delay(100);
a=(ADCDAT>>16);
senddata(globalmaximum1);
senddata1(ad);
senddata1(a);
ADCCP=1;
while(!ADCSTA){}
delay(100);
z=(ADCDAT>>16);
senddata1(z);
senddata1(flgl);
ADCCP=ad;
while(!ADCSTA){}
delay(100);
x=(ADCDAT>>16);
return 0;
}

```

```

    }
    prevrange=range;
    range=range+0x004;
}
return 1;
}
int finetrackmin(int ad){
int x,i,j,k,l,threshold=0x020,a,range,flag=1,prevrange,flg1=0,z;
k = poscell0min;
l = poscell1min;
range=0x04;
    ADCCP=ad;
    delay(100);
    while (range<0x40)
    {
    for (i=(poscell0min-range); i<=(poscell0min+range);i+=0x001)
    {

    if(i>(poscell0min-prevrange) && i < (poscell0min+prevrange))
    { i = poscell0min+prevrange; }

    DACODAT=(i<<16);
    delay(DELAY);
    while(!ADCSTA){}
    if(globalminimum1<=(ADCDAT>>16))
    {
    globalminimum1=(ADCDAT>>16);
        k=i;
    DACODAT=(k<<16);
    delay(30);
    }

    }
    poscell0min=k;
    DACODAT=(poscell0min<<16);
    for (j=(poscell1min-range); j<=(poscell1min+range);j+=0x001)
    {
    if(j>(poscell1min-prevrange) && j < (poscell1min+prevrange))
    { j = poscell1min+prevrange; }
    DAC1DAT=(j<<16);
    delay(DELAY);
    while(!ADCSTA){}

```

```

if(globalminimum1<=(ADCDAT>>16))
{
globalminimum1=(ADCDAT>>16);
        l=j;
DAC1DAT=(l<<16);
delay(30);
}
}
poscell1min=l;
DAC1DAT=(poscell1min<<16);
while (!ADCSTA){}
x=(ADCDAT>>16);
if (!(x < (globalminimum1 - threshold)))
{
ADCCP=0;
while(!ADCSTA){}
delay(100);
a=(ADCDAT>>16);
senddata(globalminimum1);
senddata1(ad);
senddata1(a);
ADCCP=1;
while(!ADCSTA){}
delay(100);
z=(ADCDAT>>16);
senddata1(z);
senddata1(flg1);
ADCCP=ad;
while(!ADCSTA){}
delay(100);
x=(ADCDAT>>16);
return 0;
        }
prevrange=range;
range=range+0x004;
}
return 1;
}
int main()
{
int i=0,chan=0,scr_globalmax=0,flg1,trc_globalmax=0;
long max=0x00,max1=0x02;

```

```
initialize_AD_DA_channels();
initialize_UART();
scr_globalmax=polscramble(i);
trc_globalmax=poltracking(i);
trc_globalmax=poltracking(i);
while(1)
{
    GP2DAT = 0x04040000;
    scr_globalmax=polscramble(0);
    GP2DAT = 0x04000000;
    trc_globalmax=poltracking(0);
    flg1=finetrack(0);
    trc_globalmax=poltracking(1);
    flg1=finetrack(1);
    trc_globalmax=poltrackingmin(0);
    flg1=finetrackmin(0);
    trc_globalmax=poltrackingmin(1);
    flg1=finetrackmin(1);
}
return 0;
}
```

# Appendix B

## MATLAB code for acquiring data from the PMD monitor

```
%-----  
% code for acquiring data from PMD monitor  
% written by Sathyanarayanan Sundhararajan  
%-----  
  
    clc;  
    clear all;  
    Data_Folder='Foldername';  
    %Variables Declarations  
    count = 0;  
    % CREATE DEVICE OBJECTS  
    %Analog Input Object  
    ai = analoginput('dtol', 0);  
    ai.InputType = 'SingleEnded';  
    %Digital Input Object for Status Check  
    dio = digitalio('dtol');  
    %ADD CHANNEL 0,1 and 2 to analoginput  
    addchannel(ai, 0:3);    % 3 AIN channels (0 and 1)  
    %CONFIGURE ANALOG INPUT SUBSYSTEM  
    set(ai, 'SampleRate', 50000);  
    set(ai, 'BufferingMode', 'auto');  
    set(ai, 'SamplesPerTrigger', Inf);
```



```

    % External Hardware Trigger
    set(ai, 'TriggerType', 'HwDigital');
    set(ai, 'TriggerRepeat', Inf);
while(1)
    data=[];
    data1=[];
    i=1;
    while (i <=4)
        start(ai);
        data1 = getdata(ai,50000);
        data=[data;data1];
        stop(ai);
        i=i+1;
    end
    plot(data);
    StartTime=datetime(clock);
    %-----
    %Write data to file:
    %-----
if isdir(Data_Folder) ~= true
    mkdir(Data_Folder);
end
TimeStamp = datestr(StartTime, 'mmm_dd_yyyy_HH-MM-SS');
i=1;
FilePath = sprintf('%s\\Scr_%s_%i.txt', Data_Folder, TimeStamp, i);
fid = fopen(FilePath, 'w');
fprintf(fid, '%4.4f\t%4.4f\t%4.4f\r\n', data');
fclose(fid);
end

```

# Appendix C

## MATLAB code for extracting DGD from polarization tracking data

```
%-----  
% code for acquiring data from PMD monitor  
% data processing code written by Sathyanarayanan Sundhararajan  
% file access part of the code by Peter Adany and Junfeng Jiang  
%-----  
clc;  
clear all;  
%paramters:  
Wavelen = 1;      %select wavelength number  
    T = 1;        %s   Enter time duration of each file  
NtoLoad = 1;      %# files to load  
NpksLoc = 50;     %# peaks to find  
GoBackN = 1e9;  
    Thresh = 0.99; %    amplitude thershold value  
%1) Get the list of file names from the given folder:  
disp('Getting file names...')  
    Dir = uigetdir(cd, 'Please select PMD_Data folder');  
    Fldr = Dir(max(regexp(Dir, '\')+1):end);
```

```

    % cd(Dir) %% Set "Dir" as the current directory
    Dir = sprintf('%s\\',Dir)
    Ext = '.txt';
    FilePathString = [Dir '*' Ext]
    %get file names:
    Files = dir(FilePathString);
    if isempty(Files),error('no files found!'),end;
    normmatrix=[];
    %2) Sort the files into chronological order
    FileCnt = length(Files);
    Date = zeros(FileCnt,3);
    for i=1:FileCnt
        NameString = Files(i).name;
        Date(i,1) = i;
        NameStringEnd = max(regexp(NameString, '.txt'))-3;
        Date(i,2) = datenum(NameString(15:NameStringEnd))
        Date(i,3) = Wavelen;
    end
    Date = sortrows(Date,2);
    %plot dates:
    %plot(Date(:,2)-Date(1,2),'.')
    ValidInd = find(Date(:,3)==Wavelen);
    Date = Date(ValidInd,:)
    Nfile = length(Date);
    clc;
    Data2=[];
    mindgd=[];dgd1=[];time=[];
    %3)Load up #NtoLoad files at a time
    SetInd = max(Nfile-GoBackN,1):NtoLoad:Nfile;
    SetLen = length(SetInd);
    val=1;
    for i0=1:SetLen
        data=[];
        FilesIndex = SetInd(i0);
        %load #(NtoLoad) data sets:
        i1 = FilesIndex;
        i2 = min(FilesIndex+NtoLoad-1,Nfile);
        y=[];
        m = 1;
        for k = i1:i2
            DataIn = load([Dir Files(Date(k,1)).name])/1e3;
            FilePath=[Dir Files(Date(FilesIndex,1)).name];

```

```

    fid = fopen(FilePath,'r');
    %%Read data in column
    Data1= fscanf(fid,'%g %g %g', [3 200000]);
    s=Data1';
    fclose(fid);
    m=1;
    ind=[4,1];
        for j=1:50000:200000
            for i=j:length(s)
                if (s(i,3) < 1)
                    break
                end
            end
            ind(m)=i;
            m=m+1;
        end
        data=[];
    %%Extracting tracking data from the text file
    for i=1:4
        trackingdata=[s((ind(i):50000*i),1) s((ind(i):50000*i),2)] ;
        for l=1:length(trackingdata)-3
            trackingdata(l)= (trackingdata(l)+ trackingdata(l+1)+
            trackingdata(l+2)+ trackingdata(l+3))/4;
        end
        a=sortrows(trackingdata(:,1));
        b=sortrows(trackingdata(:,2));
        maxthreshold=mean(a(end-20:end));
        %%Extracting values for normalization
        V11=mean(trackingdata((3000:3500),1));
        V21=mean(trackingdata((3000:3500),2));
        V22=mean(trackingdata((6800:7300),2));
        V12=mean(trackingdata((6800:7300),1));
        V13=mean(trackingdata((10600:11000),1));
        V23=mean(trackingdata((10600:11000),2));
        V14=mean(trackingdata((14400:14900),1));
        V24=mean(trackingdata((14400:14900),2));
        dev11=sqrt(var(trackingdata((3000:3500),1)));
        dev22=sqrt(var(trackingdata((6800:7300),2)));
        dev13=sqrt(var(trackingdata((10600:11000),1)));
        dev24=sqrt(var(trackingdata((14400:14900),2)));
        if ((V11 > 0.98*maxthreshold))
            if ( (dev11 < 0.02) && (dev22 < 0.02) &&

```

```

    (dev13 < 0.02) && (dev24 < 0.02))
    dpp1=(V14-V13)/(V11-V13);
    dpp2=(V23-V24)/(V22-V24);
    phy=asin(0.5*(sqrt(dpp1)+sqrt(dpp2)));
    dgd(val)=abs(phy/pi/1e10);
    mean(dgd)
    plot(dgd)
    length(dgd)
    timebase(val)=i0*4+i;
    val=val+1;
    end
end
end
end
end
figure(1)
hist(dgd.*1e12,100);
figure(2)
plot(timebase,dgd*1e12);
title('DGD')
%save result:
u = [timebase' (dgd')];
FileName1 = sprintf('%sDGD_Data_.txt',Foldr);
fp=fopen(FileName1,'w');
fprintf(fp,'%3.10e\t %3.10e\r\n',u);

```

# Appendix D

## MATLAB code for extracting DGD from polarization scrambling data

```
%-----  
%MATLAB code to calculate DGD from polarization scrambling data  
%Peter Adany  
%09/14/2007 Revised by Jiang Junfeng  
%07/13/2008 Revised by Sathyanarayanan Sundhararajan  
%-----  
clc;  
clear all;  
%paramters:  
Wavelen = 1;      %select wavelength number  
      T = 1;      %s   Enter time duration of each file  
NtoLoad = 1;      %# files to load  
NpksLoc = 50;     %# peaks to find  
GoBackN = 1e9;  
      Thresh = 0.99; %   amplitude thershold value  
%1) Get the list of file names from the given folder:  
disp('Getting file names...')  
      Dir = uigetdir(cd, 'Please select PMD_Data folder');
```

```

    Foldr = Dir(max(regex(Dir,'\')+1):end);
    % cd(Dir) %% Set "Dir" as the current directory
    Dir = sprintf('%s\\',Dir)
    Ext = '.txt';
FilePathString = [Dir '*' Ext]
%get file names:
Files = dir(FilePathString);
if isempty(Files),error('no files found!'),end;
normmatrix=[];
%2) Sort the files into chronological order
FileCnt = length(Files);
Date = zeros(FileCnt,3);
for i=1:FileCnt
    NameString = Files(i).name;
    Date(i,1) = i;
    NameStringEnd = max(regex(NameString,'.txt'))-3;
    Date(i,2) = datenum(NameString(15:NameStringEnd))
    Date(i,3) = Wavelen;
end
    Date = sortrows(Date,2);
    %plot dates:
    %plot(Date(:,2)-Date(1,2),'.')
    ValidInd = find(Date(:,3)==Wavelen);
    Date = Date(ValidInd,:);
    Nfile = length(Date);
    clc;
Data2=[];
mindgd=[];dgd1=[];time=[];
%3)Load up #NtoLoad files at a time
SetInd = max(Nfile-GoBackN,1):NtoLoad:Nfile;
SetLen = length(SetInd);
val=1;
for i0=1:SetLen
    data=[];
    FilesIndex = SetInd(i0);
    %load #(NtoLoad) data sets:
    i1 = FilesIndex;
    i2 = min(FilesIndex+NtoLoad-1,Nfile);
    y=[];
    m = 1;
    for k = i1:i2
        DataIn = load([Dir Files(Date(k,1)).name])/1e3;

```

```

        FilePath=[Dir Files(Date(FilesIndex,1)).name];
        fid = fopen(FilePath,'r');
        %%Read data in column
        Data1= fscanf(fid,'%g %g %g', [3 200000]);
        s=Data1';
        fclose(fid);
        m=1;
%%revised by sathya
%%extracting scrambling data from text file
for start=1:50000:200000
    for l=start:length(DataIn)
        if (DataIn(l,3) < 1)
            break
        end
    end
    ind(m)=l;
    m=m+1;
end
data=[];
val=1;
start=1;
for l=1:4
scramblingdata=[DataIn((start+2000:ind(l)-2000),1)
                DataIn((start+2000:ind(l)-2000),2)] ;
start=start+50000;
y= scramblingdata;
%Get time base:
    if i0==1
        %Fs = length(y)/T;           %%????
        Fs=length(y)/(NtoLoad*T);
    end
    N = length(y);
    t = linspace(0,N/Fs,N);
%Apply boxcar lowpass filter:
    FilterSelection=1;
    Nf1 = round(N/10);
    yy1=(fft(y(:,1)));
    yy2=(fft(y(:,2)));
    yy1(Nf1:(N-Nf1))=0;
    yy2(Nf1:(N-Nf1))=0;
    yy11=real(ifft(yy1));
    yy22=real(ifft(yy2));

```



```

%normalize:
y1=(yy11-min(yy11))/max(yy11-min(yy11));
y2=(yy22-min(yy22))/max(yy22-min(yy22));
Flag_MaximumOrMimimum=1 ; %0-----Maximum search
%%1-----Minimum search
if Flag_MaximumOrMimimum==1
y1=1-y1;
y2=1-y2;
end
%peak search:
Athr = Thresh+0*t; %amplitue threshold
Zone1 = max(y1',Athr)-Athr; %find peaks above level
Zone2 = max(y2',Athr)-Athr;
%get the peak indeces:
i=0;
Peak1=[];
Ipk1=[];
while sum(Zone1.^2)>0 && i<NpksLoc
i=i+1;
[Peak1(FilesIndex,i) Ipk1(FilesIndex,i)] = max(Zone1);
Inot1 = find(y1' < Athr);
Il1 = Inot1(max(find(Inot1 < Ipk1(i))));
Ih1 = Inot1(min(find(Inot1 > Ipk1(i))));
if isempty(Il1);Il1=1;end
%remove used-up peak from the search:
Zone1([Il1:Ih1]) = 0;
end
i=0;
Peak2=[];
Ipk2=[];
while sum(Zone2.^2)>0 && i<NpksLoc
i=i+1;
[Peak2(FilesIndex,i) Ipk2(FilesIndex,i)] = max(Zone2);
Inot2 = find(y2' < Athr);
Il2 = Inot2(max(find(Inot2 < Ipk2(i))));
Ih2 = Inot2(min(find(Inot2 > Ipk2(i))));
if isempty(Il2);Il2=1;end
if isempty(Ih2);Ih2=1;end
%remove used-up peak from the search:
Zone2([Il2:Ih2]) = 0;
end
%%-----

```

```

Flag_InverseSearch=0;
if Flag_InverseSearch==1
%%-----Inverse search again ---Minnum----Begin
y1MeanMax=mean(y1(Ipk1(FilesIndex)))
pos1 = find((y1'-y1MeanMax)>0);
y1(pos1)=0;
y1Inverse=(-y1+y1MeanMax)/y1MeanMax;
y1=y1Inverse;
y2MeanMax=mean(y2(Ipk2(FilesIndex)))
pos2 = find((y2'-y2MeanMax)>0);
y2(pos2)=0;
y2Inverse=(-y2+y2MeanMax)/y2MeanMax;
y2=y2Inverse;

%peak search:
Athr = Thresh+0*t; %amplitude threshold
Zone1 = max(y1',Athr)-Athr;
Zone2 = max(y2',Athr)-Athr;
%get the peak indeces:
i=0;
while sum(Zone1.^2)>0 && i<NpksLoc
i=i+1;
Peak1(FilesIndex,i) Ipk1(FilesIndex,i)] = max(Zone1);
Inot1 = find(y1' < Athr);%find indeces below thresh
Il1 = Inot1(max(find(Inot1 < Ipk1(i))));
Ih1 = Inot1(min(find(Inot1 > Ipk1(i))));
if isempty(Il1);Il1=1;end
%remove used-up peak from the search:
Zone1([Il1:Ih1]) = 0;
end
i=0;
while sum(Zone2.^2)>0 && i<NpksLoc
i=i+1;
[Peak2(FilesIndex,i) Ipk2(FilesIndex,i)] = max(Zone2);
Inot2 = find(y2' < Athr);
Il2 = Inot2(max(find(Inot2 < Ipk2(i))));
Ih2 = Inot2(min(find(Inot2 > Ipk2(i))));
if isempty(Il2);Il2=1;end
if isempty(Ih2);Ih2=1;end
%remove used-up peak from the search:
Zone2([Il2:Ih2]) = 0;
end

```

```

end
%%-----
%calculate DGD from the collected points:
dpp1 = sqrt(y1(Ipk2(FilesIndex)));
dpp2 = sqrt(y2(Ipk1(FilesIndex)));
dpp = 0.5*(mean(dpp1)+mean(dpp2));%???
phy = acos(dpp);
dgd(1) = phy/pi/1e10;
pause(.1);
end
dgd1=[dgd1 dgd];
end
end
t_d=(Date(end,2)-Date(1,2))*60*60*24;
t_d=linspace(0,t_d,length(dgd1));
figure(1)
hist(dgd1.*1e12,100);
figure(2)
plot(t_d,dgd1*1e12);
title('DGD')
%save result:
u = [t_d' abs(dgd1')];
FileName1 = sprintf('%sDGD_Data.txt',Foldr);
fp=fopen(FileName1,'w');
fprintf(fp,'%30.20e\t %30.20e\r\n',u);
fclose(fp)

```

# Appendix E

## Visual Studio 2005 C sharp code for acquiring data from the PMD monitor

```
using System;
using System.Collections.Generic;
using System.ComponentModel;
using System.Data;
using System.Drawing;
using System.Text;
using System.Windows.Forms;
using System.IO;
using System.IO.Ports;
using System.Net.Sockets;
using System.Net;

namespace serialtest2
{
public partial class Form1 : Form
{
    SerialPort serial = new SerialPort("COM1", 9600, Parity.None);
    // Defining a serial port
```

```

Socket clientSocket = null;// creating client socket
EndPoint epServer; //Creating endpoint
StreamWriter sw;
bool b = false;
bool brk = false;
public Form1()
{
InitializeComponent();
}
private void button2_Click(object sender, EventArgs e)
{
    b = true;
    sw.Close();
    timer1.Stop();
    textBox1.Clear();//clears textbox
    textBox2.Clear();//clears textbox
    textBox3.Clear();//clears textbox
    textBox4.Clear(); //clears textbox
    textBox5.Clear(); //clears textbox
    textBox6.Clear();//clear textbox
    textBox7.Clear();//clears textbox
    serial.Close(); // closes the port

}

public void writefile()
{
string filename = DateTime.Now.Day.ToString();
string initime = DateTime.Now.TimeOfDay.ToString();
TextWriter s = new StreamWriter("filename.txt");
bool nostart = true;
int row = 0;
int vstop = 0;
int run = 0;
double[,] arr1 = new double[4, 4];
int timecount = 0;
while (true)
{
    run++;
    if (brk)
        break;
}
}

```

```

string serialip = serial.ReadLine();
//s.WriteLine(serialip);
if (serialip.Length <= 8)
continue;
string stmp = serialip.Replace('\r', ' ');
String[] cols = stmp.Split(new char[] { '\t' });
if (nostart)
{
    if (cols[2].Trim() != "001")
        continue;
    nostart = false;
}
if(row == 4)
{
    row = 0;
    double dpp1 = 0, dpp2 = 0, dgd = 0,dpp11=0,dpp22=0;
    dpp1 = (arr1[3, 0] - arr1[2, 0]) / (arr1[0, 0] - arr1[2, 0]);
    dpp11 = dpp1;
    dpp2 = (arr1[2, 1] - arr1[3, 1]) / (arr1[1, 1] - arr1[3, 1]);
    dpp22 = dpp2;
    dgd = Math.Asin(0.5 * (Math.Sqrt(dpp1) +
        Math.Sqrt(dpp2))) / (Math.PI * 1e10);
    dgd *= 1e12;
    arr1 = new double[4, 4];
    timecount = 0;
}
if(row < 4)
{
    for (int j = 0; j < cols.Length-2; j++)
        timecount += Convert.ToInt32(cols[3].Trim(), 16);
    }
    row++;
}
serial.Close();
s.Close();
}

private void timer1_Tick(object sender, EventArgs e)
{
    try
    {

```

```
        textBox1.Text = serial.ReadLine();
        sw.WriteLine(serial.ReadLine());
    }
    catch (Exception es)
    {
        MessageBox.Show(es.Message);
    }
}
}
```